Kapteyn Astronomical Institute
&
SRON, Netherlands Institute for Space Research

Bachelor project

Design of a Pickett-Potter Horn to measure the CMB at 11 GHz

Author:
Bram Lap
S2224399

Supervisor:
Prof. dr A. Baryshev
dr. J.P. McKean

July 6, 2015

Abstract

In this Bachelor Thesis the design of a horn antenna to measure the Cosmic Microwave Background (CMB) at 11 GHz is discussed. The theory underlying the design and different horn antenna types are treated. From this the optimal horn design is chosen; the Pickett-Potter horn. Then the design is optimized with a bandwidth of 1 GHz using CST Microwave Studio. Having obtained the final design, the Pickett-Potter is constructed and tested for the beam pattern and the reflection of the probe. From this it can be seen that the measured beam pattern and probe reflection deviate from the simulations. This difference is due to the propagation of a higher order mode. Despite this, the constructed Pickett-Potter horn was still suited for our observation, when rotated 90°.

Contents

1 Introduction

The footprint of the Big Bang, known as the Cosmic Microwave Background (CMB), is still visible today. It was first discovered in 1964 by Penzias and Wilson [14] [15] (shown in Figure 2). They discovered that on top of the flux received from Cas A and the atmosphere, there was another flux, corresponding to a temperature of roughly 2.7 K. This temperature directly points back to the oldest light seen in the Universe, originating from the epoch of recombination. In this epoch, the temperature of the Universe dropped below the threshold of 6000 K, allowing electrons and protons to combine to form the first atoms. This allowed photons to travel freely trough space, since the probability of scattering of electrons decreased drastically. This combination was very uniform throughout the Universe (especially on large scales). Even today we see that this radiation is uniform, even in regions of the Universe that nowadays are not causally connected. Hence in some early stage of the Universe they must have been. Therefore the discovery of the 2.7 K CMB is strong evidence for a Big Bang like Universe.

Figure 2: Penzias and Wilson with their Horn telescope.

The objective for this Bachelor project was to build a radio telescope that would measure the temperature of the CMB. For the project, four students participated (W. Mulder, M. Zandvliet, F. Sweijen and myself) each with their own - though strongly connected - subprojects. In this Bachelor Thesis the focus will be on the underlying physics, the design and testing of the constructed horn.

1.1 How to measure the CMB

The CMB is uniform at large scales and is almost a perfect black body. The black body radiation is described by the Planck Function [7], were the brightness of the object is plotted as function of frequency. This was done for the CMB in [7]. From this plot a preferred observing frequency can be chosen. One might choose to observe at a frequency of 175 GHz, since around that frequency the brightness of the CMB is the highest. However, for us this was not possible, since the available equipment (filters and amplifiers etc.) limited us to choose a frequency between 4-12 GHz. Eventually we choose to observe at 11 GHz, corresponding to the highest possible frequency (i.e. highest brightness) allowed by the available filter.
Observations in the radio regime are possible using two techniques; basic antennas or interferometry. The latter is not suited for measuring the temperature of the CMB, because an interferometer only measure the spatial fluctuations on the sky. Thus a uniform signal, from any extend source, will not be picked up by an interferometer. Also interferometry is a more advanced technique than a basic antenna. Therefore, for our observation a basic antenna was preferred. We used the horn antenna of Penzias and Wilson, shown in Figure 2, as a starting point.
Our observation of the CMB comes down to the observation of electromagnetic radio waves. Hence it is good to note that we are operating in the Rayleigh-Jeans regime, where the relationship between temperature and brightness is linear.
The incident electromagnetic radio waves will cause a time-varying current across a surface. This current will be measured in the form of a power, which corresponds to a temperature. This seems straight forward, but there are all sorts of calibration, electronic and design issues involved which make the measurement of the CMB much harder than sketched above. In this thesis the focus will be on the horn design, for the calibration and electronic issues see [7] [12] [21].

2 Electromagnetism

As stated before, the observation of the CMB is an observation of electromagnetic waves. The incident electromagnetic waves, originating from the CMB, will need to propagate through our horn, inflict a time-varying current, resulting in a measurable power. The design of the horn influences how the horn 'sees' the photons of the CMB and how they propagate through the horn. To understand this, and in the end, know how to optimize the horn design, the theory of electromagnetism is needed.

2.1 Maxwell's equations

In the field of electromagnetism electric- and magnetic fields are brought together. This was done by James Clerk Maxwell in 1862, resulting in the famous Maxwell's equations. Since the incident electromagnetic wave is a sinusoidal time-varying field we assume that all the fields have a time dependence $e^{\mathrm{j}\omega\mathrm{t}}$.

$$\mathbf{E}(\mathbf{r},\mathrm{t}) = \mathbf{E}(\mathbf{r})e^{\mathrm{j}\omega\mathrm{t}}, \quad \mathbf{H}(\mathbf{r},\mathrm{t}) = \mathbf{H}(\mathbf{r})e^{\mathrm{j}\omega\mathrm{t}}$$

Where ω being the angular frequency of the wave. Then the Maxwell's equations have the following form [13]:

$$\begin{aligned} \nabla' \times \mathbf{E} &= -\mathbf{J}_\mathrm{m} - \mathrm{j}\omega\epsilon\mathbf{H} \\ \nabla' \cdot \mathbf{E} &= \frac{\rho}{\epsilon} \\ \nabla' \times \mathbf{H} &= \mathbf{J} + \mathrm{j}\omega\epsilon\mathbf{E} \\ \nabla' \cdot \mathbf{H} &= \frac{\rho_\mathrm{m}}{\mu} \end{aligned} \tag{2.1}$$

Where $\mathbf{E(r)}$ is the electric field and $\mathbf{H(r)}$ is the magnetic field ($= \frac{\mathbf{B}}{\mu_0}$ in vacuum). These fields are driven by ordinary electric and current densities $\rho(\mathbf{r})$ and $\mathbf{J(r)}$, and in addition by the magnetic charge and current density ρ_m, $\mathbf{J}_\mathrm{m}\mathbf{(r)}$[1]. In order to know the beam pattern of the horn (the response of the horn to incoming radiation as a function of angle) and the propagation of the incident electromagnetic wave through the horn, equations 2.1 need to be solved for every infinitesimal volume element within the horn. This can be done by using boundary conditions, that are given by the properties of the material and the structure of the horn. Here we use the boundary conditions for a perfect conductor, since the material of the horn will be highly conducting, enabling the electromagnetic waves to propagate. The boundary conditions for a perfect electric conductor are [13]:

$$\begin{aligned} \hat{\mathbf{n}} \times \mathbf{E} &= 0 \\ \hat{\mathbf{n}} \cdot \mathbf{H} &= 0 \\ \mathbf{J}_s &= \hat{\mathbf{n}} \times \mathbf{H} \\ \rho_s &= \hat{\mathbf{n}} \cdot \epsilon_0\mathbf{E} \end{aligned} \tag{2.2}$$

2.2 Modes

The Maxwell's equations can be solved with the boundary conditions from equation 2.2. These solutions are linear, hence the solutions can be decomposed into linear super-positions of orthogonal solutions, called "modes". These solutions are chosen because they are easy to use in enclosed spaces, such as waveguides. The three types of modes are: [19] [2]:

1. Transverse electromagnetic (TEM) modes, that are modes with neither electric nor magnetic field in the direction of propagation, e.g. free-space waves.
2. Transverse Electric (TE) modes, modes with no electric field in the direction of propagation.
3. Transeverse Magnetic (TM) modes, are modes with no magnetic field in the direction of propagation.

For a hollow metallic object filled with a homogeneous material (e.g. air) and where the wavelength is of the order of the mechanical dimensions, only the TE and TM modes are supported. Since this is applicable for our horn, only the TE and TM modes have to be taken into account.
Since the behaviour of these modes is directly depended on the geometry of the horn, it would also influence the propagation of the TE and TM modes. The minimal frequency needed for a mode to propagate is called the cutoff frequency (ω_c). This cutoff frequency can be converted to a cutoff wavelength (λ_c), i.e. an expression for the minimal spacing required for a mode to occur.
The general mathematical formulation of the TE and TM modes are given in the following sections. These formulations will be used to determine the modes present in different horn antenna types, to eventually use these to determine the beam pattern of these horn antenna types (see Section 3).

[1] Although ρ_m and $\mathbf{J(r)}_\mathrm{m}$ are fictitious, they will enable us to calculate the beam pattern.
[2] See page 395 of reference [19]

2.2.1 TE modes

For the TE modes the conditions $\mathbf{E}_\mathrm{z} = 0$ and $\mathbf{H}_\mathrm{z} \neq 0$ must hold, as defined in Figure 3. The transverse electric field is then entirely determined by the transverse magnetic field, via $\mathbf{E}_\mathrm{T} = \eta_\mathrm{TE}\mathbf{H}_\mathrm{T} \times \hat{\mathbf{z}}$ [13]. Then the field components for the TE modes are obtained from [13], which gives:

$$\begin{aligned} &\nabla_\mathrm{T}^2 \mathrm{H_z} + \mathrm{k_c^2 H_z} = 0 \\ &\mathbf{H}_\mathrm{T} = -\frac{\mathrm{j}\beta}{\mathrm{k_c^2}} \nabla_\mathrm{T} \mathrm{H_z} \\ &\mathbf{E}_\mathrm{T} = \eta_\mathrm{TE}\mathbf{H}_\mathrm{T} \times \hat{\mathbf{z}} \end{aligned} \tag{2.3}$$

Where $\nabla_\mathrm{T}' = \hat{\mathbf{x}}\partial_\mathbf{x} + \hat{\mathbf{y}}\partial_\mathbf{y}$, η_TE is the wave impedance and $\mathrm{k_c}$ is the cutoff wavenumber, which is given by:

$$\mathrm{k_c^2} = \omega^2 \epsilon\mu - \beta^2, \tag{2.4}$$

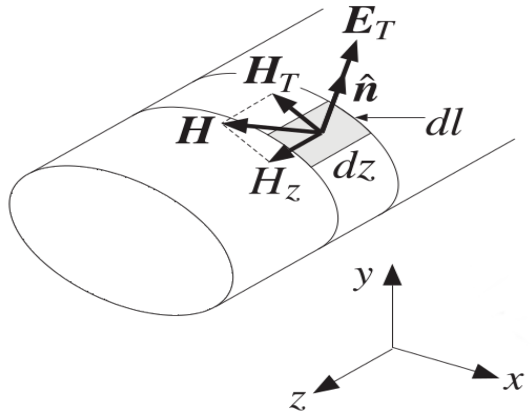

Figure 3: Definition of geometric axis [13].

with β being the propagation wavenumber along the guide direction, which is defined as: $\beta = 2\pi/\lambda_\mathrm{g}$. Here λ_g is the wavelength of the observing frequency (λ_0) within the object, defined as:

$$\lambda_\mathrm{g} = \frac{\lambda_0}{\sqrt{1 - (\lambda/\lambda_c)^2}}. \tag{2.5}$$

The relationship between E_T and H_T is identical to that of a uniform plane wave propagating in the z-direction [3].

2.2.2 TM modes

The TM modes require that $\mathbf{H}_\mathrm{z} = 0$ and $\mathbf{E}_\mathrm{z} \neq 0$, as defined in Figure 3. Hence the transverse magnetic field is completely determined by the transverse electric field, via $\mathbf{H}_\mathrm{T} = \eta_\mathrm{TM}^{-1}\hat{\mathbf{z}} \times \mathbf{E}_\mathrm{T}$ [13]. The components of the TM are given by [13]:

$$\begin{aligned} &\nabla_\mathrm{T}^2 \mathrm{E_z} + \mathrm{k_c^2 E_z} = 0 \\ &\mathbf{E}_\mathrm{T} = -\frac{\mathrm{j}\beta}{\mathrm{k_c^2}} \nabla_\mathrm{T} \mathrm{E_z} \\ &\mathbf{H}_\mathrm{T} = \frac{1}{\eta_\mathrm{TM}} \hat{\mathbf{z}} \times \mathbf{E}_\mathrm{T} \end{aligned} \tag{2.6}$$

With ∇_T' and $\mathrm{k_c}$ being the same as defined in Section 2.2.1, while η_TM is the wave impedance for the TM mode. Also here, the relationship between E_T and H_T is identical to that of a uniform plane wave propagating in the z-direction.

2.2.3 Propagation of modes: the scattering matrix

To obtain the overall transmission and reflection properties for the TE and TM modes, a scattering matrix is useful. This concept can be described as a layer, seen in Figure 4. Here $\mathrm{c_1}$ is the amplitude of the incident wave on the left and $\mathrm{b_2}$ is the amplitude of the incident wave on the right side of the layer. In Figure 4 $\mathrm{R_i}$ (i = 1 or 2) is the reflection coefficient, i.e. the ratio between the amplitude of the reflected wave with respect to the amplitude of the incident wave. Likewise $\mathrm{T_{i,j}}$ (i = 1 or 2, j = 1 or 2 and j≠i) is the transmission coefficient, which is the ratio of the amplitude of the transmission and the amplitude of the incident wave. Hence $\mathrm{T_{12}}$ is the transmission coefficient from 1 to 2 and $\mathrm{T_{21}}$ vice versa. With $\mathrm{R_1}$ the reflection coefficient of the incident wave in region 1, which is equal to $-\mathrm{R_2}$. Where $\mathrm{R_2}$ is the reflection coefficient of the incident wave in region 2. From Figure 4 we obtain that:

$$\begin{aligned} \mathrm{b_1} &= \mathrm{R_1 \cdot c_1 + T_{21} \cdot b_2} \\ \mathrm{c_2} &= \mathrm{R_2 \cdot b_2 + T_{12} \cdot c_1}. \end{aligned} \tag{2.7}$$

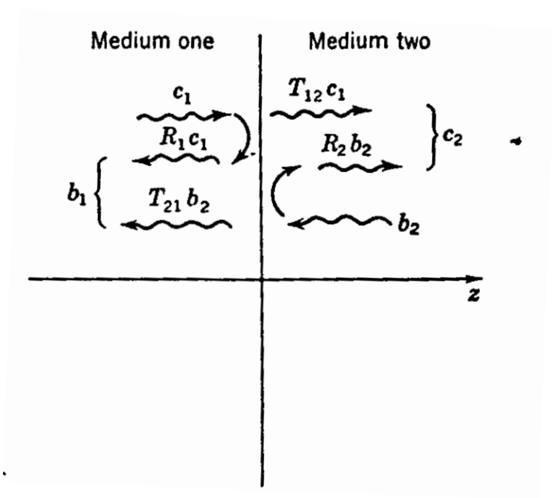

Figure 4: General scattering layer [5].

These equations can be rewritten in matrix notation, resulting in:

$$\begin{pmatrix} \mathrm{b_1} \\ \mathrm{b_2} \end{pmatrix} = \begin{pmatrix} \mathrm{S_{11}} & \mathrm{S_{12}} \\ \mathrm{S_{21}} & \mathrm{S_{22}} \end{pmatrix} \begin{pmatrix} \mathrm{c_1} \\ \mathrm{c_2} \end{pmatrix}, \tag{2.8}$$

[3] However, not exactly a free-space wave, where $\mathrm{E_z = H_z} = 0$!

where the 2D matrix is called the scattering matrix. The matrix element S_{11} is the reflection coefficient for region 1, S_{22} is the reflection coefficient for region 2 and S_{21} or S_{12} is the transmission coefficient from region 1 to region 2 and vice versa.

The scattering matrix will be used in two situations. The first being the mode propagation within the horn antenna, but as discussed earlier we will assume [4] that our antenna is a perfect electric conductor. Hence there will be little to no scattering involved, i.e. the scattering matrix will mainly be used to calculate the transmission.
While in the second situation, being the transfer of the incoming radiation into the probe, both the transmission as well as the scattering will be important. See Section 5.3 for a more detailed discussion.

2.3 Beam pattern uniformly illuminated aperture

The radiation field from an aperture antenna is determined from the the field over the aperture of the antenna. The aperture fields become the sources of the radiated fields at large distances. $\mathbf{E}_\mathrm{a}$ and $\mathbf{H}_\mathrm{a}$ are the tangential fields over the aperture A, as shown in Figure 5.
Here we assume that these fields correspond to the calculated TE and TM modes present in that part of the horn, i.e. no TEM modes. This approximation is valid since a TEM mode can only propagate by following currents in the wall, for which you need a voltage. However, in a single conducting system (e.g. a horn antenna) these currents and voltages cancel out, therefore TEM cannot propagate. On the other hand, the TE and TM modes only need a voltage or current in the wall, along which they can propagate. Hence the TE and TM modes will be present within the system.
In this sense the existence, propagation and balance of the TE and TM modes determines the characteristics of the given horn. To determine the radiation pattern, the radiated fields E($\mathbf{r}$) and H($\mathbf{r}$) have to be calculated at some observation point far away from the aperture.

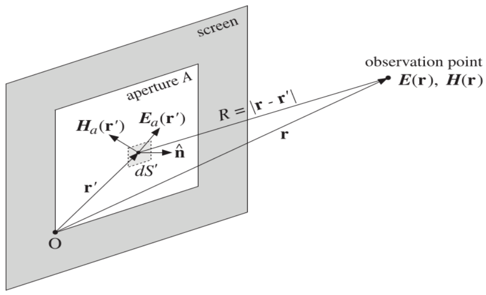

Figure 5: Aperture and the corresponding radiated fields [13].

By replacing the TE and TM modes at the aperture of the antenna by an equivalent electric and magnetic surface currents, which generate electromagnetic fields that propagate into the far-field, the radiation pattern can be calculated. For this the field equivalent principle is used, which states that the aperture fields may be replaced by equivalent electric and magnetic surface currents. The equivalent surface currents are [13]:

$$\begin{aligned} \mathbf{J} &= \hat{\mathbf{n}} \times \mathbf{H}_\mathrm{a} \quad \text{(electric surface current)} \\ \mathbf{J}_\mathrm{m} &= -\hat{\mathbf{n}} \times \mathbf{E}_\mathrm{a} \quad \text{(magnetic surface current)} \end{aligned} \tag{2.9}$$

With the addition of the fictitious ρ_m and $\mathbf{J}_\mathrm{m}$ a complete symmetry between the two 'electrical' and the two 'magnetic' Maxwell's equations shown in eq. 2.1 arises. This leaves the four Maxwell equations invariant [13]:

$$\begin{aligned} &\mathbf{E} \to \mathbf{H} \quad \mathrm{J} \to \mathbf{J}_\mathrm{m} \quad \mathbf{A} \to \mathbf{A}_\mathrm{m} \\ &\mathbf{H} \to -\mathbf{E} \quad \rho \to \rho_\mathrm{m} \quad \varphi \to \varphi_\mathrm{m} \\ &\epsilon \to \mu \quad \mathbf{J}_\mathrm{m} \to -\mathbf{J} \quad \mathbf{A}_\mathrm{m} \to -\mathbf{A} \\ &\mu \to \epsilon \quad \rho_\mathrm{m} \to -\rho \quad \varphi_\mathrm{m} \to -\varphi \end{aligned} \tag{2.10}$$

Where $\varphi, \mathbf{A}$ and $\varphi_\mathrm{m}, \mathbf{A}_\mathrm{m}$ are the corresponding scalar and vector potentials defined in the literature [13][5]. From this transformation it can be seen that the first two equations in eq.2.1 transform in the last two. Hence, by obtaining an expression for the electric field $\mathbf{E}$ and applying a duality transformation, we can find an expression for the magnetic field H.

The next step is to rewrite the Maxwell's equations in equation 2.1 in terms of the scalar and vector potentials, which satisfy the Lorentz conditions and Helmholtz wave equations [13]. This gives:

$$\begin{aligned} \mathbf{E} &= -\nabla'\phi - \mathrm{j}\omega\mathbf{A} - \frac{1}{\epsilon}\nabla' \times \mathrm{A}_\mathrm{m} \\ \mathbf{H} &= -\nabla'\phi_\mathrm{m} - \mathrm{j}\omega\mathbf{A}_\mathrm{m} + \frac{1}{\epsilon}\nabla' \times \mathrm{A}. \end{aligned} \tag{2.11}$$

Plugging in the scalar and vector values defined in [13], we obtain an expression for the E and $\mathbf{H}$ fields in terms of the current and charge densities.

$$\begin{aligned} \mathbf{E} &= \frac{1}{\mathrm{j}\omega\mu\epsilon}\int_\mathrm{V}\Big[\mathrm{k}^2\mathbf{J}\mathrm{G} + (\mathbf{J}\cdot\nabla'')\nabla'\mathrm{G} - \mathrm{j}\omega\mu\epsilon\mathrm{J}_\mathrm{m} \times \nabla''\mathrm{G}\Big]\mathrm{dV'} \\ \mathbf{H} &= \frac{1}{\mathrm{j}\omega\mu\epsilon}\int_\mathrm{V}\Big[\mathrm{k}^2\mathbf{J}_\mathrm{m}\mathrm{G} + (\mathbf{J}_\mathrm{m}\cdot\nabla')\nabla''\mathrm{G} + \mathrm{j}\omega\mu\epsilon\mathrm{J} \times \nabla''\mathrm{G}\Big]\mathrm{dV'} \end{aligned} \tag{2.12}$$

[4] And justified in Section 5
[5] Equation 18.2.6

With V being the volume over which the charge and current densities are nonzero and G the Green's function for the Helmholtz equation [13]:

$$\mathrm{G} = \mathrm{G}(\mathbf{r}\text{-}\mathbf{r'}) = \frac{e^{-\mathrm{jk}(\mathbf{r}-\mathbf{r'})}}{4\pi|\mathbf{r}-\mathbf{r'}|}, \tag{2.13}$$

. with the definition of **r** and **r'** as shown in Figure 5.
For an aperture antenna with the effective surface currents given by equation 2.12, the volume integral is reduced to a surface integral over the aperture A.

$$\begin{aligned}\mathbf{E} &= \frac{1}{\mathrm{j}\omega\epsilon}\int_{\mathrm{A}}[(\hat{\mathbf{n}}\times\mathbf{H}_{\mathrm{a}})\cdot\nabla'(\nabla'\mathrm{G}) + \mathrm{k}^2(\hat{\mathbf{n}}\times\mathbf{H}_{\mathrm{a}})\mathrm{G} + \mathrm{j}\omega\epsilon(\hat{\mathbf{n}}\times\mathbf{E}_{\mathrm{a}})\times\nabla'\mathrm{G}]\mathrm{dS'}\\ \mathbf{H} &= \frac{1}{\mathrm{j}\omega\epsilon}\int_{\mathrm{A}}[-(\hat{\mathbf{n}}\times\mathbf{E}_{\mathrm{a}})\cdot\nabla'(\nabla'\mathrm{G}) - \mathrm{k}^2(\hat{\mathbf{n}}\times\mathbf{E}_{\mathrm{a}})\mathrm{G} + \mathrm{j}\omega\epsilon(\hat{\mathbf{n}}\times\mathbf{H}_{\mathrm{a}})\times\nabla'\mathrm{G}]\mathrm{dS'}\end{aligned} \tag{2.14}$$

Next, we need to make a far-field approximation of the solutions given by equation 2.12, to obtain the radiation field [13] [6]. Hence we need to transform these fields to far-field, which is done by a Fourier transform. The radiation vectors are given by a two-dimensional Fourier transform-like integral over the aperture of the antenna [13]:

$$\begin{aligned}\mathbf{F}(\theta,\phi) &= \int_{\mathrm{A}}\mathbf{J}_{\mathrm{s}}(\mathbf{r'})e^{\mathbf{jk\cdot r'}}\mathrm{dS'} = \int\hat{\mathbf{n}}\times\mathbf{H}_{\mathrm{a}}(\mathbf{r'})e^{-\mathbf{jk\cdot r'}}\mathrm{dS'}\\ \mathbf{F}_{\mathrm{m}}(\theta,\phi) &= \int_{\mathrm{A}}\mathbf{J}_{\mathrm{m}}(\mathbf{r'})e^{-\mathbf{jk\cdot r'}}\mathrm{dS'} = -\int\hat{\mathbf{n}}\times\mathbf{E}_{\mathrm{a}}(\mathbf{r'})e^{\mathbf{jk\cdot r'}}\mathrm{dS'}\end{aligned} \tag{2.15}$$

Since the far-field solutions of Maxwell's equations are best described in spherical coordinates, the radiation fields are given as a function of the angles ϕ and θ (see Figure 6).
It is reasonable to assume that the surface of the aperture is flat. This means that the equations given by 2.15 become two normal 2-D Fourier transform integrals. Hence by taking the aperture plane in the xy-plane, we set $\hat{\mathbf{n}} = \hat{\mathbf{z}}$. Therefore dS' = dx' dy', which results in:

$$\begin{aligned}\mathbf{F}(\theta,\phi) &= \int_{\mathrm{A}}\mathbf{J}_{\mathrm{s}}(\mathbf{r'})e^{\mathbf{jk\cdot r'}}\mathrm{dx'\ dy'} = \hat{\mathbf{z}}\times\int\mathbf{H}_{\mathrm{a}}(\mathbf{r'})e^{-\mathbf{jk\cdot r'}}\mathrm{dS'}\\ \mathbf{F}_{\mathrm{m}}(\theta,\phi) &= \int_{\mathrm{A}}\mathbf{J}_{\mathrm{m}}(\mathbf{r'})e^{-\mathbf{jk\cdot r'}}\mathrm{dx'\ dy'} = -\hat{\mathbf{z}}\times\int\mathbf{E}_{\mathrm{a}}(\mathbf{r'})e^{\mathbf{jk\cdot r'}}\mathrm{dx'\ dy'}\end{aligned} \tag{2.16}$$

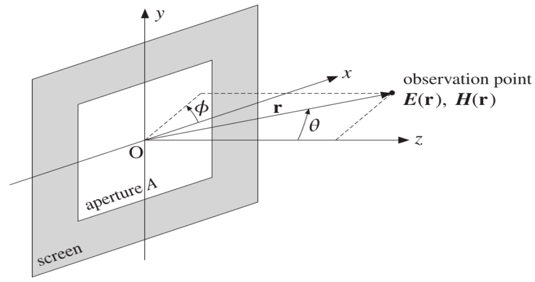

Figure 6: Radiation fields from aperture [13].

Here $e^{\mathbf{jk\cdot r'}} = e^{\mathrm{jk_x x' + jk_y y'}}$ and $\mathrm{k_x} = \mathrm{k}\cos(\phi)\sin(\theta), \mathrm{k_y} = \mathrm{k}\sin(\phi)\sin(\theta)$. With the two-dimensional Fourier transforms of the aperture fields being:

$$\begin{aligned}\mathbf{f}(\theta,\phi) &= \int_{A}\mathbf{E}_{\mathrm{a}}(\mathbf{r'})e^{\mathbf{jk\cdot r}}\mathrm{dx'\ dy'} = \mathrm{E_a(x', y')}\int_{A}e^{\mathrm{jk_x x' + jk_y y'}}\mathrm{dS}\\ \mathbf{g}(\theta,\phi) &= \int_{A}\mathbf{H}_{\mathrm{a}}(\mathbf{r'})e^{\mathbf{jk\cdot r}}\mathrm{dx'\ dy'} = \mathrm{H_a(x', y')}\int_{A}e^{\mathrm{jk_x x' + jk_y y'}}\mathrm{dx'\ dy'}\end{aligned} \tag{2.17}$$

In uniform apertures, which we will assume later on, the fields $\mathbf{E}_{\mathrm{a}}$ and $\mathbf{H}_{\mathrm{a}}$ are constant over the aperture. Since $\mathbf{E}_{\mathrm{a}}$ is constant, the Fourier transform in equation 2.17 becomes:

$$\mathrm{f}(\theta,\phi) = \frac{1}{\mathrm{A}}\int_{A}e^{\mathbf{jk\cdot r'}}\mathrm{dS'}\quad\text{(uniform-aperture pattern)} \tag{2.18}$$

Hence by assuming that the tangential aperture fields $\mathbf{E}_{\mathrm{a}}$ and $\mathbf{H}_{\mathrm{a}}$ are equal to the TE and TM modes at the aperture, i.e. no TEM modes, the radiation pattern of an aperture can be calculated. This can be done, by replacing the TE and TM modes at the aperture with equivalent electric and magnetic surface currents. These currents will produce electromagnetic waves, which operate as sources for the radiation fields. To obtain the final radiation fields, the Fourier transform of the current densities, i.e. the tangential aperture fields, is taken.

[6] See Chapter 15 of citation

3 Horn antenna theory and characteristics

The basics of horn antenna theory is that an incident electromagnetic wave will cause a time-varying current across the aperture surface, resulting in modes at the aperture that can propagate through the horn into the probe. This process can be reversed, using the Reciprocal Theorem. So now the circular waveguide modes will start to propagate in the direction of the aperture, out of the horn. These modes will eventually reach the aperture, resulting in an emitted electromagnetic wave.
In this way an important general aspect of radio telescopes is introduced; the beam pattern. The beam pattern describes how the telescope, in this case a horn antenna, sees the power incoming radiation as a function of angle. The power pattern of a horn antenna is square of the radiation field at the aperture of the horn, calculated in Section 2

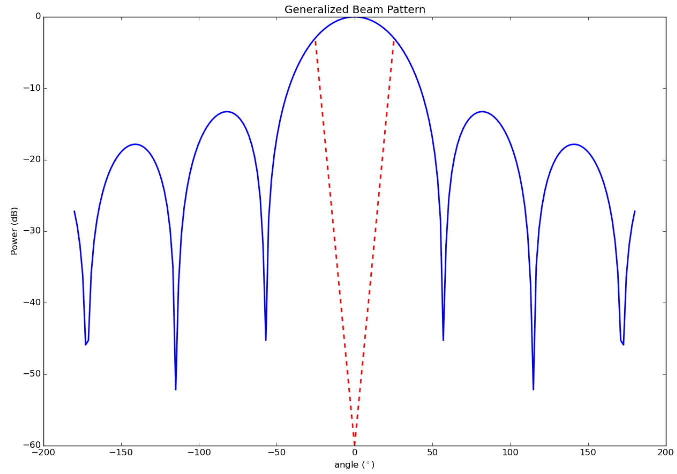

Figure 7: General representation of a beam pattern.

In Figure 7 a general representation of a beam pattern is shown. This pattern is normalized with respect to the global maximum and converted into decibels, hence the maximum of the graph corresponds to 0 dB [7]. From the beam pattern other horn characteristics can be calculated, such as the main beam, the sidelobe level, half-power beamwidth, beam solid angle, the gain and effective area.
The main beam is given by the area from the highest power (the global maximum), till the first local minimums on both sides of the global maximum. In Figure 7, this is from roughly from -50°till 50°. Resulting in a main beam of 100°. The other maximums are named sidelobes, were the first local maximum gives the sidelobe level. The half-power beamwidth (HPBW) is the total angle at which the received power is reduced to -3 dB, since P(db) = $10 * \log_{10}(0.5)$ = -3 dB. This is shown in Figure 7 as the angle between the two red dotted lines.
In general the beam pattern has a 3D shape and the power is a function of θ and ϕ ($\mathrm{P}(\theta, \phi)$). Assuming that the beam pattern is symmetric, we can calculate the beam solid angle with [20]:

$$\Omega_A = \frac{\pi}{4} \cdot \mathrm{HPBW}^2 = \int_0^{2\pi} \int_0^{\pi} \mathrm{P_n}(\theta, \phi) \mathrm{d}\Omega \tag{3.1}$$

Where the HPBW is given in radians, Ω_A in steradians[8] and $\mathrm{d}\Omega = \sin(\theta)\mathrm{d}\theta\mathrm{d}\phi$.
The beam solid angle is a measure of how large the object appears to an observer at a given point. It can also be used for estimating the antenna temperature produced by a compact source covered by the solid angle Ω_A having uniform brightness temperature $\mathrm{T_B}$ [1].
Due to the beam of the power pattern, the horn antenna also has directional properties. These are represented in the gain of the horn antenna, i.e. the ratio between the received power by the antenna with respect to the power received of an (hypothetical) isotropic antenna [20]. The gain is given by [20]:

$$\mathrm{G_{max}} = \frac{4\pi}{\Omega_A} = \frac{4\pi A_e}{\lambda^2}. \tag{3.2}$$

With $\mathrm{A_e}$ the effective area and λ is the observed wavelength. From this the effective area of the horn aperture can be calculated, by rewriting equation (3.2).

Another horn characteristic, which can be determined without the beam pattern, is the far-field distance. This is a measure of how far a point source must be from the horn antenna to satisfy the assumption that the incident waves are (nearly) planar. This distance is given by [20]:

$$\mathrm{R_{ff}} \approx \frac{2D^2}{\lambda}. \tag{3.3}$$

[7] The power in dB is calculated as follows: $\mathrm{P(db)} = 10 \cdot \log_{10}(\mathrm{P}/\mathrm{P_{max}})$. Where $\mathrm{P_{max}}$ is the maximum power in watt
[8] 1 str = 1 rad^2 = $(\frac{180}{\pi})^2$degrees^2

Generally a horn antenna consist of good electrically conducting material, that has been designed in such a manner that it will radiate electromagnetic power in an efficient manner. The horn antenna is a type of antenna that has a flared shape, as shown in Figure 8. This flaring section allows radio waves to be directed into a beam. The directivity makes these antennas excellent instruments for measuring the CMB, because the sky can be sampled more frequently (i.e. narrow beam) and the antenna gain is high. Horn antennas also have little loss, resulting in a high directivity of the gain. Next to the horn antenna being a reliable choice, they are easy to manufacture, making them an excellent choice for our observation of the CMB.

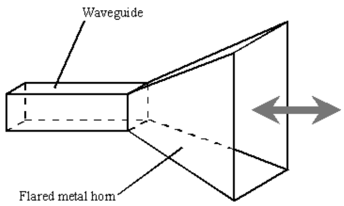

Figure 8: Schematic of a rectangular horn antenna, showing the flared section and the waveguide. Credits: Margaret Rouse [10].

A horn antenna normally consists of two parts; a flared horn section and a waveguide, as show in Figure 8. Here the term 'horn' refers to the total horn, i.e. the flared horn section with the waveguide, unless specifically said otherwise. The flared-horn section is where the incident electromagnetic waves enter the aperture and (if possible) propagate into the horn. At the end of the flaring-section there is the waveguide, that guides the wave until they enter a copper probe. The received signal is weak and thus needs to be further processed. The back-end of the measurement system is where the signal is further processed, see [12].

3.1 Different horn types

As discussed in Section 2 different types of horn antennas result in different electric and magnetic fields at the aperture of the horn. These fields give rise to a different beam pattern, as discussed in Section 3. In this section a more detailed discussion will be given on what the different beam patterns are for the four selected horn shapes. The discussed horn shapes are; the Rectangular horn, the Circular horn, the Potter horn and the Pickett-Potter horn. Here it is assumed, that for each of these horn the fields at the aperture are uniform, i.e. equation 2.18 is applicable.

3.1.1 Rectangular Horn

The Rectangular horn antenna, also known as a pyramidal horn antenna, is one of the commonly used horn antenna types. Since they are easy to fabricate, have a high gain and are operational at a large frequency range [11]. This type of horn is obtained by flaring a rectangular waveguide, were it is assumed that the modes that can exist within the waveguide propagate into the flared horn section. The design of the Rectangular horn is shown in Figure 9.

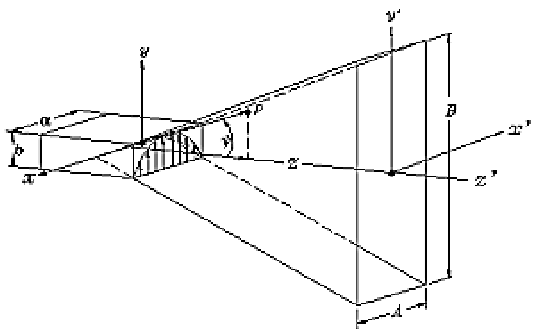

Figure 9: Design of a rectangular horn antenna [4].

The Rectangular horn is determined by the parameters 'a', for the x-axis and 'b', for the y-axis. To calculate the modes for the Rectangular horn, the Maxwell's equations for this configuration need to be solved [19]. The solutions are given by:

$$\begin{aligned} &\mathrm{E_z = A' \sin(k_x x) \sin(k_y y)} && \text{For TM waves} \\ &\mathrm{H_z = B' \cos(k_x x) \cos(k_y y)} && \text{For TE waves} \end{aligned} \tag{3.4}$$

With A' and B' being values corresponding to the amplitude of the electromagnetic wave. Applying the boundary conditions [9] to equation 3.4 the following can be found:

$$\begin{aligned} \text{Where:} \quad & \mathrm{k_x = \pi m}, & \mathrm{m} = 1, 2, 3, ... \\ & \mathrm{k_y = \pi n}, & \mathrm{n} = 1, 2, 3, .. \end{aligned}$$

With m and n being the integers representing the mode number.
Assuming that most of the energy is stored in the dominant $\mathrm{TE_{10}}$ mode, equation (2.18) can be used to find the radiation pattern for a Rectangular horn antenna, this gives:

$$\mathrm{f}(\theta, \phi) = \frac{1}{\mathrm{ab}} \int_{\text{-a/2}}^{\text{a/2}} \int_{\text{-b/2}}^{\text{b/2}} \mathrm{e}^{\mathrm{j}\mathbf{k}_\mathrm{x}\mathrm{x}+\mathrm{j}\mathbf{k}_\mathrm{y}\mathrm{y}} \mathrm{dx\ dy} = \frac{\sin(\mathrm{k_x a}/2)}{\mathrm{k_x a}/2} \frac{\sin(\mathrm{k_y a}/2)}{(\mathrm{k_y a}/2)} \tag{3.5}$$

Where $\mathrm{k_x = k\sin(\theta)\cos(\phi)} =$, $\mathrm{k_y = k\sin(\theta)\sin(\phi)}$ and $\mathrm{k} = \frac{2\pi}{\lambda}$. This gives:

$$\mathrm{f}(\theta, \phi) = \frac{\sin(\frac{\pi \mathrm{a}}{\lambda}\sin(\theta)\cos(\phi))}{\frac{\pi \mathrm{a}}{\lambda}\sin(\theta)\cos(\phi))} \frac{\sin(\pi\frac{\mathrm{a}}{\lambda}\sin(\theta)\sin(\phi))}{\frac{\pi \mathrm{a}}{\lambda}\sin(\theta)\cos(\phi))} \tag{3.6}$$

[9] $\mathrm{E_z} = 0$ at $\mathrm{x = a}$ and $\mathrm{y = b}$

Along the principle, that is in the xz-plane ($\phi = 0°$), the beam pattern as a function of the angle is plotted in Figure 10. The plot of the beam pattern in the yz-planes ($\phi = 90°$) looks like the beam pattern in Figure 10, since the beam patterns are symmetric.

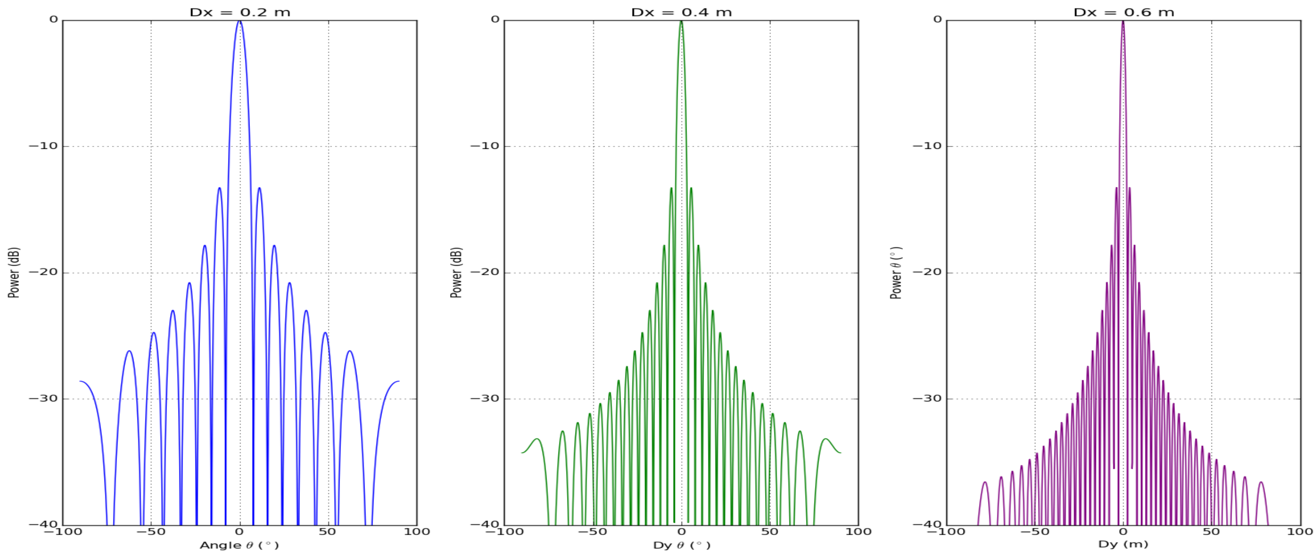

Figure 10: The Beam Pattern of a rectangular horn as function of y position, i.e. the xz-plane ($\phi = 0°$). Plot was made with the Python script in 11.1. Credits for Maik Zandvliet [12] and Frits Sweijen [7].

3.1.2 Conical horn

The Conical horn structure is one of the most simple antenna structures and can be quite compact in size. The response of a Conical horn to the incoming radiation is similar to that of a Rectangular or Pyramidal horns. Since the beam pattern and therefore the gain, can be calculated easily from the physical dimensions of the horn. [3].
The general design of a Conical horn is shown Figure 11. As seen from this figure, the Conical horn is conical flared section, which is usually connected to a circular waveguide. The performance of this type of horn antenna can be determined by two parameters; the axial length l of the flared-section and the diameter of the horn aperture $\mathrm{d_m}$.

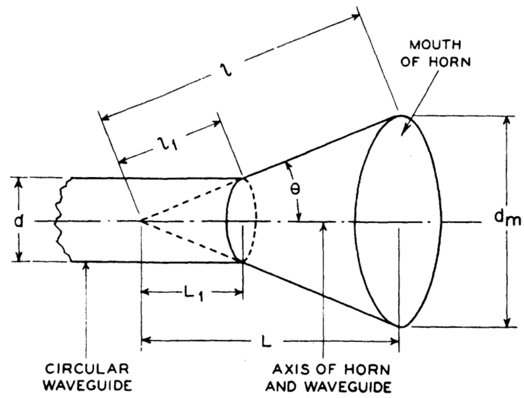

Figure 11: Design of a rectangular horn antenna [3].

As with the Rectangular horn, the modes the Conical horn must be obtained [19]. They are given by:

$$\mathrm{E_z} = \mathrm{A\ J_n(k_c r)cos(n\phi)} \qquad \text{For TM waves}$$
$$\mathrm{H_z} = \mathrm{B\ J_n(k_c r)cos(n\phi)} \qquad \text{For TE waves}$$

Using that $\mathrm{H_z} = 0$, the remaining components for the TM waves are [19]:

$$\begin{aligned} \mathrm{E_r} &= -\frac{\mathrm{j}\beta}{\mathrm{k_c}}\mathrm{AJ'_n(k_c r)cos(n\phi)} \\ \mathrm{E_\phi} &= -\frac{\mathrm{jn}\beta}{\mathrm{k_c^2 r}}\mathrm{AJ_n(k_c r)sin(n\phi)} \end{aligned} \tag{3.7}$$

And using $\mathrm{E_z} = 0$ for TM waves [19]:

$$\begin{aligned} \mathrm{E_r} &= -\frac{\mathrm{jn}\omega\mu}{\mathrm{k_c^2 r}}\mathrm{BJ_n(k_c r)sin(n\phi)} \\ \mathrm{E_\phi} &= -\frac{\mathrm{jn}\omega\mu}{\mathrm{k_c}}\mathrm{BJ'_n(k_c r)cos(n\phi)} \end{aligned} \tag{3.8}$$

Where $\mathrm{k_c^2} = \gamma^2 + \mathrm{k}^2 = \mathrm{k}^2 - \beta^2$, where $\mathrm{k} = \frac{2\pi}{\lambda}$.
For a Conical horn aperture, we need to calculated the circular aperture with a radius 'a' in cylindrical coordinates. This implies that $\mathrm{f}(\theta, \phi)$ will be independent of ϕ. For computing the integral from equation 2.18 we set $\phi = 0$ and

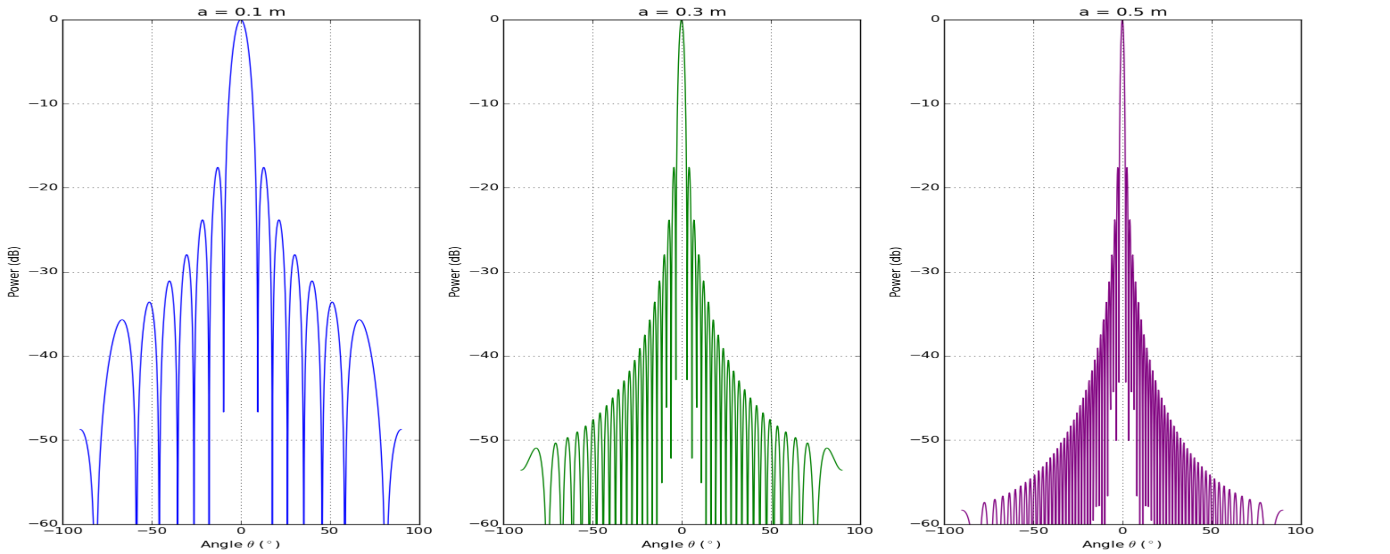

Figure 12: The Beam Pattern of a Conical horn aperture. Plot was made with the Python script in 11.1. Credits for Maik Zandvliet [12] and Frits Sweijen [7].

assume that the TE_{11} mode is the dominant mode [8] , this gives:

$$\mathrm{f}(\theta) = \frac{1}{\pi \mathrm{a}^2} \int_0^{\mathrm{a}} \int_0^{2\pi} e^{\mathrm{jk}\rho \sin(\theta') \cos(\phi')} \mathrm{d}\rho' \mathrm{d}\phi' \tag{3.9}$$

$$\text{Using: } \mathrm{J}_0(\mathrm{x}) = \frac{1}{2\pi} \int_0^{2\pi} e^{\mathrm{jx}\cos(\phi')} \mathrm{d}\phi' \quad \text{and} \quad \int_0^1 \mathrm{J}_0(\mathrm{xr})\mathrm{r}\ \mathrm{dr} = \frac{\mathrm{J}_1(\mathrm{x})}{\mathrm{x}} \tag{3.10}$$

Where J_1 is the Bessel function of the first order and J'_1 is it's derivative, equation 3.9 gives:

$$\mathrm{f}(\theta) = 2\frac{\mathrm{J}_1(\mathrm{ka}\ \sin(\theta))}{\mathrm{ka}\ \sin(\theta)} = 2\frac{\mathrm{J}_1(\mathrm{ka}\ \sin(\theta))}{\mathrm{ka}\ \sin(\theta)} = \frac{\lambda \mathrm{J}_1(\frac{2\pi \mathrm{a}}{\lambda}\sin(\theta))}{\pi \mathrm{a}\ \sin(\theta)} \tag{3.11}$$

In Figure 12, the beam pattern for a Conical horn, given by equation 3.11, is plotted for different values of the parameter 'a', as function of θ. This beam pattern is symmetric, since the aperture of a Conical horn is symmetric resulting in a symmetric beam pattern.

3.1.3 Potter Horn

The third type of horn that was selected for further discussion was the Potter horn. This type of horn was invented by P. D. Potter in 1963 [16]. The Potter horn, shown in Figure 13, focuses on one of the important characteristics of a horn antenna for most applications, which is the sidelobe level. It is important because it determines the main-beam efficiency and the response to spurious wide-angle radiation, to obtain low sidelobe levels.
To obtain a low sidelobe level the phase centers of the electric- and magnetic-plane must be coincident [16]. In his paper, Potter presents a technique which enables complete phase centering by using a phasing section in the horn. As a result -30 dB sidelobe level is obtained in the electric field plane. Leaving the magnetic field plane unaffected. This method of balancing modes, is know as a 'dual-mode conical horn'. In this technique, next to the the dominant TE_{11} mode, the TM_{11} mode is excited at the throat of the horn.
At the aperture of the horn antenna, these two modes will be balanced such that the sidelobe level is suppressed. Hence the performance of the dual-mode conical horn is determined by a balance between the TE_{11} and TM_{11} modes. To see the combined result we start at with the electric- or magnetic field of these two modes. The electric field of the TE_{11} mode is given by [16]:

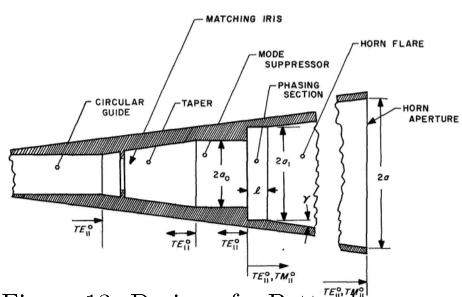

Figure 13: Design of a Potter horn antenna [16].

$$\begin{aligned}
\mathrm{E}_{\theta \mathrm{H}} &= -\frac{\omega\mu}{2\mathrm{R}}\Big(1 + \frac{\beta_{11\mathrm{H}}\cos(\theta)}{\mathrm{k}}\Big)\mathrm{J}_1(\mathrm{K}_{11\mathrm{H}}\mathrm{a})\left[\frac{\mathrm{J}_1(\mathrm{ka}\ \sin(\theta))}{\sin(\theta)}\right]\sin(\phi)e^{-\mathrm{jkR}} \\
\mathrm{E}_{\phi \mathrm{H}} &= -\frac{\mathrm{ka}\omega\mu}{2\mathrm{R}}\Big(\frac{\beta_{11\mathrm{H}}}{\mathrm{k}} + \cos(\theta)\Big)\mathrm{J}_1(\mathrm{K}_{11\mathrm{H}}\mathrm{a})\left[\frac{\mathrm{J'}_1(\mathrm{ka}\ \sin(\theta))}{1 - \Big(\frac{\mathrm{k}\ \sin(\theta)}{\mathrm{K}_{11\mathrm{H}}}\Big)^2}\right]\cos(\phi)e^{-\mathrm{jkR}}
\end{aligned} \tag{3.12}$$

The electric field of the TM_{11} mode is given by [16]:

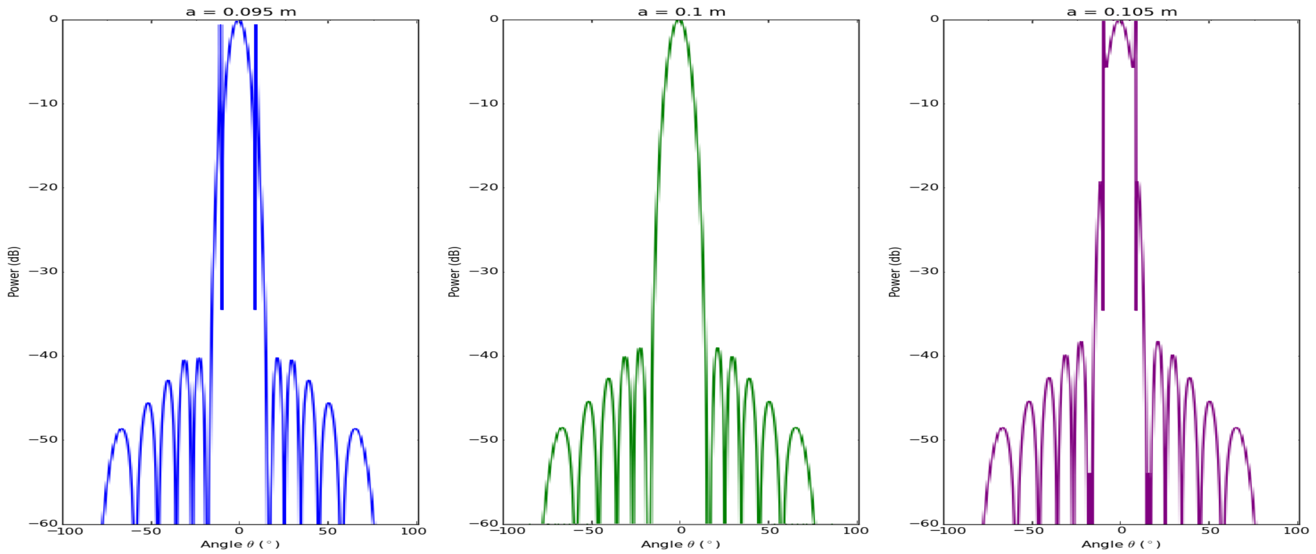

Figure 14: The Beam Pattern of a Potter horn aperture. Plot was made with the Python script in 11.1 [16]. Credits for Maik Zandvliet [12] and Frits Sweijen [7].

$$\mathrm{E}_{\theta\mathrm{E}} = -\left(\frac{\mathrm{kaK_{11E}}}{2\mathrm{R}}\right)\left(\frac{\beta_{11\mathrm{E}}}{\mathrm{k}} + \cos(\theta)\right)\left[\frac{\mathrm{J'}_1(\mathrm{K_{11E}a})}{1-\left(\frac{\mathrm{K_{11E}}}{\mathrm{k}\ \sin(\theta)}\right)^2}\right]\left[\frac{\mathrm{J}_1(\mathrm{ka}\ \sin(\theta))}{\sin(\theta)}\right]\sin(\phi)e^{-\mathrm{jkR}}$$

$$\mathrm{E}_{\phi\mathrm{E}} = 0 \tag{3.13}$$

Where ω is the radian frequency, k is the free-space propagation constant ($= \mathrm{j}\omega\sqrt{\mu_0\epsilon_0}$ [18]), μ is the permeability, 'a' the aperture radius, J_1 is the first order Bessel function of the first kind, $\mathrm{J'}_1$ the first derivative of J_1 with respect to its argument and $\mathrm{K_{11H}}$ is the first root of $\mathrm{J'}_1$ (=1.841).
Equation 3.12 and 3.13 can be combined to get the total electric field of the dual-mode horn antenna, i.e. subtracting $\mathrm{E}_{\theta\mathrm{H}}$ from $\mathrm{E}_{\theta\mathrm{E}}$. This results in,

$$\mathrm{E}_{\theta\mathrm{T}} = \left[\left(1 + \frac{\beta_{11\mathrm{H}}}{\mathrm{k}}\cos(\theta)\right) - \alpha\frac{\left(\beta_{11\mathrm{H}} + \cos(\theta)\right)}{1-\left(\frac{\mathrm{K_{11E}}}{\mathrm{k}\ \sin(\theta)}\right)^2}\right]\left[\frac{\mathrm{J}_1(\mathrm{ka}\ \sin(\theta))}{\sin(\theta)}\right]. \tag{3.14}$$

Here, α is an arbitrary constant defining the relative power in the TE_{11} and TM_{11} modes. Here $\alpha = 0.653$ is chosen, since for this value the E- and H-plane half-power beamwidth are equal and the phase centers coincide, resulting in a sidelobe level of -40 dB. $\mathrm{E}_{\theta\mathrm{T}}$ is plotted as a function of θ, for different values of the aperture radius in Figure 14.

3.1.4 Pickett-Potter Horn

The final type of horn that was further investigated was the Pickett-Potter horn. This type of horn antenna, invented by H. M. Pickett is a variation on the Potter horn (see section 3.1.3).
The Pickett-Potter is the Potter horn without the phasing section, such as shown in Figure 15. The coincidence of the TE_{11} and TM_{11} modes is done by the step-transition from the flared horn section to the circular waveguide (indicated in Figure 15 at $1.30\lambda_0$). This step transition generates a small fraction of the TM_{11} mode, as well as the propagating TE_{11} mode. At the aperture of the horn, this results in an E-plane aperture distribution that is more tapered with respect to a stand single-mode conical horn [9].
The result is that the Pickett-Potter horn is a horn antenna with the advantages of a Potter horn (i.e. low sidelobes), but easier to construct, since the phasing section is left out. The beam pattern of the Pickett-Potter horn will be the same as for the Potter horn (as shown in Figure 14), since the balancing of the modes is the same, but how this balance is achieved is different.
There is however, one major disadvantage of the Pickett-Potter horn that is that the low sidelobe level comes at the cost of the total bandwidth [16][17].

Figure 15: General sketch of a Pickett-Potter horn antenna [9].

4 Selection of the preferred horn antenna type

In this section the most suited horn antenna type, for our observation of the CMB, is selected from the four horn antenna types that were discussed in Section 3.1. The CMB has an expected value of around 2.7 Kelvin, which is small with respect to the temperature of the atmosphere, i.e. $\sim$ 300 K. Hence the precision we need for our measurement system is of the order of 0.1 K. This corresponds to a power level of -35 dB [10]. Therefore the main selection constraint is that the sidelobe level of the beam pattern is lower then -35 dB. Related to this is that the beam pattern of the horn antenna must have a shape as shown in Figure 7. With such a shaped beam pattern and a sidelobe level of -35 dB, we can be certain that the measured power is from the main beam and some spurious wide-angle radiation received by the sidelobes.
Another, related, design constraint is the half-power beamwidth of the beam. Since we will be measuring the atmospheric temperature as a function of zenith angle [7][21] to determine the temperature of the CMB, precision in the zenith direction is important. The maximum half-power beamwidth that the measurement system is allowed to have is 15°. As shown in the thesis of F.Sweijen [7].
Besides the design constraints mentioned above, the horn antenna has to be constructed by ourselves within a reasonable amount of time ($\sim$ 2 days). Therefore the construction level of the horn is important. The horn needs to be easy to fabricate and must be robust with respect to small construction errors. For the latter it helps that we observe at 11 GHz, which corresponds to a wavelength of roughly 3 cm, hence it is less prone to construction errors.

4.1 Definite horn horn antenna type

An overview of the four horn antennas types and their performance regarding the selection criteria is listed below.

Horn antenna type	**Sidelobe level (dB)**	**HPBW (full angle in degrees)**	**Construction level**
Rectangular horn	-13	4 - 1.6	Easy
Conical horn	-17	6.6 - 1.4	Medium
Potter horn	-40	10 - 8.2	Hard
Pickett-Potter horn	-40	10 - 8.2	Medium

Table 1: Ferformance selected horn types.

The analysis of the sidelobe level shown in Table 1 is based on the beam patterns shown in Figures 10, 12 and 14. The beam pattern of the Potter and the Pickett-Potter horn are the same, since only the method of phase coincidence changes, leaving the beam pattern intact. From these figures it can be seen that the Rectangular and Conical horn have a sidelobe level of roughly -20 dB, while the Potter en Pickett-Potter horn have a sidelobe level of -40 dB.
For the HPBW again the beam patterns in Figures 10, 12 and 14 are used. As can be seen from these figures, the the HPBW of the Potter and Pickett-Potter horn is somewhat broader, than the Rectangular and Conical horn, while remaining below 15°.
The analysis for the construction level of these four horn types is based on the schematics shown in Figures 9, 11, 13 and 15. By looking at these schematics, combined with some technical insight regarding the actual construction of the horn, the selected horn types were rated. This resulted in the conclusion that a conical shape is much more difficult to construct than a rectangular shape, therefore the the Rectangular horn received an 'Easy', while the Conical horn and the Pickett-Potter horn received a 'Medium'. The Potter horn received 'Hard', due to the presence of the phasing section.
On the basis of Table 1 it can be concluded that the Pickett and Pickett-Potter horn have the best performance regarding the main selection constraint, i.e. the sidelobe level. Hence, the Rectangular and Conical horn do not qualify. As seen from Table 1 the Pickett-Potter horn is easier to construct than the Potter horn. Therefore, we selected the Pickett-Potter horn as the most suited horn antenna type for our observation of the CMB.

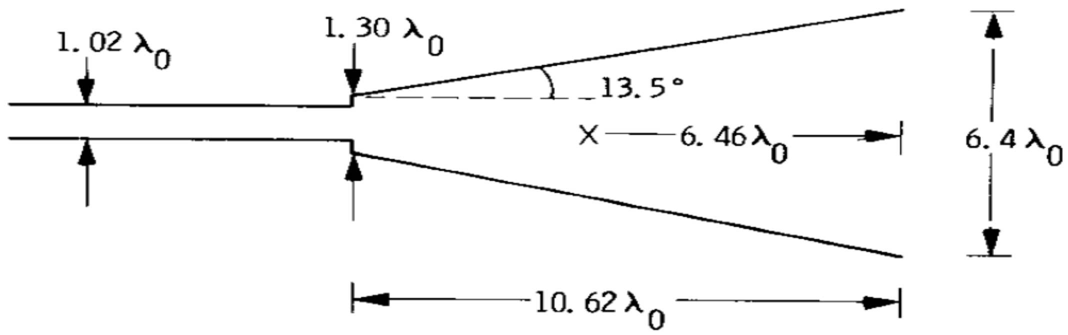

Figure 16: Design of a Pickett-Potter horn aperture [16].

[10] $= 10 \cdot \log_{10}(\frac{0.1}{300})$

5 Design parameters and optimization for the Pickett-Potter horn

As the basis for our design, we used the design made by Pickett, shown in Figure 16. However, before construction of the Pickett-Potter horn could begin, the antenna had to be optimized. The optimization was needed to fine-tune the design to obtain the optimal beam pattern, i.e. one with the preferred sidelobe level and HPBW. The optimization consisted of two parts; the flared Conical horn and the probe within the circular waveguide. Both simulations were done by using the program Computer Simulated Technology - Microwave Studio (CST MWS).

5.1 CST Microwave Studio

CST MWS enables three dimensional electromagnetic wave simulations for high frequencies [6]. It provides a fast and accurate analysis of high frequency devices, including horn antennas.
In the environment of CST MWS the user can design their object of interest, with the correct dimension, shapes, material and operating frequency. Waveguide ports can be used to excite an electromagnetic pulse, to calculate the existing modes, based on the geometry of the object. CST MWS does this by solving Maxwell's equations for each mesh-cell. Then, by calculating the scattering-matrix for each mesh-cell, the propagation of the different modes is simulated. These mode simulations are then used to calculate the far-field, i.e. beam pattern, of the simulated object.
CST MWS also has an optimization module, where different techniques and algorithms can be selected, each having their own specifics that are suited. In this way the user is able to select the most suited method for optimizing the design.
The above was done for two parts of the horn separately, the flared conical horn and the probe in the circular waveguide. These simulations were done separately to reduce the calculation time.

5.2 Flared Conical Horn optimization

The design parameters of the flared conical horn are the slant angle, the step-size, the radius of the waveguide and the axial length of the horn. To speed-up the optimization, the number of free parameters needed to be reduced from four to two. Hence the slant angle, which is the angle of the flared section, was set to 13.5° and the axial length of the horn was set to $10.62 \cdot \lambda_0 = 289$ mm. These parameter values correspond to the values set by Pickett, as discussed in his paper [9].
The remaining parameters were the step-size, i.e. the radius at the transition from the horn to the circular waveguide, and the radius of the circular waveguide.

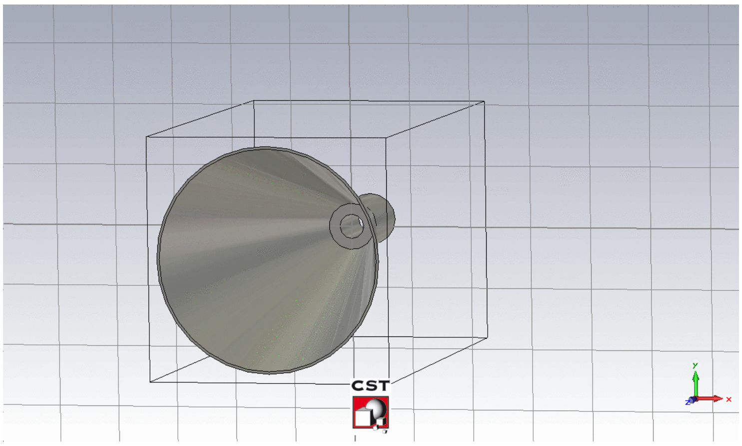

Figure 17: Slanted conical horn in CTS MW (tilted view).

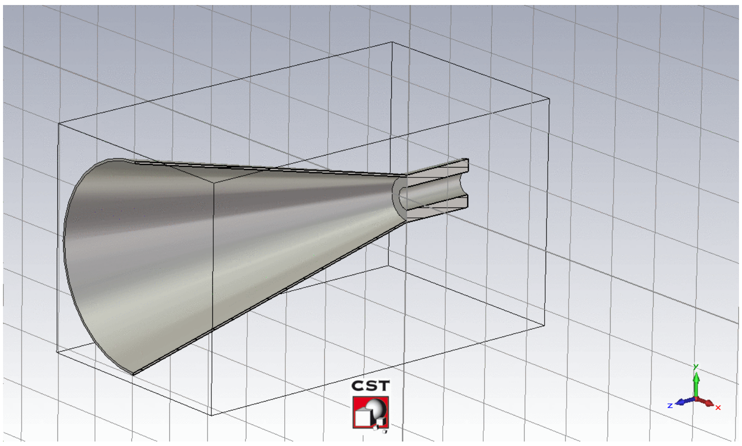

Figure 18: flared concical horn in CTS MW (cross cut x-axis).

To achieve the required sidelobe level, the TE_{11} and the TM_{11} mode needed to be balanced correctly. This is only attained for a specific set of step- and circular waveguide radii. In the literature the following constraints were found for the the step-radius and the radius of the circular waveguide [22]:

$$\begin{aligned} 1.84 < \mathrm{ka_w} < 3.83 \\ 3.83 < \mathrm{kA} < 5.33 \end{aligned} \tag{5.1}$$

Where a_w is the waveguide radius and A the radius of the step discontinuity. Using $k = 2\pi/\lambda_0$, with λ_0=27.27 mm, gives:

$$\begin{aligned} 7.987 \text{ mm} < \mathrm{a_w} < 16.624 \text{ mm} \\ 16.624 \text{ mm} < \mathrm{A} < 23.135 \text{ mm} \end{aligned} \tag{5.2}$$

Equation (5.2) gives the minimum and maximum values for both the radius of the circular waveguide and the radius of the step-size. An overview of the parameters and their values or range is given in Table 2. With these values the optimization for the beam pattern was started.

Parameter	Range or value
Observing frequency	11 GHz
Slant angle	13.5°
Length horn	298 mm
Wall thickness	2 mm
a_w	7.987 - 16.624 mm
A	16.624 - 23.135 mm

Table 2: Parameter values for the optimization of the Pickett-Potter Horn antenna design.

5.2.1 Method and measurement setup for the flared Conical Horn optimization

The values given in Table 2 were used to draw the horn antenna in CST MWS, see Figure 17 and Figure 18. Note that in these schematics there is no back-end in the waveguide, since this is a configuration in which CST MWS is able to calculate the beam pattern. For more details see Section 5.2.1.2. The horn, shown in Figures 17 and 18, consists of Perfectly Electric Conducting (PEC) material, i.e. there is zero resistivity. This will reduce the computation time, since non-zero resistivity properties, such as scattering, are not calculated. Despite the fact that our horn will consist of copper, the approximation of copper being a PEC is valid, since copper is a highly electrically conducting material.

As mentioned, the CST Microwave Studio has an optimization module, with a very broad application, ranging from optimizing S-parameters, the gain, the far-field pattern with a parameter sweep or optimization algorithms. The CST MWS Optimization module was used for our horn design, to check if the TE_{11} and TM_{11} flared horn modes would couple to the TE_{11} mode in the circular waveguide. To, eventually, find the horn antenna design which has the optimal beam pattern, both of these simulations were done for the central frequency of 11 GHz. The method for the optimization are described below.

5.2.1.1 From horn modes to waveguide modes?

After the horn antenna was drawn in CST MWS, two ports were added, one at both ends of the horn. Port 1, located at the aperture, would calculate the horn modes, while the Port 2, located at the end of the waveguide, would calculate the modes in the waveguide. Then CTS MW would use Port 1 as a source, to calculate how the modes at Port 1 would propagate trough the flared horn can couple to the waveguide modes, i.e. the modes calculated at Port 2. To store the result a field monitor was added to the horn antenna design.
In CST MWS it is not possible to select specific modes, e.g. TE_{11} or TM_{32}. Instead of this you're able to select the number of modes you want CST MWS to calculate at each port. From these calculated modes, a selection can be made, which then will be excited by MWS. For Port 1 eight modes needed to be selected to obtain the preferred TE_{11} and TM_{11} modes with the right polarization, i.e. along with the direction of the probe. At Port 2 only one mode was selected, since this was directly the dominant TE_{11} mode. The calculated modes, at each port, are shown in Figure 19. In Figure 5.2.2.1 the coupling of the flared horn modes to the waveguide modes is shown.
The results are shown in Section 5.2.2.1.

5.2.1.2 To optimize the beam pattern

Once the coupling of the TE_{11} and the TM_{11} horn modes to the TE_{11} circular waveguide mode was checked, the horn antenna design could be optimized to find the optimal beam pattern. There were two optimization goals, that was to obtain the lowest sidelobe level as possible while maintaining a HPBW smaller than 15°(full angle) [7]. This at the central frequency of 11 GHz, not for the entire bandwidth, to reduce the simulation time.

The basis horn antenna design, as shown in Figure 17 and Figure 18, was used. At the end of the waveguide a waveguide port, the same as in Section 5.2.1.1, was added[11]. This port, now Port 1, was used as the source and a far-field monitor was added to calculate the far-field for this horn antenna configuration. Thus, the TE_{11} mode in the circular waveguide would be excited and would start to propagate in the direction of the aperture. At the transition this TE_{11} waveguide mode would transist into a TE_{11} and TM_{11} horn mode (as checked in Section 5.2.1.1). The balance between these to flared horn modes would determine the far-field pattern of that specific horn antenna configuration.
Since there are no S-parameter in this simulation for which CST MWS can optimize for to obtain the optimal far-field pattern, a parameter sweep was used. CST MWS supports this type of optimization, in which the user can specify a certain parameter space. For each possible set of parameters, CST MWS would then calculate the beam pattern. In this case the parameter space was defined by the radius of the waveguide (a_w) and the radius step-size (A). Two parameter sweep cycles were used for finding the optimal a_w and A. The first would coarsely scan the selected parameter space, given by Table 2. The result of the first scan was used for the second scan. This second parameter sweep would scan the most promising part of the parameter space. For the results see Section 5.2.2.2.
Since the beam pattern of the horn is determined by the shape of the aperture and in our case the aperture of the horn is symmetric, it is valid to assume that the resulting beam pattern is also symmetric in three dimensions.

[11] There is no waveguide port at the aperture of the horn

5.2.2 Results for the flared Conical horn optimization

This section shows the result obtained from the simulations described in Section 5.2.1.1 and 5.2.1.2. In Section 5.2.2.1 the mode propagation and coupling discussed, while Section 5.2.2.2 describes the beam pattern optimization.

5.2.2.1 Results mode propagation

The modes present at the horn aperture and circular waveguide are shown in Figure 19. Figures 19a, 19b, 19c and 19d show the five distinct modes present, while Figure 19f shows the single circular waveguide mode. Here the polarizations for the TE_{11}, TE_{21} and TM_{11} are left out. Out of the horn modes, only the TE_{11} and TM_{11}, couple to the TE_{11} circular waveguide mode. Here we assume that, beside the TE_{11} and TM_{11}, no higher order modes couple to the TE_{11}. This assumption is valid since it is a requirement of the Pickett-Potter horn design.
Figure 20 shows the results of the check needed to assure that the dominant TE_{11} and TM_{11} horn modes would transfer into the TE_{11} mode in the circular waveguide. As seen from Figure 20 only the TE_{11} and TM_{11} horn modes propagate into the circular waveguide, i.e. transferring their energy to the TE_{11} circular waveguide mode.

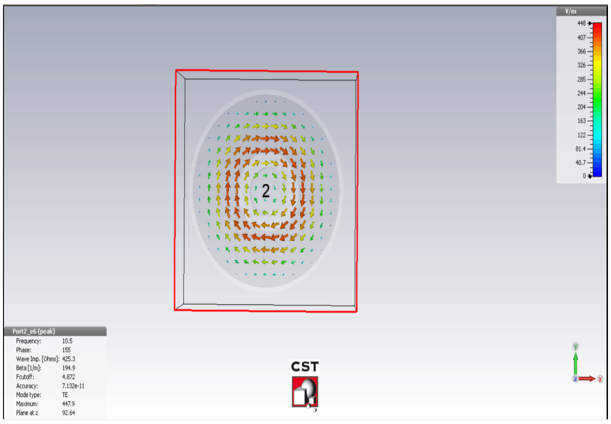

(a) TE01 horn mode.

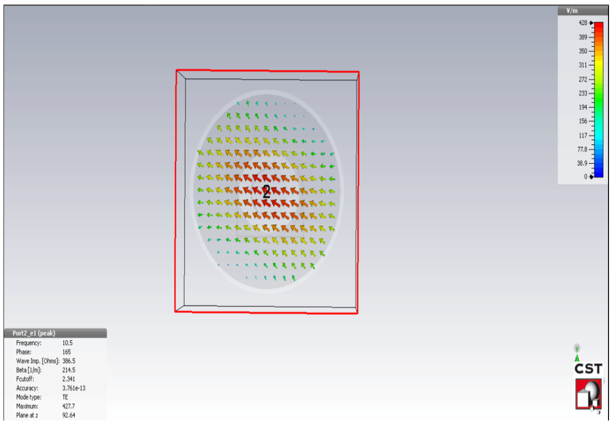

(b) TE11 horn mode.

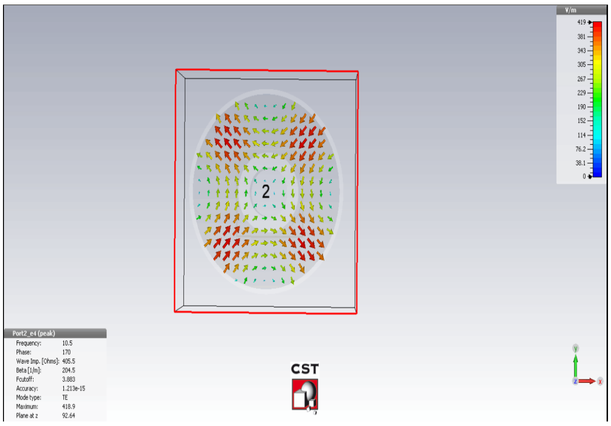

(c) TE21 horn mode.

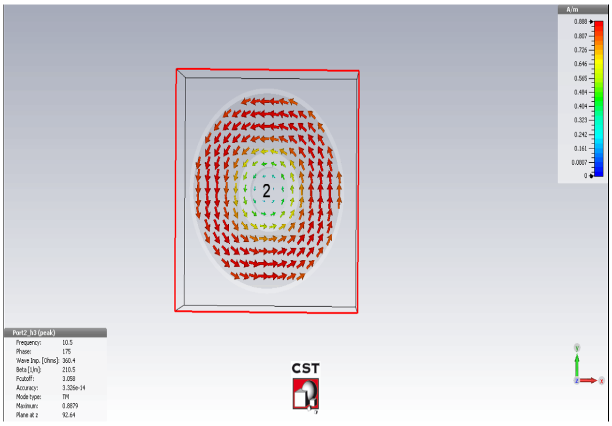

(d) TM01 horn mode.

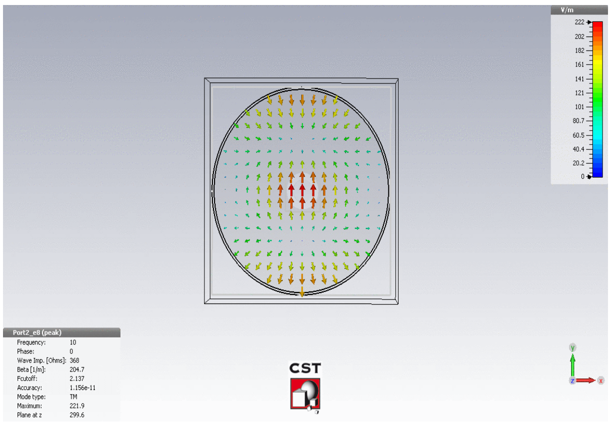

(e) TM11 horn mode.

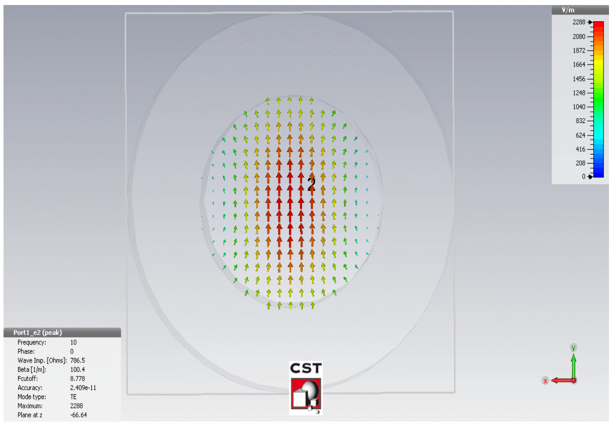

(f) TE11 waveguide mode.

Figure 19: Propagation of modes from the flared horn section to circular waveguide.

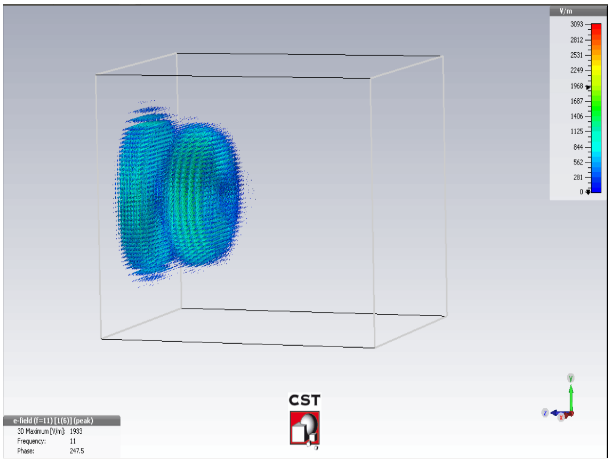

(a) TE01 mode.

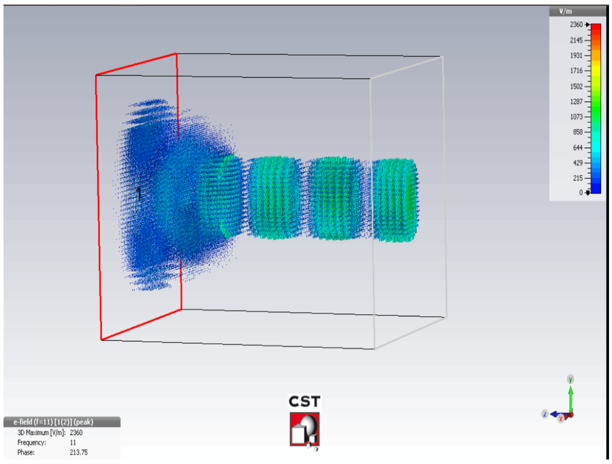

(b) TE11 mode.

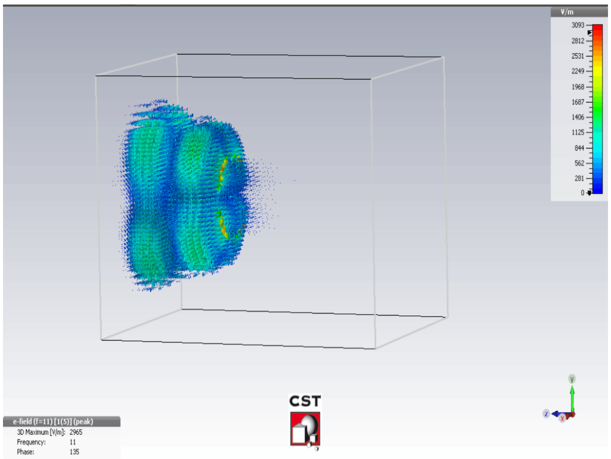

(c) TE21 mode.

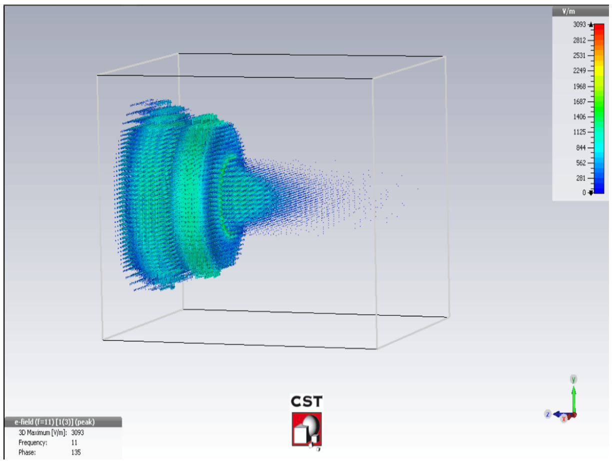

(d) TM01 mode.

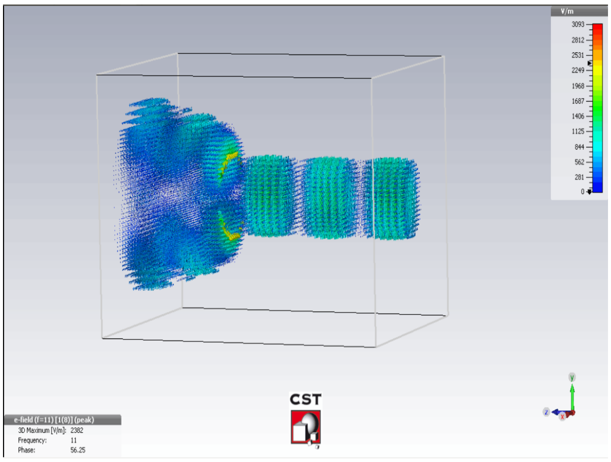

(e) TM11 mode.

Figure 20: Transition from the flared horn to the circular waveguide. As can be seen only the TE_{11} and TM_{11} couple to the TE_{11} waveguide mode.

5.2.2.2 Results for the beam pattern optimization

The results in Section 5.2.2.1 show that the principle of the Pickett-Potter horn, i.e. using a step to transfer the TE_{11} and TM_{11} horn modes into the TE_{11} circular waveguide mode works. With this verification, the design of the Pickett-Potter horn can be optimized.

As discussed in Section 5.2.1.2 the optimization of the horn design was done via a two cycle parameter sweep. In the first a coarse scan would be made to determine which part of the initial parameter space (given in Table 2) was the most promising. In this scan a parameter step size of 2 mm was chosen for the radius of the step (A) and a parameter step size of 1.5 mm for the radius of the waveguide (a_w). The results of the first parameter sweep are shown in Figure 21 and Table 3.

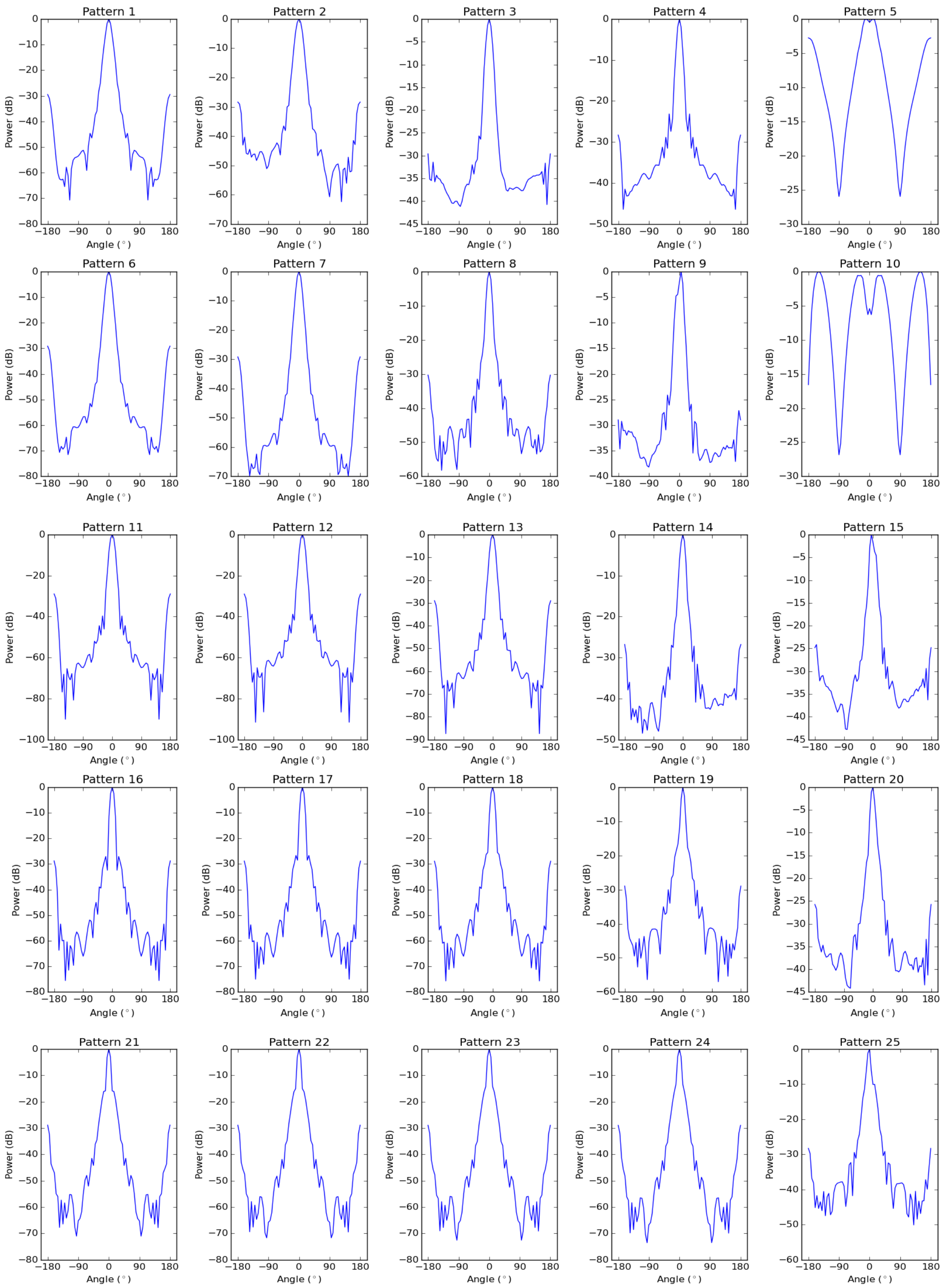

Figure 21: Beam patterns of first parameter sweep.

Beam Pattern	Radius step (A)(mm)	Radius waveguide (a_w)(mm)	HPBW(°)
01	17.00	8.00	12.84
02	17.00	10.00	15.68
03	17.00	12.00	13.78
04	17.00	14.00	11.75
05	17.00	16.00	11.75
06	18.50	8.00	12.58
07	18.50	10.00	12.39
08	18.50	12.00	11.08
09	18.50	14.00	3.77
10	18.50	16.00	3.77
11	20.00	8.00	11.80
12	20.00	10.00	11.73
13	20.00	12.00	11.65
14	20.00	14.00	12.69
15	20.00	16.00	20.28
16	21.50	8.00	10.59
17	21.50	10.00	10.59
18	21.50	12.00	10.63
19	21.50	14.00	8.60
20	21.50	16.00	13.69
21	23.00	8.00	9.57
22	23.00	10.00	9.74
23	23.00	12.00	9.95
24	23.00	14.00	10.06
25	23.00	16.00	13.36

Table 3: A, a_w and the Half Power Beam Width per Beam pattern for the first scan.

The data from this first sweep was analyzed with a Python script (11.2)). Obtaining the beam pattern for each configuration (Figure 21) and the HPBW per configuration is shown in Table 3.

From the beam patterns shown in Figure 21, it can be seen that the beam patterns in the range from 8 mm - 12 mm for a_w and from 16 mm - 19 mm for A show the most promising beam pattern. Since these beam patterns show the lowest sidelobe level and the HPBW is of the preferred size, i.e. smaller than 15°.
With the results of the first parameter sweep, a second was initiated. In this scan a parameter step size of 0.5 mm was selected for the radius of the step (A) that ranged from 16 mm - 19 mm. For the radius of the waveguide a parameter step size of 0.5 mm and a range of 8 mm - 12 mm was chosen. The output data for the second parameter sweep was analyzed using the Python script shown in Appendix III. The results of the second parameter sweep are shown in Figure 22 and Table 4.

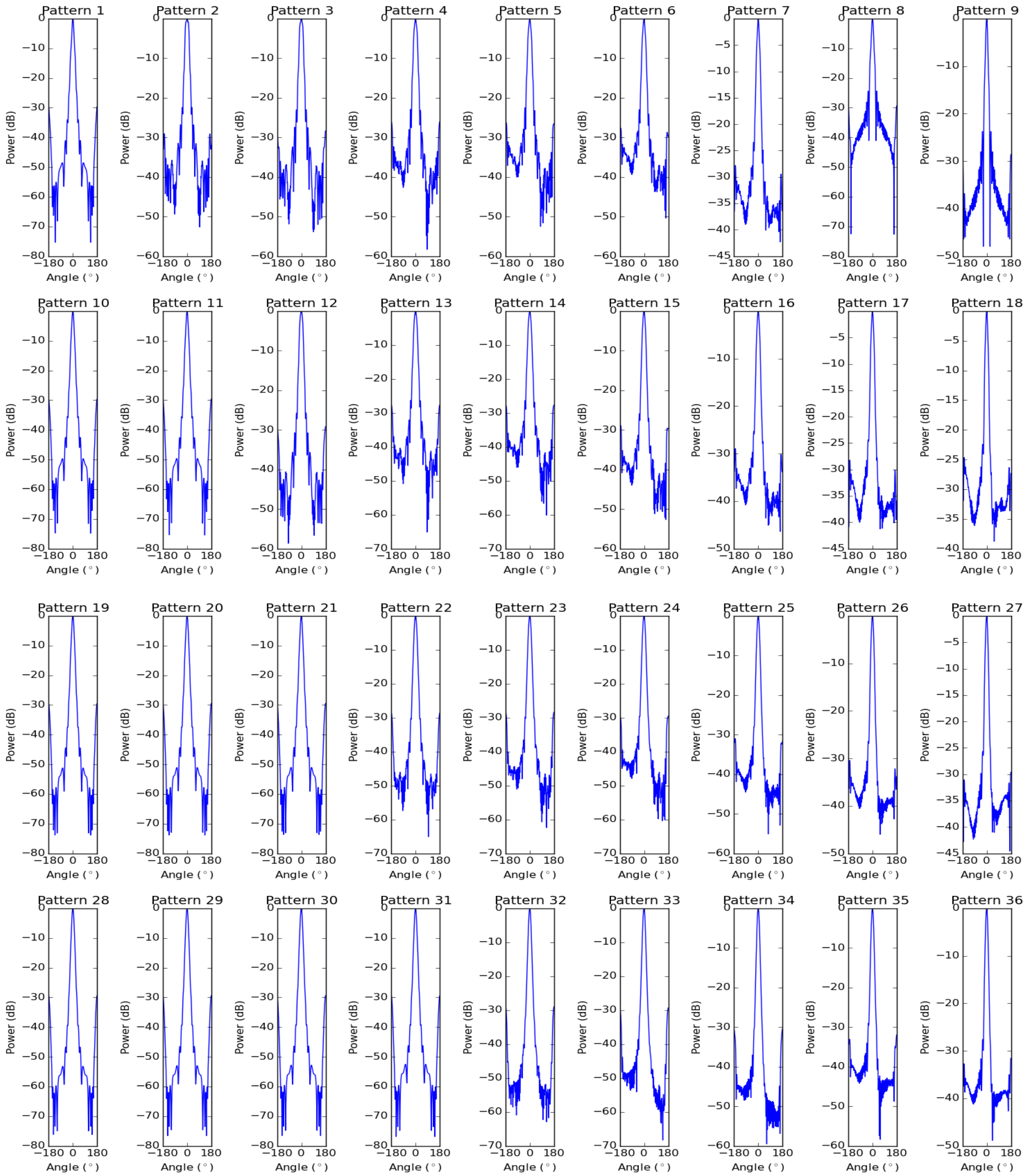
Pattern 1
Pattern 2
Pattern 3
Pattern 4
Pattern 5
Pattern 6
Pattern 7
Pattern 8
Pattern 9
Pattern 10
Pattern 11
Pattern 12
Pattern 13
Pattern 14
Pattern 15
Pattern 16
Pattern 17
Pattern 18
Pattern 19
Pattern 20
Pattern 21
Pattern 22
Pattern 23
Pattern 24
Pattern 25
Pattern 26
Pattern 27
Pattern 28
Pattern 29
Pattern 30
Pattern 31
Pattern 32
Pattern 33
Pattern 34
Pattern 35
Pattern 36
Power (dB)
Angle (°)

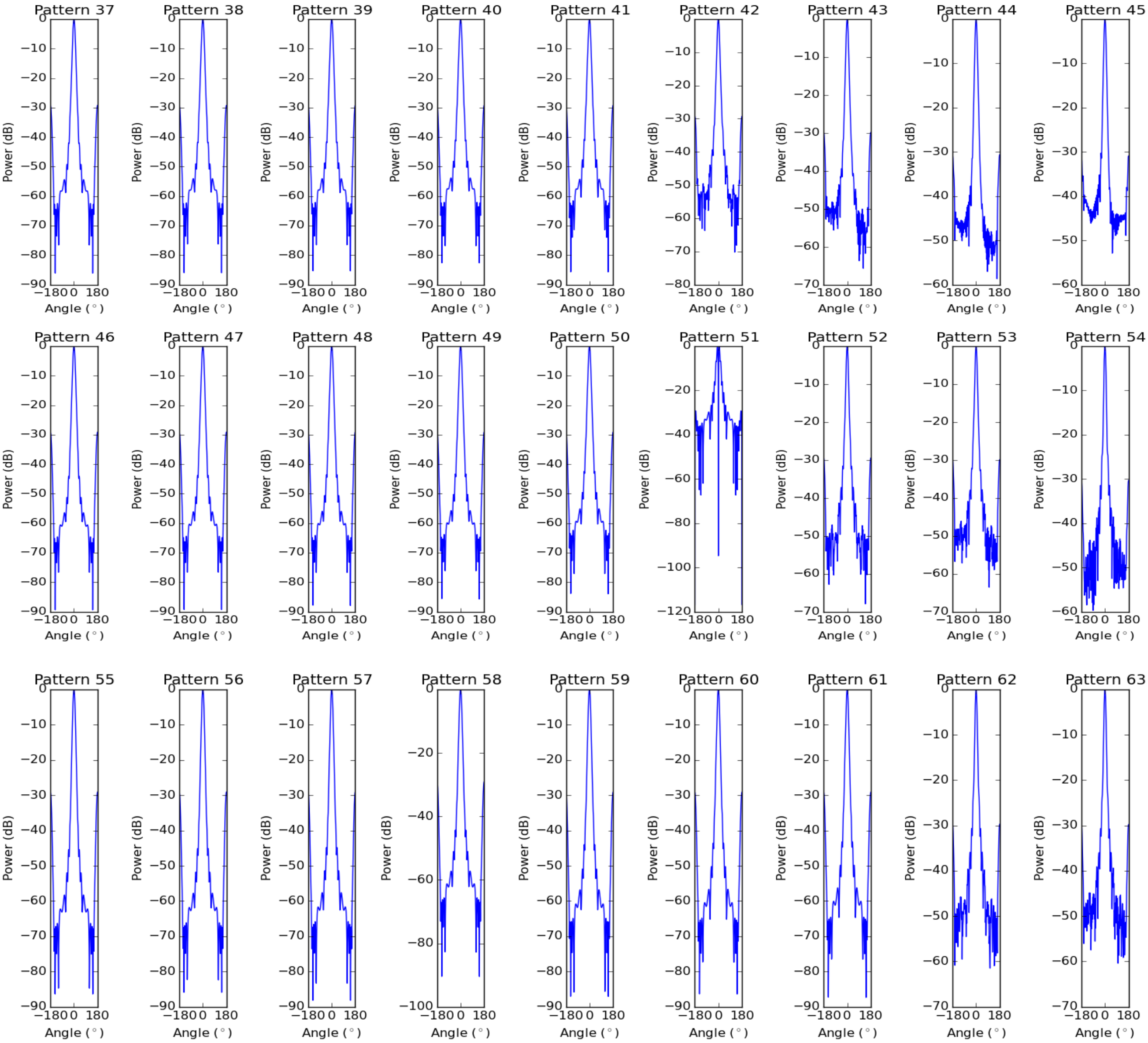

Figure 22: Beam patterns of second parameter sweep.

Pattern	A(mm)	a_w(mm)	HPBW(°)		Pattern	A(mm)	a_w(mm)	HPBW(°)		Pattern	A(mm)	a_w(mm)	HPBW(°)
01	16.00	8.00	12.08		22	17.00	9.50	16.54		43	18.00	11.00	12.97
02	16.00	8.50	27.25		23	17.00	10.00	16.38		44	18.00	11.50	12.88
03	16.00	9.00	25.91		24	17.00	10.50	15.93		45	18.00	12.00	12.83
04	16.00	9.50	22.06		25	17.00	11.00	15.60		46	18.50	8.00	13.26
05	16.00	10.00	22.06		26	17.00	11.50	15.11		47	18.50	8.50	13.22
06	16.00	10.50	16.19		27	17.00	12.00	14.35		48	18.50	9.00	13.15
07	16.00	11.00	14.24		28	17.50	8.00	13.50		49	18.50	9.50	13.11
08	16.00	11.50	12.34		29	17.50	8.50	13.42		50	18.50	10.00	13.02
09	16.00	12.00	12.40		30	17.50	9.00	13.33		51	18.50	10.50	21.56
10	16.50	8.00	12.40		31	17.50	9.50	13.19		52	18.50	11.00	12.09
11	16.50	8.50	12.81		32	17.50	10.00	14.24		53	18.50	11.50	12.06
12	16.50	9.00	21.93		33	17.50	10.50	14.23		54	18.50	12.00	11.50
13	16.50	9.50	20.03		34	17.50	11.00	14.16		55	19.00	8.00	13.03
14	16.50	10.00	18.34		35	17.50	11.50	14.07		56	19.00	8.50	12.99
15	16.50	10.50	17.53		36	17.50	12.00	13.83		57	19.00	9.00	12.94
16	16.50	11.00	16.55		37	18.00	8.00	13.44		58	19.00	9.50	12.89
17	16.50	11.50	15.46		38	18.00	8.50	13.38		59	19.00	10.00	12.92
18	16.50	12.00	14.41		39	18.00	9.00	13.31		60	19.00	10.50	12.86
19	17.00	8.00	13.36		40	18.00	9.50	13.12		61	19.00	11.00	12.81
20	17.00	8.50	13.24		41	18.00	10.00	13.04		62	19.00	11.50	11.48
21	17.00	9.00	13.11		42	18.00	10.50	12.97		63	19.00	12.00	11.36

Table 4: A, a_w and the Half Power Beam Width per Beam pattern second scan.

Figure 22 shows that for a larger step-radius (A) the beam pattern becomes more smooth. This indicates that the larger the radius the less prone the horn design is for sidelobes. Table 4 shows us that at increasing waveguide radius (a_w) the HPBW decreases.
With the results from Figure 22 and Table 4, Pattern 57 was selected as the final preferred beam pattern. Pattern 57 has a step radius of 19 mm and a waveguide radius of 10 mm. This beam pattern was selected because the sidelobes were of the order of -45 dB and the HPBW was 12.92°, satisfying both of our design constraints the best as possible. A detailed analysis of the beam pattern is shown in Figure 23.

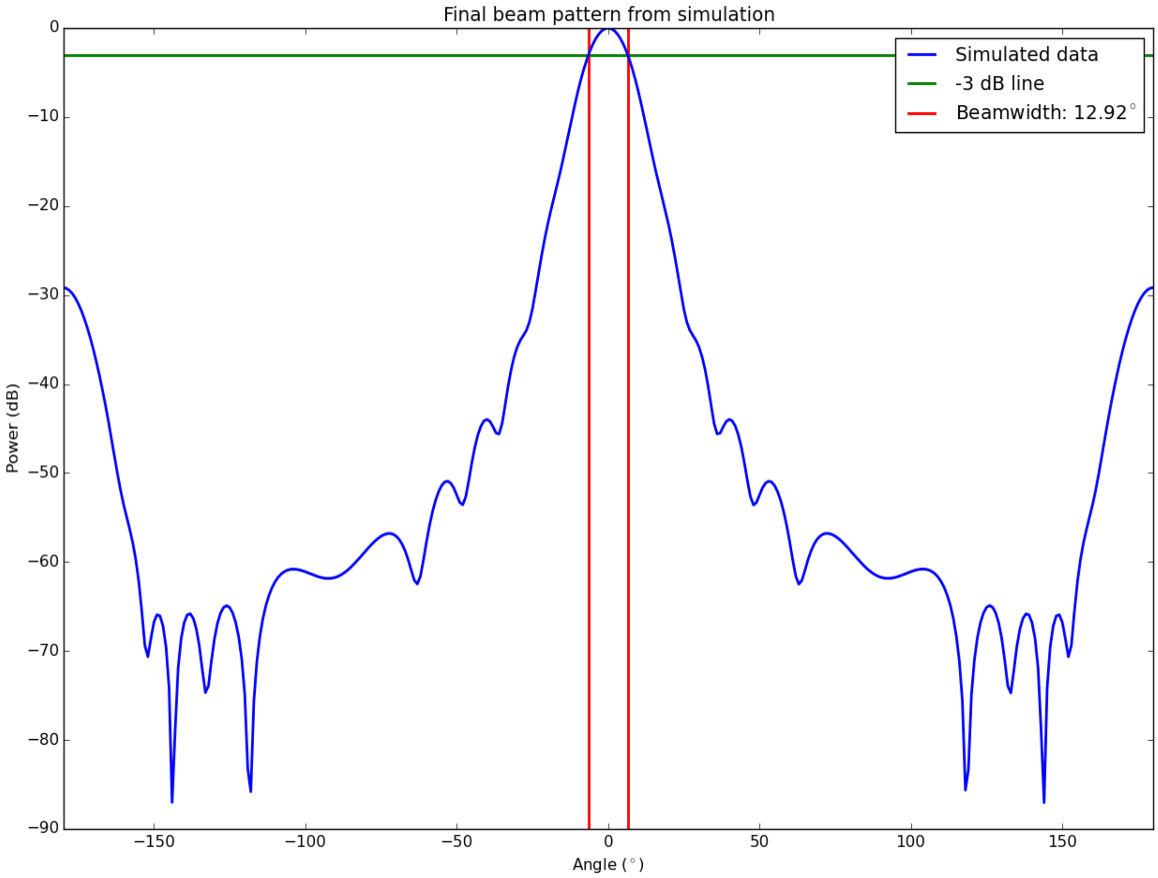

Figure 23: The beam pattern that was chosen from the results obtained in the second parameter sweep. Here A = 19 mm and a_w= 10 mm.

5.3 Probe parameter optimization

After the optimization of the beam pattern the position and length of the probe needed to be optimizated. This is to ensure that the energy transfer from the TE_{11} circular waveguide mode into the probe (S_{21}) is maximal and the reflection (S_{11}) is as low as possible. The parameter for which the optimization was done, was the transmission, i.e. the matrix element S_{21} (see Section 2.2.3). The initial guess for the length of the probe is $\lambda_0/4$ and the position of the probe is $\lambda_0/4$ with respect to the back-end of the circular waveguide [1]. Hence both parameters are set to 6.8175 mm.

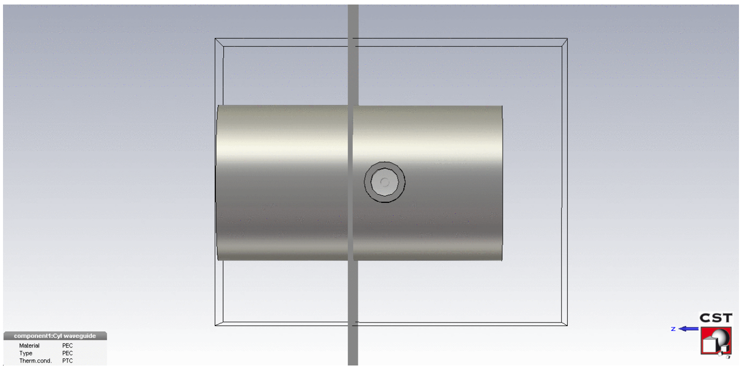

Figure 24: Circular waveguide and probe in CTS MW (front view).

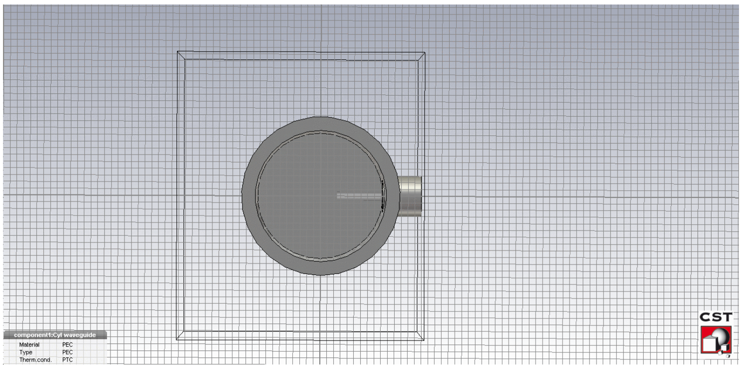

Figure 25: Circular waveguide and probe in CTS MW (side view).

With these starting conditions the circular waveguide and the probe were drawn in CST MWS, see Figure 24 and 25. As with the horn, the waveguide would need to consist of a Perfectly Electric Conducting (PEC) material, this would reduce the computation time.
The dimensions for this design are shown in Table 5. All of these dimensions were known from previous optimizations (such as a_w) or are standard values (such as the design parameters for the probe), except for the length of the waveguide. The minimal requirement for this parameter is that the waveguide has to support at least one guide-wavelength (λ_g), which is the wavelength of the observing frequency within the circular waveguide. If this requirement is not met and the length of the waveguide is smaller than λ_g, the dominant modes will not be able to propagate into the circular waveguide [19][12]. λ_g is given by:

$$\lambda_g = \frac{\lambda_0}{\sqrt{1-(\omega_c/\omega)^2}}. \tag{5.3}$$

Here ω is the observed angular frequency in radians and ω_c is the cutoff frequency. The latter is given by [19][13]:

$$\omega_c = \frac{m c_m \pi}{a_w} \Rightarrow \omega_c = \frac{c_m \pi}{a_w}, \tag{5.4}$$

with m the order of the mode, which for the dominant mode threaded here is equal to one, and c_m is the speed of light in that medium.
The dimensions of the probe, e.g. the diameter of the copper and the diameter of the Teflon, were chosen to be standard values given by [2]. These values are also shown in Table 5.

Since we are observing a bandwidth, instead of a single frequency, the optimization of the probe needed to be done for the entire bandwidth. Thus, the frequency range from 10.5 to 11.5 GHz needed to be taken into account.

Parameter	**Value(mm)**
Observed frequency range	10.5 - 11.5 GHz
Main observing frequency	11 GHz
λ_g	33.3
a_w	10
Length waveguide	19
Wall thickness horn	2
Position probe	26.482
Length probe	6.818
Diameter teflon	4.2
Diameter copper probe	1.2
Diameter mantle probe	5

Table 5: Dimensions of the probe optimization.

[12] See page 399 equation (20)
[13] See page 398 equation (14)

5.3.1 Method for the probe optimization

In the optimization for the beam pattern an effective but time intensive parameter sweep was needed, since there was no S-parameter (see Section 2.2.3) for which CST MWS could optimize.
The optimization of the position and length of the probe within the circular waveguide, enabled an optimization of the S-parameters. Since the transition of the TE_{11} waveguide mode into the probe can be expressed in a transition from one medium to another medium using S-parameters, here the optimization criteria was to optimize the transmission of the mode, i.e. the S_{21}. This was done only for the dominant TE_{11} circular waveguide mode.

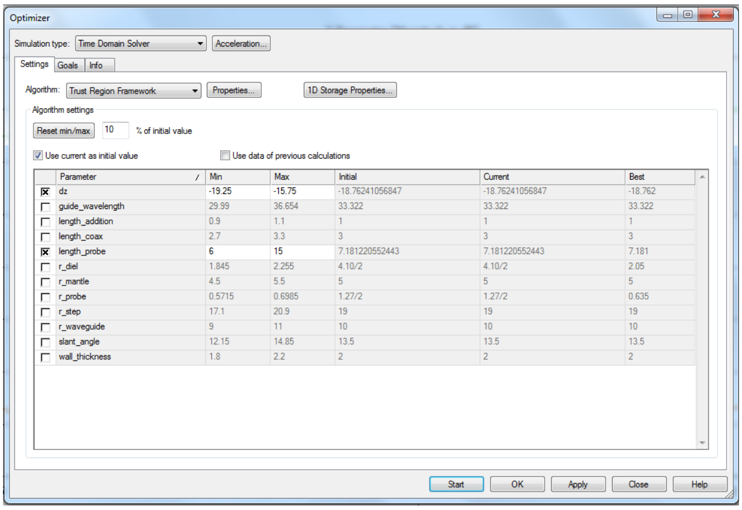

Figure 26: General CST MWS optimization window.

In the simulation of the circular waveguide with the probe design, as seen in Figure 24 and 25, was used. At both the beginning of the circular waveguide as at the end of the probe a waveguide port was positioned. The waveguide port at the beginning of the waveguide was named Port 2 and the port at the end of the probe was named Port 1. Port 2 was used as the source.

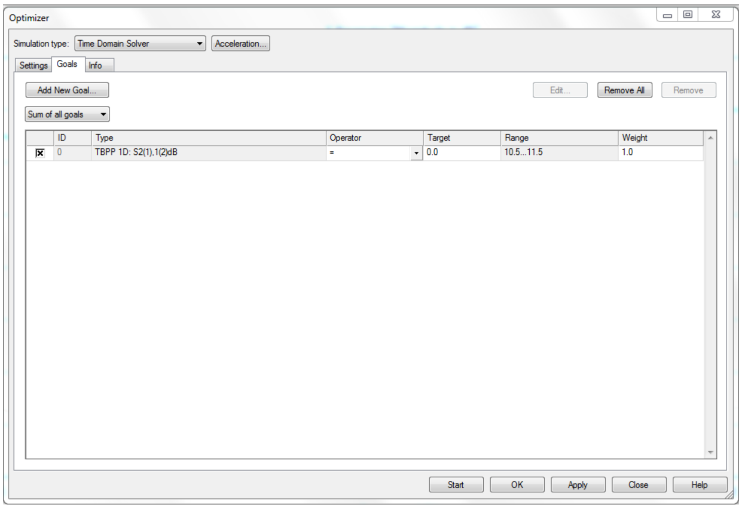

Figure 27: General CST MWS optimization window, the goals tab.

The number of modes that were excited at Port 2 was eight, while the number of modes excited at Port 1 was one. The selected number for Port 2 might seem weird, since only the dominant TE_{11} circular waveguide mode was needed for this optimization. The reason for this is due a bug in CST MWS, since with one mode at both Port 1 and Port 2, the TE_{11} waveguide mode would not propagate into the waveguide. With eight modes calculated at Port 2, the TE_{11} waveguide mode would propagate and couple to the probe.

The next step would be to select an optimization algorithm. CST MWS has different local and global S-parameter optimization algorithms, each with their advantages and disadvantages. The algorithm selected here was the 'Trust Region Framework', which is one of CST MWS local optimizers. The Trust Region Framework builds a linear model on the primary data in a "trust" region around the initial point. The modeled solution will be used until the algorithm converges. The main advantage of the Trust Region Framework is that it takes advantage of the S-parameter sensitivity information to reduce the number of cycles needed and to speed-up the optimization process. From the CST MWS optimization module the Trust Region Framework is the most robust optimization algorithms [6].
The optimizer window overview is shown in Figure 26. Under 'Setting' the window shows the optimizer choice, the parameter space definition and the precision, and under 'Goals', see Figure 27 for the objectives that can be set. Here the Trust Region Framework-algorithm was selected and the parameter space ranged from 3 - 15 mm for the length of the probe and from 30 - 10 mm for the position with respect to the back of the waveguide. As goal the maximization of $S_{21} = 0$ in dB's for the entire bandwidth, was set. The results of this optimization are shown in Section 5.3.2

5.3.2 Results probe optimization

The result of the CST MWS optimization discussed in Section 5.3 resulted in a probe length of 7.2 mm and a position of the probe, with respect to the back-end of the circular waveguide, of 15.1 mm. The S_{21} parameter is plotted in Figure 28a , were a zoomed plot for the observed bandwidth is shown in Figure 28b .
The brown line in Figure 28a and 28b is the S-parameter, which describes the magnitude of the transmision of Port 2 to Port 1, for mode 2 (the TE_{11} circular waveguide mode with the correct polarization) to mode 1 (the dominant probe mode). The pink line in these same Figures shows the S-parameter and describes the magnitude of the transmision of Port 2 to Port 1, for mode 8 (the TM_{11} circular waveguide mode with the correct polarization) to mode 1 (the dominant probe mode). The former is the one for which was optimized and is therefore of most interest.

Besides the S_{21}, also the S_{11}, i.e. the reflection, as function of frequency can be calculated using CST MWS. This is shown in Figure 29.

For our observation of the CMB we need a precision of 0.1 Kelvin. Hence, the deviation of the S_{21} parameter on the entire bandwidth from the ideal value (i.e. 1) had to be smaller than 0.1. As can be seen from Figure 28b, the averaged value of the S_{21} parameter in the observed bandwidth is approximately - 0.15 dB. Which corresponds to a value of 0.966 K on a linear scale. Therefore the deviation on a linear scale is: 1.0 - 0.966 = 0.034 K, i.e. smaller than the required 0.1 K. The deviation of $3.4 \cdot 10^{-2}$ K was thought to be acceptable for our measurement, hence no further optimization of the probe was needed.

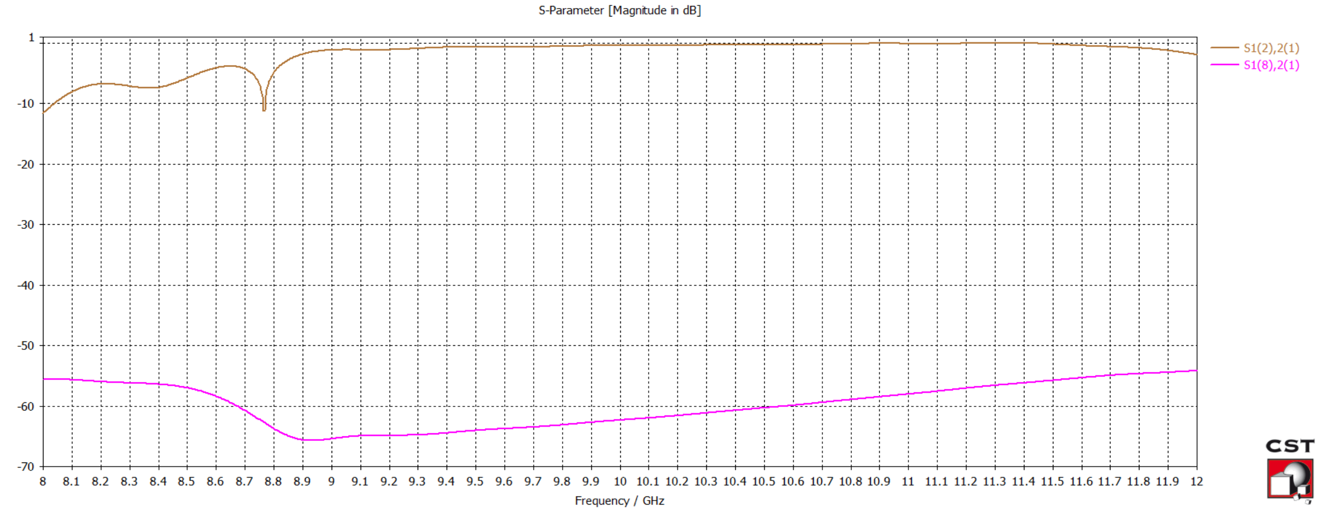

(a) S_{21} as function of frequency.

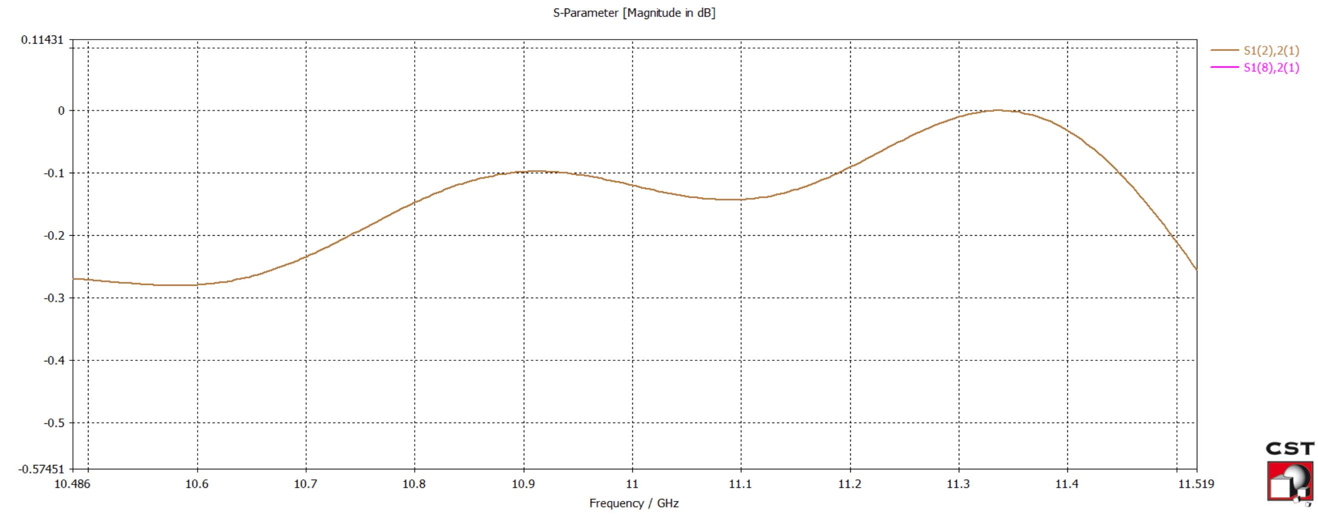

(b) S_{21} as function of frequency, zoomed-in at 10.5-11.5 GHz.

Figure 28: Results for S_{21} simulation.

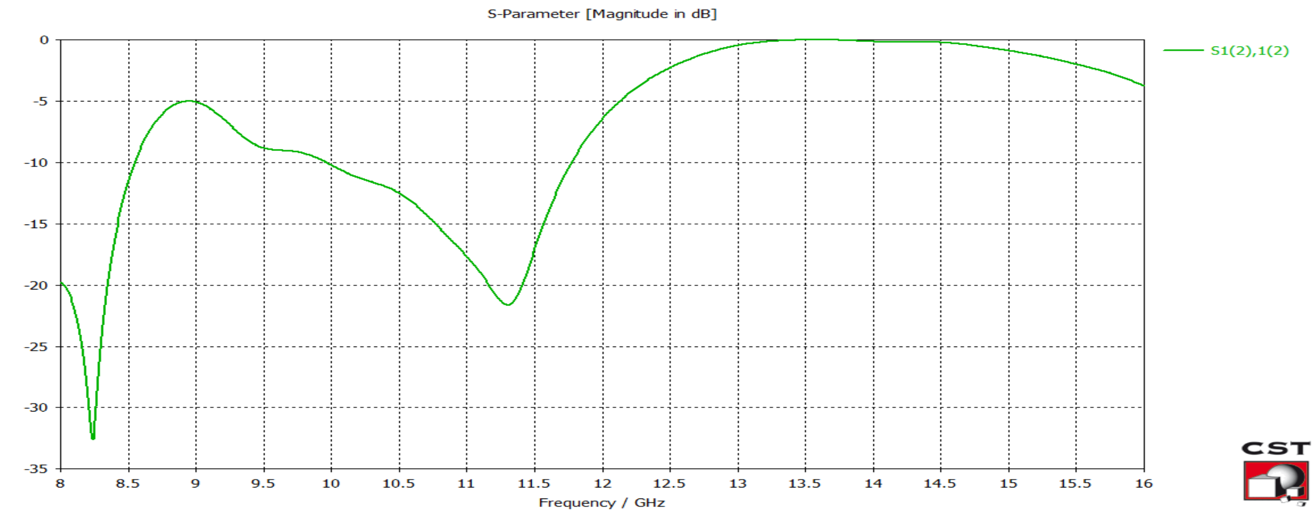

(a) S_{11} as function of frequency at 8-16 GHz.

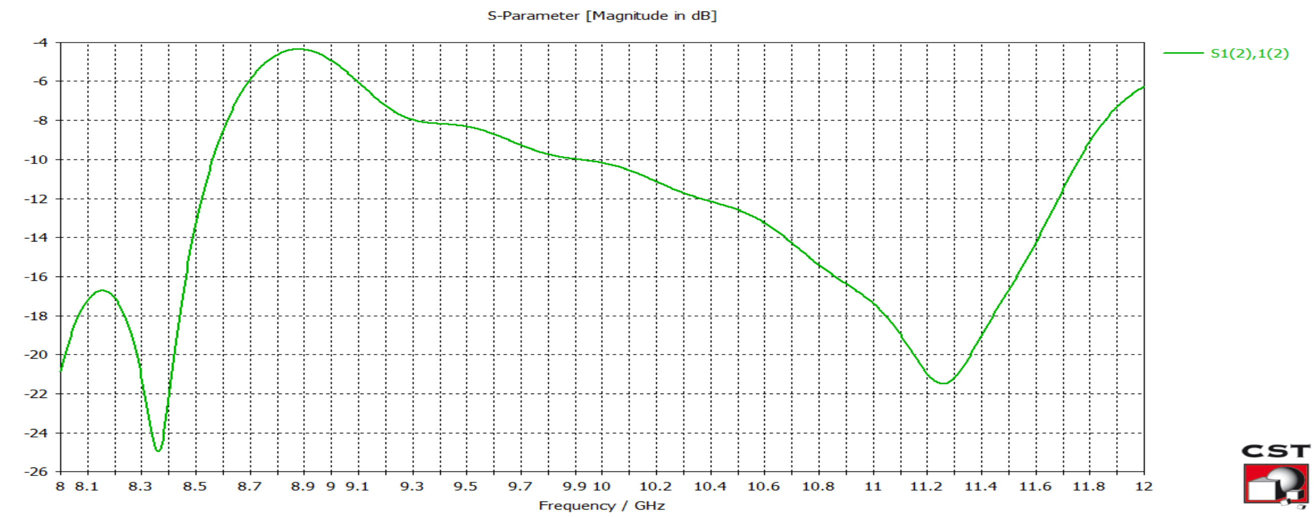

(b) S_{11} as function of frequency, zoomed-in at 10-12 GHz.

Figure 29: Results for S_{11} simulation.

5.4 Final result flared Conical horn and probe optimization

Combining the result of the flared Conical horn optimization (Section 5.2.2.2) and the probe optimization (Section 5.3.2), the design parameters of the Pickett-Potter horn were set. The values for the design parameters are summarized in Table 6. These values were used to draw a blue print of the Pickett-Potter horn, which is shown in Figure 30 . Now it was time to build the horn!

Parameter	**Value**
Slant angle	13.5°
Length horn	289.64 mm
a_w	10 mm
A	19 mm
λ_g	33.3
Length waveguide	19
Wall thickness horn	2
Position Probe	15.1 mm
Length probe	7.18
Diameter teflon	4.2
Diameter copper probe	1.2
Diameter mantle probe	5

Table 6: Final parameter values Pickett-Potter Horn design.

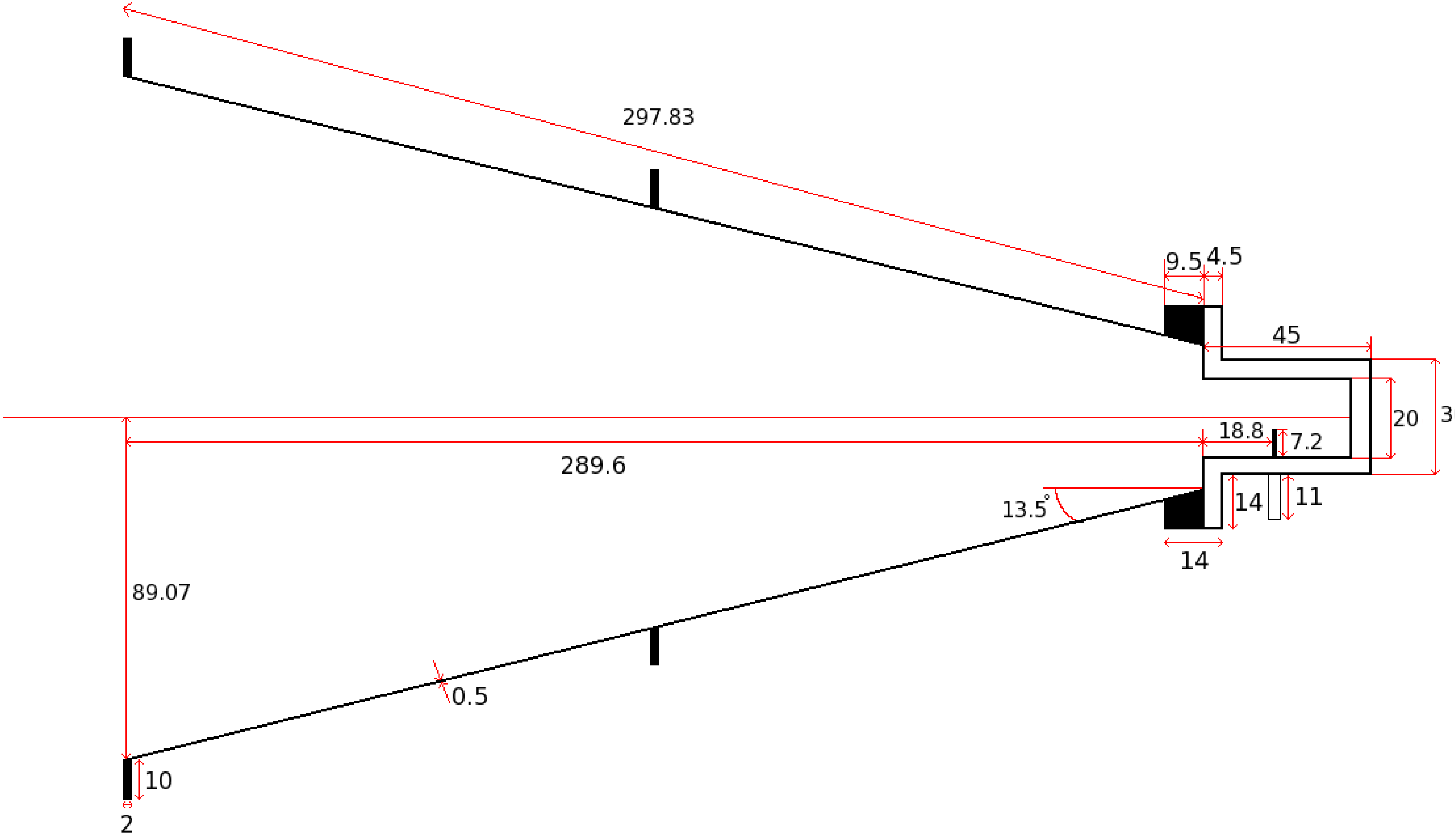

Figure 30: Blue print of horn antenna. Credits: Maik Zandvliet. [12]

6 Construction of the Pickett-Potter Horn

With the design parameters and the blue print at hand, the construction of our Pickett-Potter horn could begin. This consisted of two main sub-constructions; the construction of the flared conical horn and the circular waveguide. A general description on both these sub-constructions is discussed below. The different steps for the construction of the flared Conical horn are shown in Figure 31, with the steps for the construction of the circular waveguide shown in Figure 32. Since the descriptions of the sub-constructions is given on the main issues and methods, Table 7 and 8 will provide more details on the materials and equipment that were used during the construction of this Pickett-Potter horn.

6.1 Constructing the flared Conical horn

The flared Conical horn consisted out of four major sections; a conical shaped horn, a support ring with a 178 mm inner and 188 mm outer diameter, a support ring with a 108 mm inner and 118 outer diameter and a flench. All these sections consist of copper, since the horn needed to be a good conductor of electricity.
The conical shaped horn was bent out of a sheet of copper. The sheet of copper, seen in Figure 31a, was cut out of a rectangular sheet of copper with a thickness of 2 mm. This was done by R. Hesper and myself. This copper sheet was bent in a conical shape by using a roller and some improvisation. Next, the two support rings of copper were cut out of a copper sheet of 5 mm thick. This was done by Rob van der Schuur, who works at the workshop of SRON.

To get an impression of the size and shape of the horn, see Figure 31b. Here the two sides of the horn are bent towards each other, while being situated on an aluminum block, to keep the aperture in the correct shape. Then, the two ends of the sheet were duck-taped, to keep the horn in place while putting the rings at the correct position around the horn.

With the rings in the correct position, the ring at the aperture of the horn needed to be soldered to the conical shaped horn. To achieve the soldering temperature the entire setup, as shown in Figure 31b, was put on a heating plate. By preheating the setup, the soldering temperature would be obtained faster than with only heating locally. Then the soldering flux was applied, to clean up the copper such that it can be soldered. At first the flux was in a semi-liquid state, like a syrup, but as it got warmer it started to become more like a liquid, allowing it to flow between the conical shaped sheet and the support ring. Next, the horn and the support ring were heated up locally with two heat guns, one of which is shown in Figure 31c. While I and Ronald were heating the horn locally, Rob soldered the first support ring to the conical shaped copper sheet.

Then Ronald made a flench out of a 60 mm (in diameter) copper cylinder, using a lathe. This required some creativity, since the inner radius of the flench needed to decrease with the slope of the conical horn. Then six holes were tapped, which could enable us to bolt the circular waveguide and flared conical horn to each other.
With the flench ready it needed to be soldered to the conical horn. To achieve this the same setup was used as for the soldering of the support ring at the aperture of the horn. The horn would be fitted into the flench, after which it was put on the heating plate. Here the flench was directly seated on the heating plate, with the rest of the horn resting on top of it. As with the first support ring, the preheating would ensure that the soldering temperature was reached sooner than with local heating only. With the preheating finished, the soldering flux was applied to assure that the solder would stick to the copper. Then the heating guns were used to locally heat the copper to the soldering temperature. The result of this step is shown in Figure 31d and 31e.
For the soldering of both the support horn at the aperture and the flench solder, a high temperature, i.e. $t_{\mathrm{melt}} = 217°\mathrm{C}$ (see Table 7), was used. The force pushing the sheet out of its conical shape was the greatest at these solder points. This also being the reason why these two points were soldered before the second support ring.

The next step was to solder the second support ring (solder Sn 62) to the conical horn and to solder the two ends of the conical copper sheet together (solder Sn95.5). The former is shown in Figure 31d and Figure 31e, while the latter is shown in Figure 31f. With the same approach as used before, i.e. with the use of the soldering flux, heating plate and the heating guns, the second support ring and the two ends of the conical copper sheet were soldered. Figure 31d shows the soldering setup and Figure 31g shows the final constructed flared Conical horn.

Materials	**Specifics**
Copper sheet for the horn	600 x 400 mm of 2mm thick
Copper cylinder	40 mm long and 60 mm in Diameter
Copper sheet for the support rings	600 x 400 mm of 5 mm thichk
Solder	1. 60-40 (regular solder, $T_{melt} = 180°C$. 2. Sn 62 (regular solder,$T_{melt} = 179°C$). 3. Resist-2 Silver solder 2mm ($T_{melt} = 221°C$).
Solder flux	Skandia soldering flux S-39
Equipment	**Specifics**
Heating plate	Labotech DHP 20
Heating gun	Metabo HE 2300 Control

Table 7: Materials and equipment that were needed for the construction of the flared conical section.

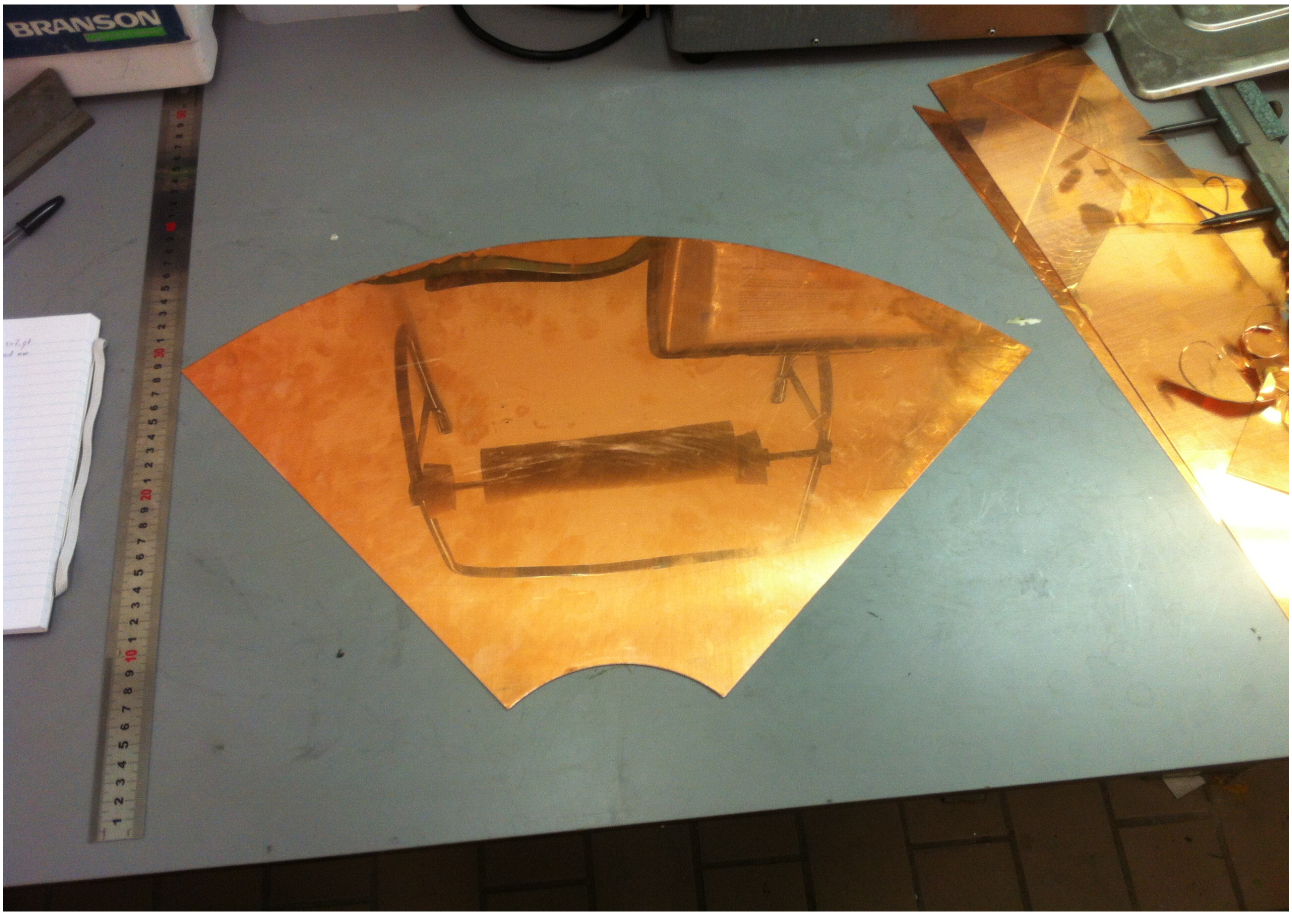

(a) Cutted copper sheet.

(b) Putting together the conical copper sheet and support rings.

(c) One of the two heating guns that was used.

(d) The Conical shaped sheet, with the first support ring and flench attached.

(e) The Conical shaped sheet, with the first support ring and flench attached, zoomed-in at the top.

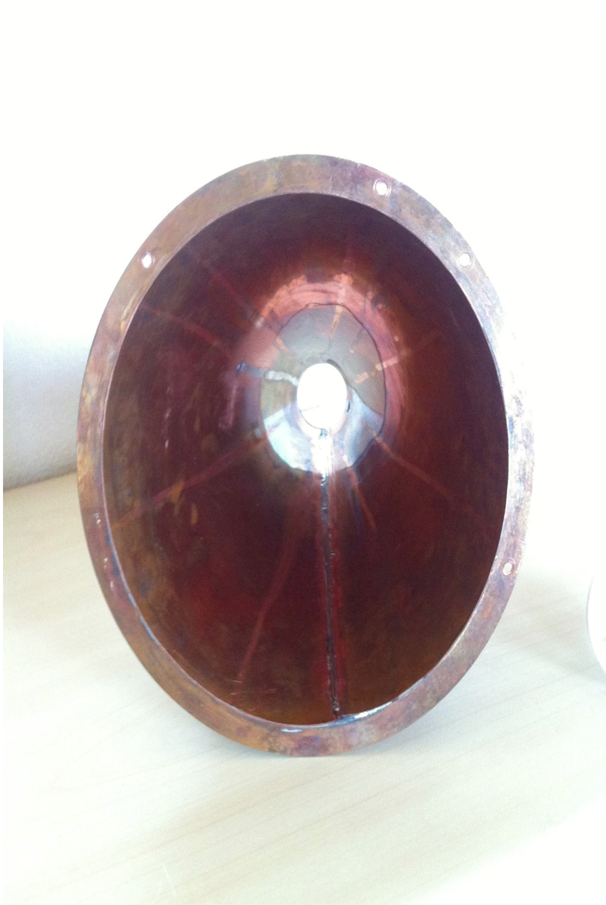

(f) The constructed flared Conical horn showing the gap caused by the two side of the conical copper sheet.

(g) The constructed flared conical horn, were the Aquarius bottle is put to get an impression of scale.

Figure 31: The construction of the flared Conical horn.

6.2 Constructing the circular waveguide and the probe

The circular waveguide was cut out of an aluminum cylinder with the dimension shown in Figure 30 and a more detailed description in Figure 32a. All of the work was done on the lathe of Ronald Hesper. Since I had no experience in using a lathe, Ronald was doing the main part of the job, while I was assisting him were I could.
The aluminum cylinder, having a diameter of 60 mm to match the diameter of the flench, with which we started is shown in Figure 32b. At the workshop of SRON, the cylinder was cut to a piece of 50 mm long. Then the first step would be to cut the cylinder in the correct dimensions, i.e. a diameter of 60 mm at the front of the waveguide that would drop to 30 mm after 5 mm. This was done by spanning the cylinder in Ronald's lathe and cutting off the aluminum at the end of the 'future' waveguide, see Figure 32c. Since the dimensions were quite crucial, the cutting needed to be done very precisely and a regular check of the diameter was needed (Figure 32d).
After cutting away the bulk of the material, a plateau for the probe was made by milling off 1 mm of the waveguide, as shown in Figure 32f.
Then the inner part of the waveguide needed to be made. First a hole, of 33 mm deep, with a regular metal drill was drilled into the front end of the circular waveguide. Having drilled a hole, a cutter was used to obtain the right dimensions for the waveguide, i.e. 19 mm diameter and 33.3 mm deep (Figure 32g).
Next, was to drill the holes for the probe. In total there were three holes drilled; one for the probe and two for bolts attaching the probe to the waveguide. The first was at 18.8 mm with respect to the beginning of the waveguide, with the other two 6.25 mm away from the hole for the probe. This can be seen in Figure 32g.
To assure that we could attach the circular waveguide to the flared conical horn with bolts, six holes were drilled that matched the holes in the flench. These holes were cut in such a way that the alignment of the probe would correspond to the gap (Figure 31f) caused by the two ends of the conical copper sheet. This alignment was selected, since the probe would be less prone to detect features caused by the imperfections at this gap.
The resulting circular waveguide is shown in Figure 32e.

Now that the circular waveguide was complete, the probe needed to have the correct dimensions. Therefore the Teflon and the copper wire needed to be cut, the result is shown in Figures 32f and 32g. In this Figure the probe is the copper object on the lower left. The white material is the Teflon and the copper that sticks out transfers the incoming radiation into the probe. This signal will go into the back-end of the measurements system for further processing [12].

Materials	**Specifics**
Aluminum cylinder	60 mm diameter and 50 mm long
Probe	See the specifcs given by[2]
Bolts	6 M3's
Rings	6 M3 rings
Equipment	**Specifics**
Lathe including the milling stage	Meco Maximat V10

Table 8: Materials and equipment that were needed for the construction of the circular waveguide.

6.3 Final result

Having completed the construction of the flared conical horn and the circular waveguide with the probe (see Figure 33b), the Pickett-Potter horn was assembled, as shown in Figure 33a and 33d.
The dimension of the circular waveguide and the probe were quite controllable and hence the parameters given in Table 6 correspond to the true parameter values. The dimension for the flared Conical horn were more difficult to control, due to the bending of the copper, hence the true parameter values differ, by a few tenth of a millimeter, from those obtained from the simulation (see Table 6). However, these imperfections can be neglected since they are smaller than the observed wavelength.

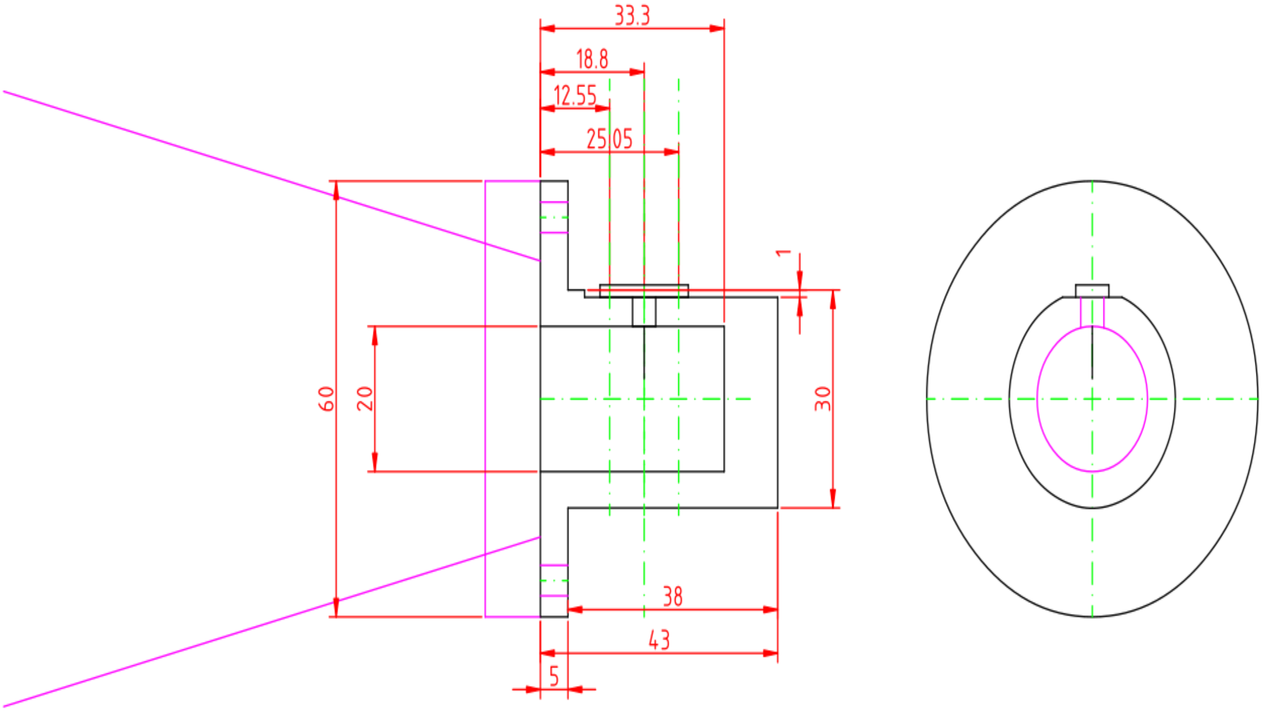

(a) Blue print circular waveguide, detailed. Credits: Ronald Hesper.

(b) The initial aluminum cylinder.

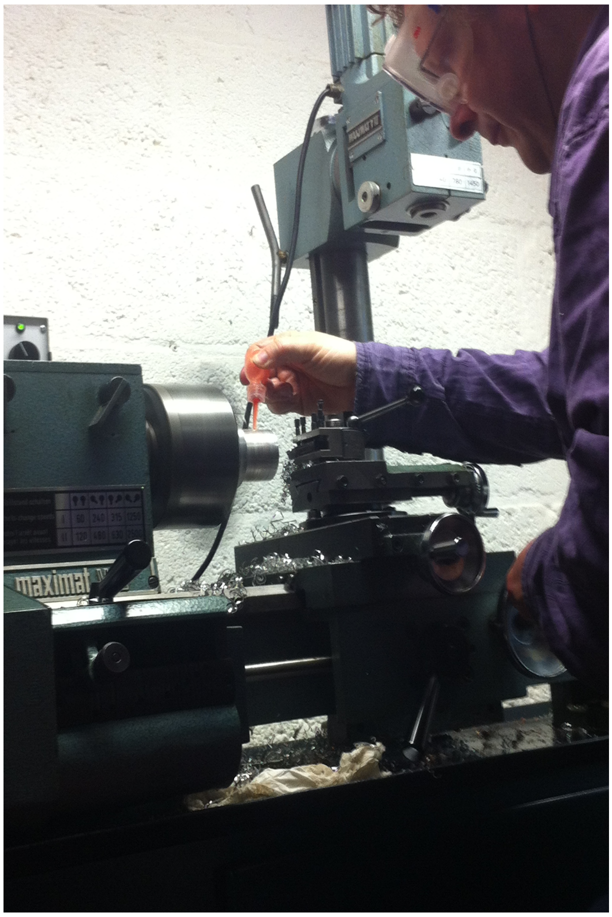

(c) Cutting of aluminum with the lathe.

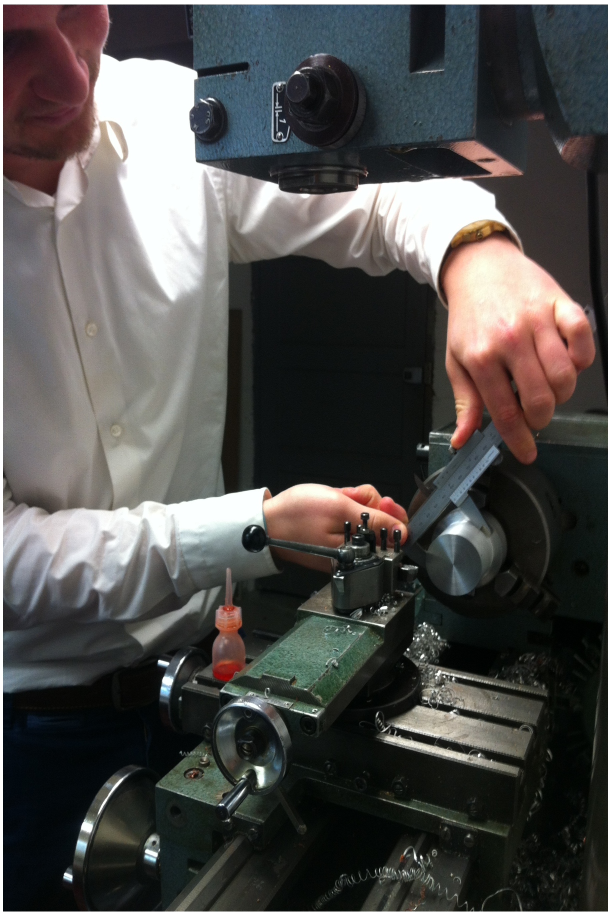

(d) A regular measurement of the diameter of the waveguide was needed.

(e) The circular waveguide, the probe and connecting bolts for the flench (3cm).

(f) Circular waveguide with the probe (top view).

(g) Circular waveguide with the probe (front view).

Figure 32: The construction of the circular waveguide.

(a) The assembled Pickett-Potter horn (side view).

(b) The horn, waveguide and probe un-assembled.

(c) The assembled Pickett-Potter horn, zoomed-in on the circular waveguide (front view).

(d) The assembled Pickett-Potter horn (top view).

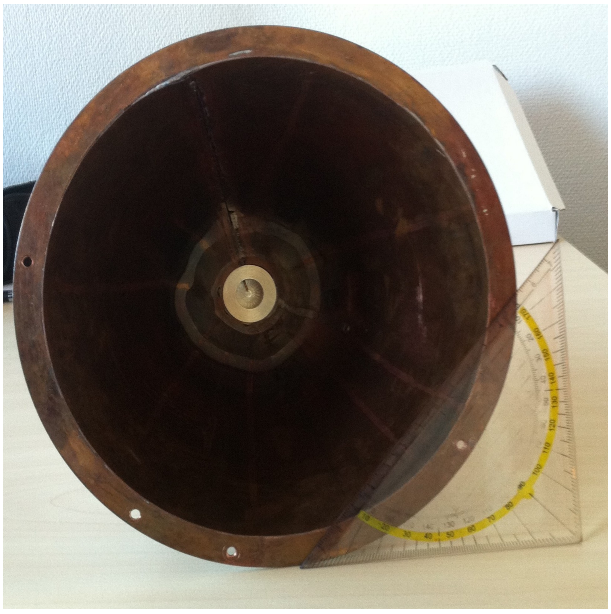

(e) The assembled Pickett-Potter horn, seen through the aperture).

(f) The assembled Pickett-Potter horn, zoomed-in at the waveguide and the probe.

Figure 33: The Pickett-Potter horn.

7 Testing the Pickett-Potter horn

Now that the horn antenna was constructed and assembled the performance of the horn needed to be determined. The performance of the horn is set by two characteristics. The first is the beam pattern, which was discussed in Sections 2.3 and 3. The other characteristic being the level of reflection by the probe. Both of the characteristics were measured by using a setup at SRON, as will be discussed below.

7.1 Scanning the beam pattern of the horn

As discussed in Section 3, the beam pattern defines how the horn antenna will responds to the incoming radiation, i.e. the power as a function of angle. There are multiple methods for determining the beam pattern of a horn antenna. One method is to position a source that is transmitting a known power, in the far-field of the antenna. The antenna will then be rotated, such that for each measurement of the power, the power is received under a different angle. Plotting the received power as a function of the angle, the beam pattern of the antenna is obtained. Since the far-field of this antenna is at 1.2 m (see Table 9) this type of measurement would be possible. However, an easier method for determining the beam pattern was used, i.e. by measuring the near-field and transforming that to the far-field.

7.1.1 Method for measuring the beam pattern

The near-field is measured by using a known source that transmits radiation onto the horn. The source and the horn are both connected to a Vector Network Analyzer (VNA, Figure 34k). The VNA will measure both the power transmitted by the source as the received power by the horn. Using this as an input, the VNA will calculate the amplitude and phase. This data will be Fourier transformed to obtain the far-field beam pattern.

Here the source was mounted on a 3D frame that allowed the positon, in the x-, y- and z-direction as defined in Figure 34b, to be changed automatically. By varying the position of the source in the y- and z-direction, the amplitude and phase were measured as function of position. After that, the source was shifted in the x-direction by $\lambda_0/4$ and the same scan done. Then the two data sets were combined as follows:

$$\mathrm{D} = \frac{(\mathrm{d}_1 - \mathrm{d}_2 \cdot \mathrm{j})}{2} \tag{7.1}$$

Where d_1 is the data from the first measurement, d_2 the data from the second measurement and D is the combined data. This procedure was needed to eliminate for possible standing wave features, due to reflections, e.g. by the horn or surrounding material.
The combined data set (D) was then transformed to the far-field by using a Fourier Transformation. The normalized power is obtained by taking the square of the magnitude, while first having normalized the data, i.e. dividing all the magnitudes by the maximum magnitude. The result will be a 2D plot, were the normalized power is plotted as a function of angle, which is the beam pattern.
The analysis of the beam pattern, to determine the half-power beamwidth (HPBW) and sidelobe level, was done with the Python script shown in Appendix IV. With the HPBW, the beam solid angle, the gain and effective area can be calculated. Thus by obtaining the beam pattern of the horn, we were able to obtain the main specifics our of Pickett-Potter horn.
The other horn specifics, such as the beam solid angle, maximum gain, effective area and the far-field distance were calculated with the equations from Section 3.

7.1.2 Measurement setup for the beam pattern scan

For our measurement, a rectangular waveguide with a copper flaring was used as the source, as shown in Figure 34c and 34d. The flaring section was added to assure the radiation from the waveguide didn't couple to the sides of the waveguide, allowing a smooth transition out of the rectangular waveguide. This source was placed in the electronically controlled frame (Figure 34a). Hence the position would be precise and automatically obtained via a computer. The latter being one of the main reasons for choosing this method. The horn was placed on a platform to assure that the middle of the aperture was in front of the source, such as shown in Figure 34h. To assure that only the beam pattern of the horn was measured and to reduce reflections of the horn, absorbing material was used to cover up the horn, the source and some surrounding materials, as seen in the Figures 34e, 34f, 34g and 34h. Some iterations were needed to optimized this, with Figures 34j and 34i showing the final measurement setup. With this setup the near field was scanned. In this scan both y- and the z-axis were scanned from -20 cm till +20 cm with respect to the middle of the horn, both in 81 steps for the y- and z-axis, resulting in 6561 different positions. At each of these 6561 positions, 21 frequencies between 10-12 GHz were sampled. The results and further analysis of the data is only done for 11 GHz, since this was the main observing frequency.

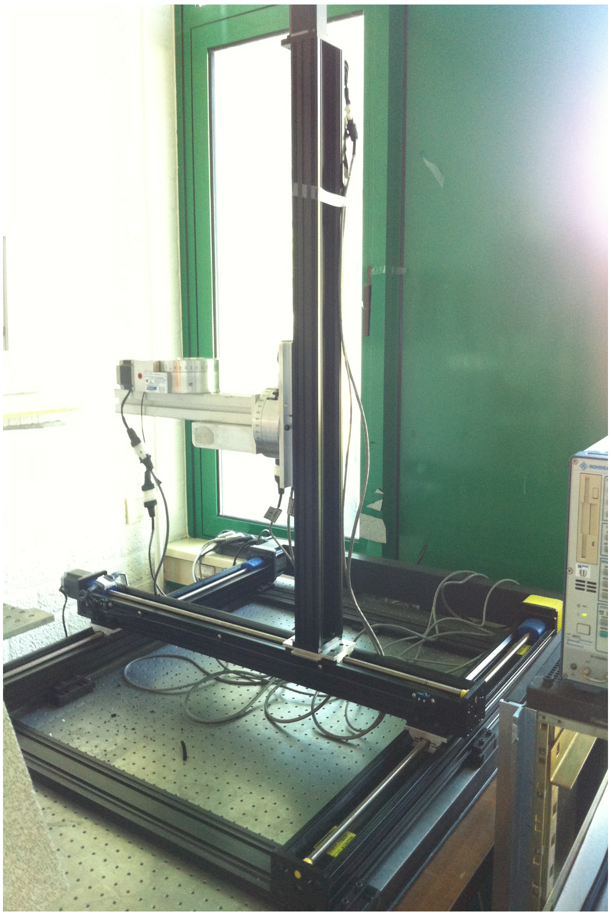

(a) Frame for the source.

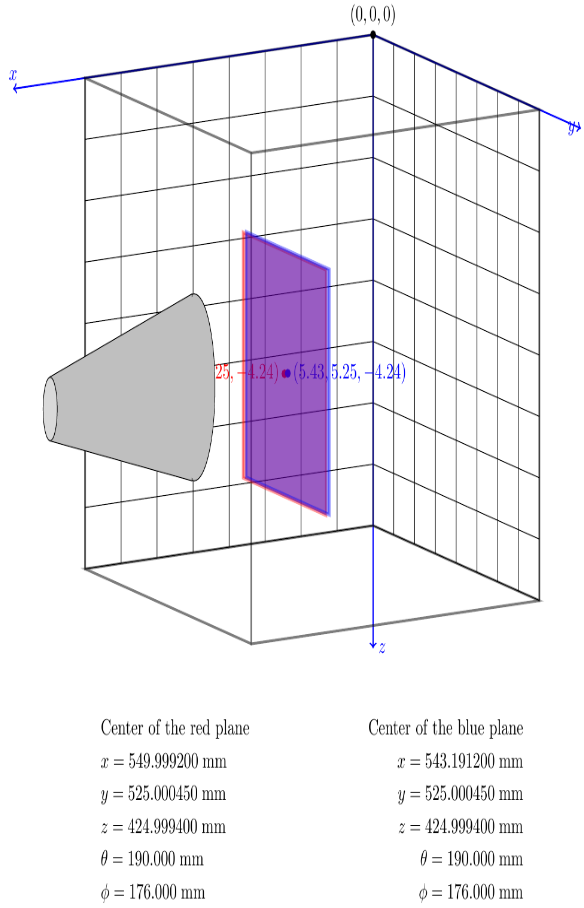

(b) Definition of frame coordinates and coordinates of measurement. Credits: Willeke Mulder.

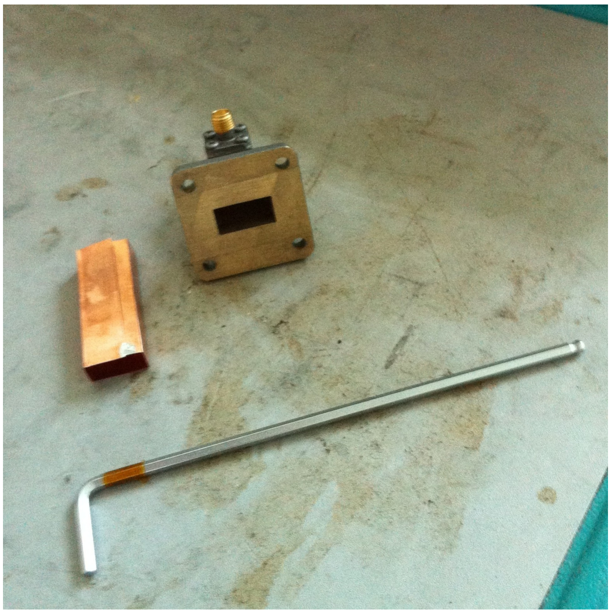

(c) Rectangular waveguide and copper flaring section.

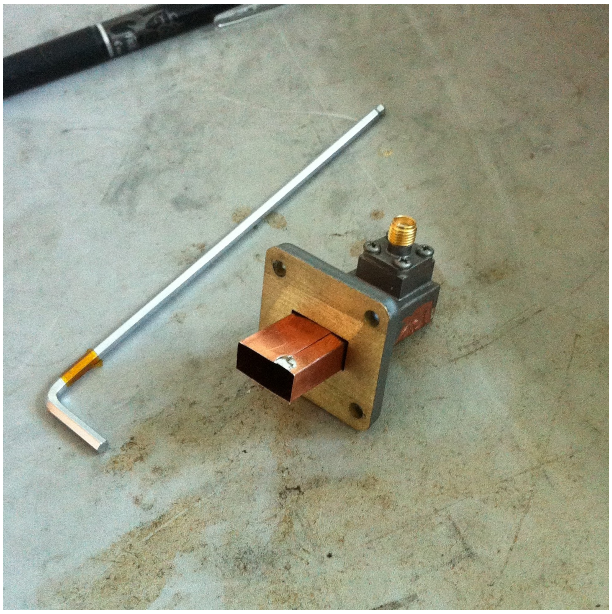

(d) Rectangular waveguide and copper flaring section assembled.

(e) The source on the frame.

(f) Zoomed-in on the source with absorption material.

(g) The Pickett-Potter horn cover with absorption material.

(h) The horn in front of the source.

(i) Definite setup (back).

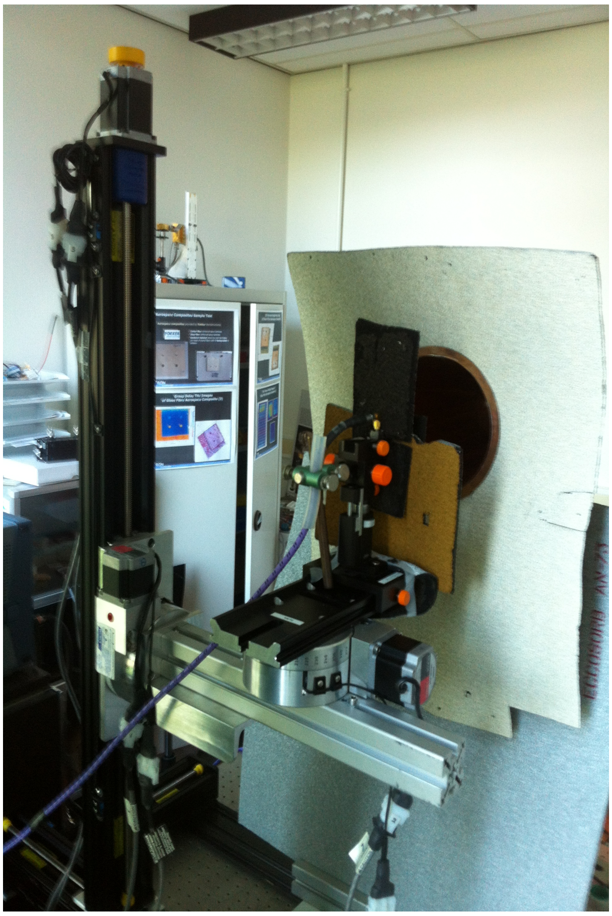

(j) Definite setup (front).

(k) The Vector Network Analyzed (VNA).

Figure 34: Measurement setup beam pattern.

7.1.3 Results for the beam pattern scan

The amplitude and phase, for the two independent measurements, were measured by the VNA and stored in a text file. The data from the text-file was analyzed by the Python script from Appendix IV (11.4)). Resulting in the near-field power pattern and phase for the central frequency of 11 GHz, shown in Figure 35. Figure 35a shows the near-field beam pattern, Figure 35b cross cut the beam pattern along the y- and z-direction when the power is at its maximum, while Figure 35c shows the near-field phase. The Python script also provides the far-field pattern at 11 GHz, which is shown in Figure 36a. The latter is further analyzed (by the Python script in Appendix II), giving the cross cut the power pattern (Figure 36b) and the calculation of the beam size (Figure 36c).

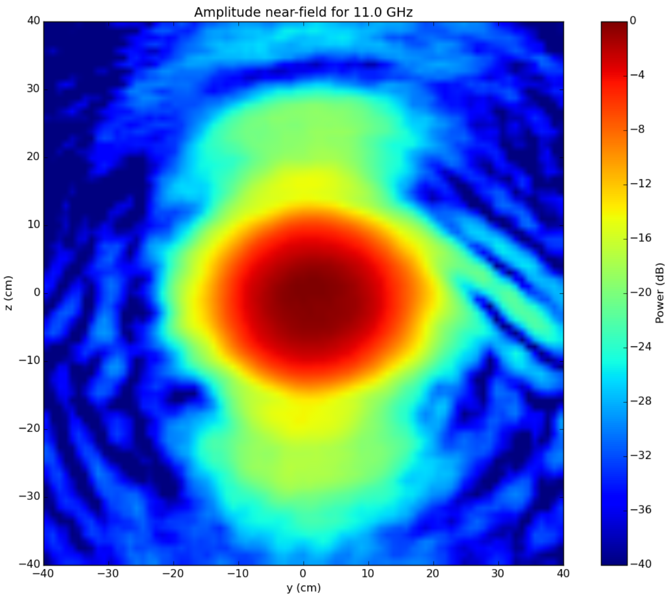

(a) The near-field power pattern.

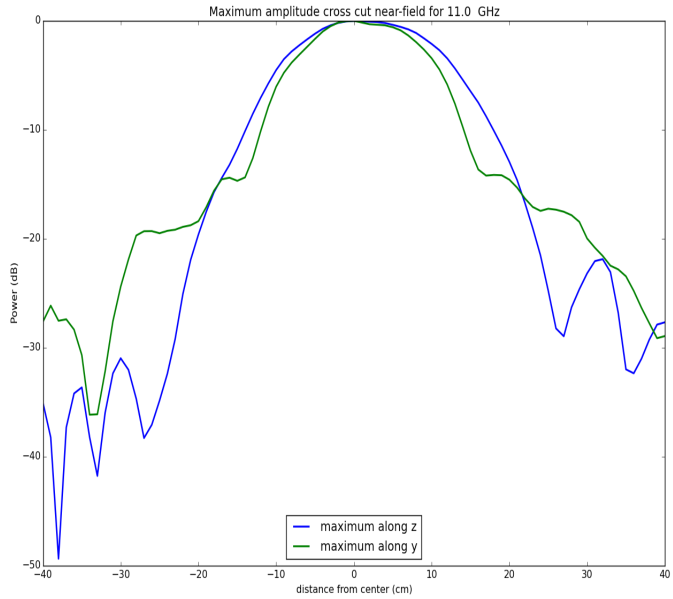

(b) The near-field power pattern cross cut at maximal amplitude.

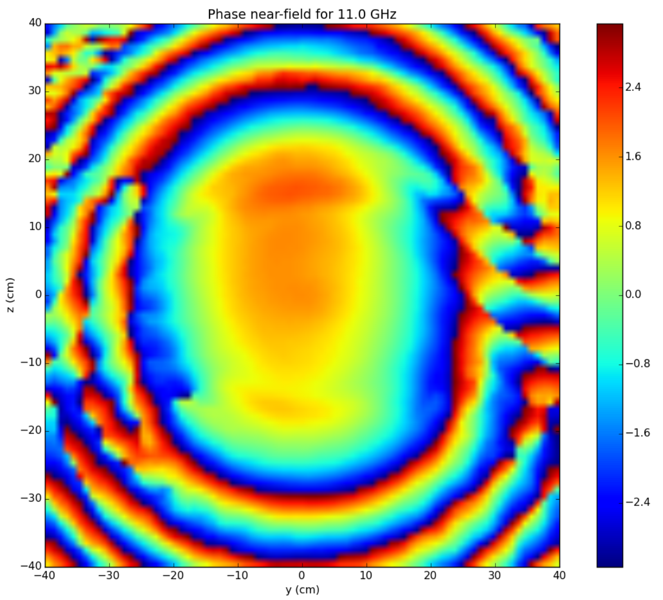

(c) The near-field phase.

Figure 35: Near-field results

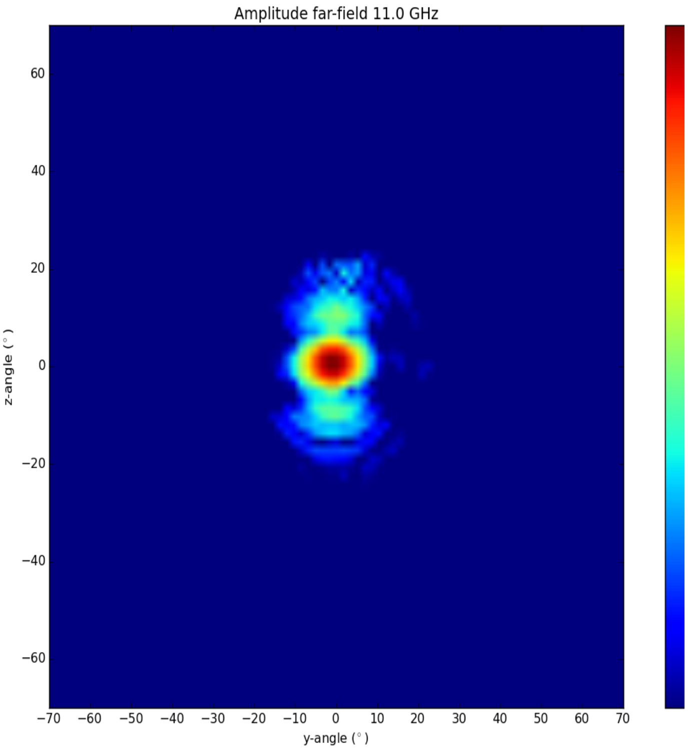

(a) The far-field power pattern.

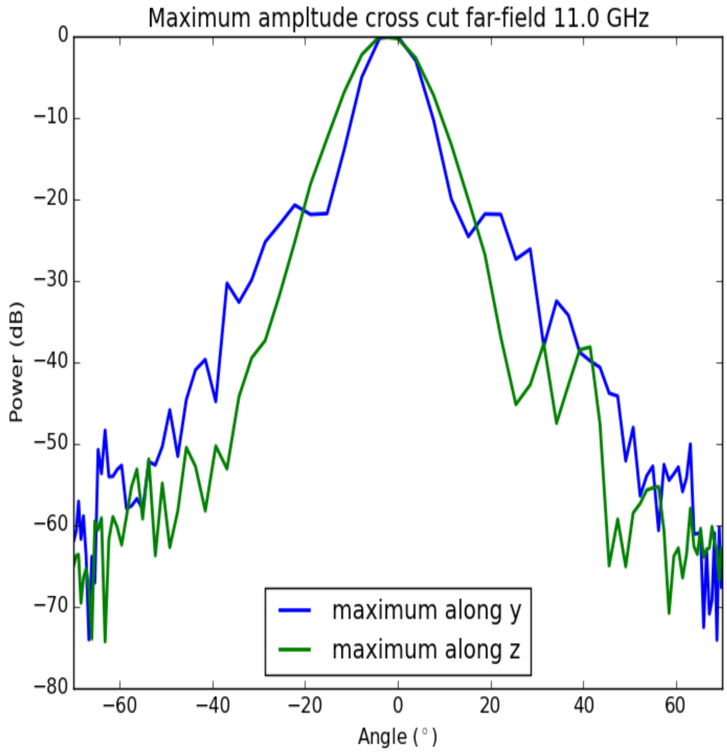

(b) The far-field power pattern cross cut at maximal amplitude.

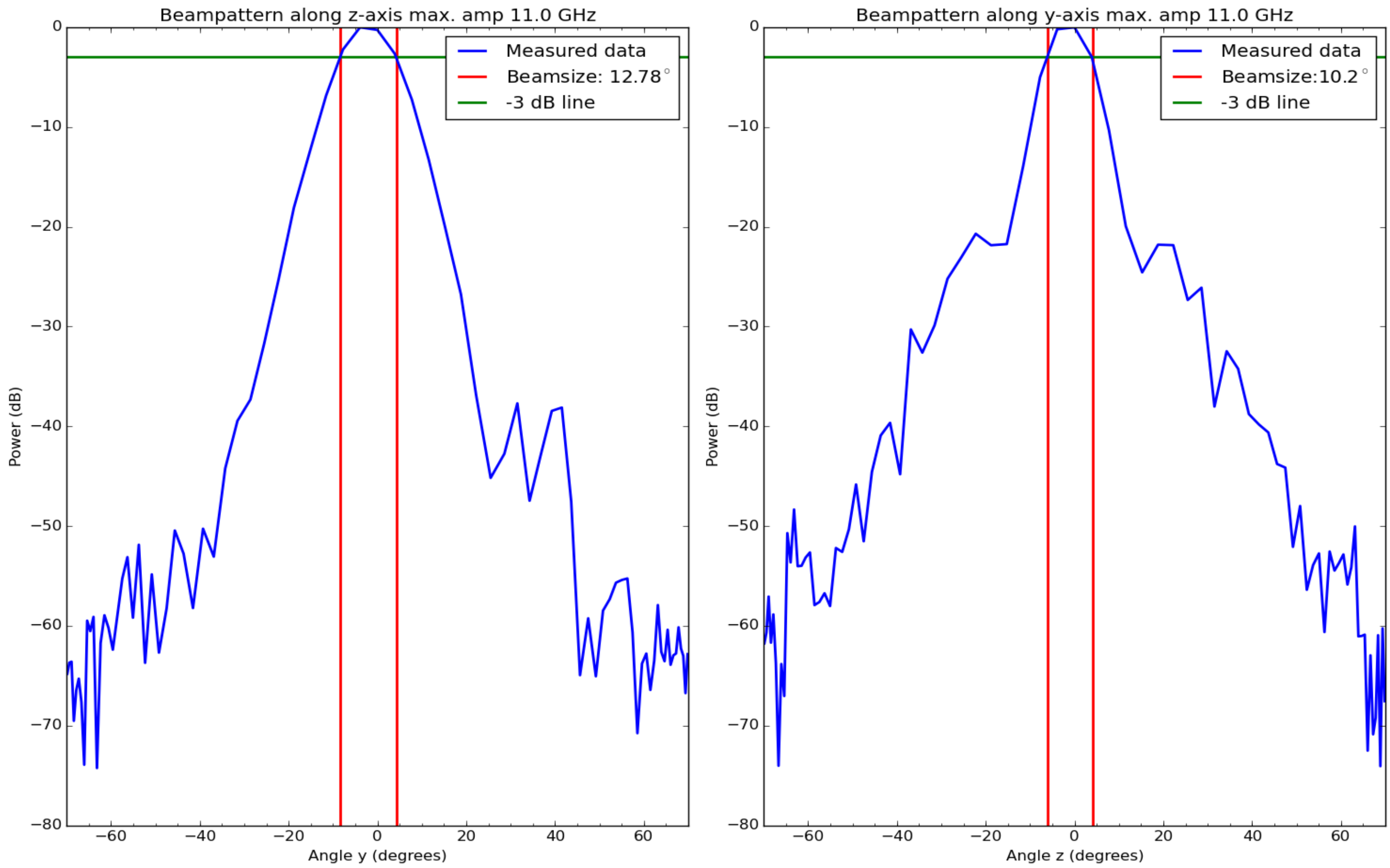

(c) The far-field power pattern cross cut at maximal amplitude for both y- and z-axis. The red lines indicate were the -3 dB line and the data intercept.

Figure 36: Result for the far-field power pattern or the beam pattern.

7.2 Reflection of the probe

The reflection of the probe needed to be measured to assure that the graph shown in Figure 28b was correct. This is used to verify if the optimization was done correctly and to compare a simulation with the measured data. The reflection of the probe as a function of frequency can be measured by using a Vector Network Analyzer (VNA, Figure 34k). By connecting the end of the probe (see Figure 32f) to the VNA, the VNA will be able to measure the S_{11} parameter. The VNA does this by sending in a signal with known phase and amplitude, after which is measured how much of this signal is reflected in a certain frequency band. These values will then be registered by a computer, which is connected to the VNA.

7.2.1 Measurement setup for measuring the probe reflection

After a calibration procedure of both the VNA ports, the horn was connected to the VNA, as shown in Figures 38a and 38b. To measure the reflection, the probe had to be pointed in a direction were there was little to no reflection, i.e. a stealthy area (Figure 38c). Then the computer program 'VNA-grab', would read out the S_{11} parameter as a function of frequency and stored it in a text-file. This data was plotted by using the Python script from Appendix V. The result is shown in Section 7.2.2.

7.2.2 Results for the measurement of probe reflection

The reflection measured from the probe is shown in Figure 37. Where the red lines indicate the bandwidth we're interested in.

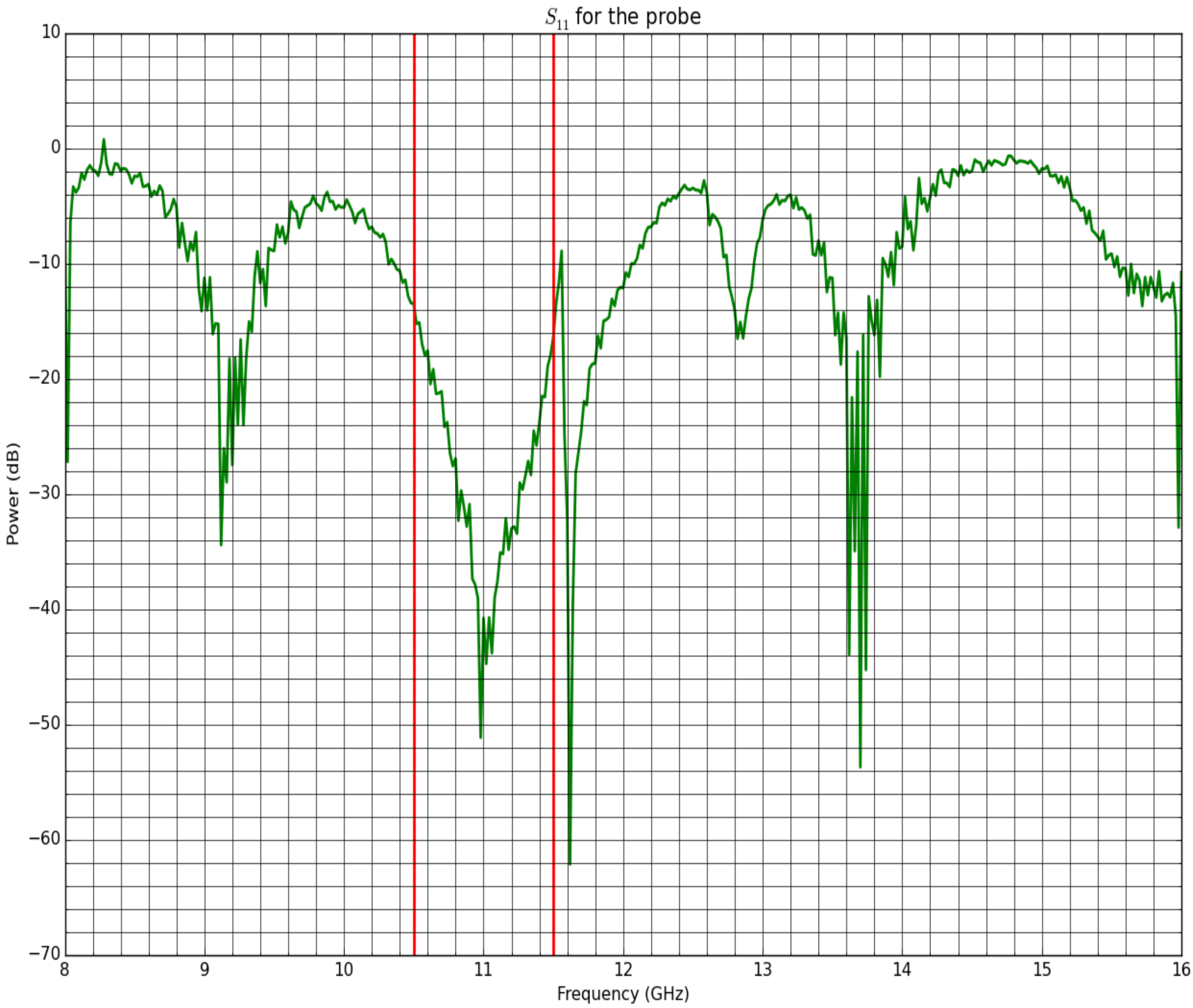

Figure 37: Measured reflection of the probe.

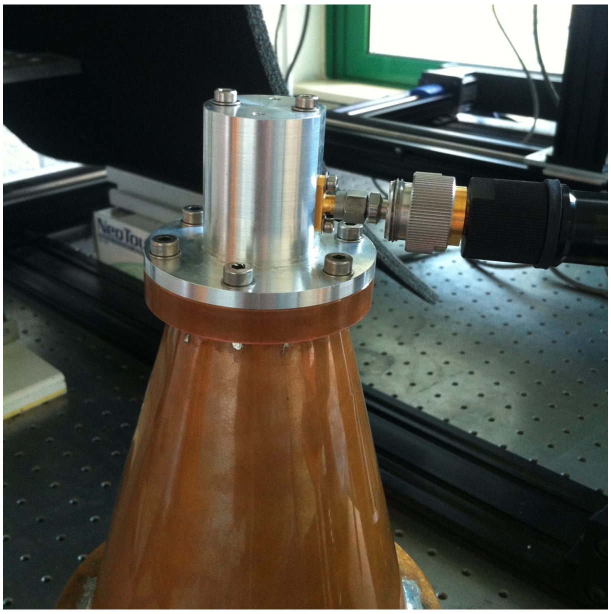

(a) The horn connected to the VNA.

(b) The horn connected to the VNA, zoomed-in on the circular waveguide.

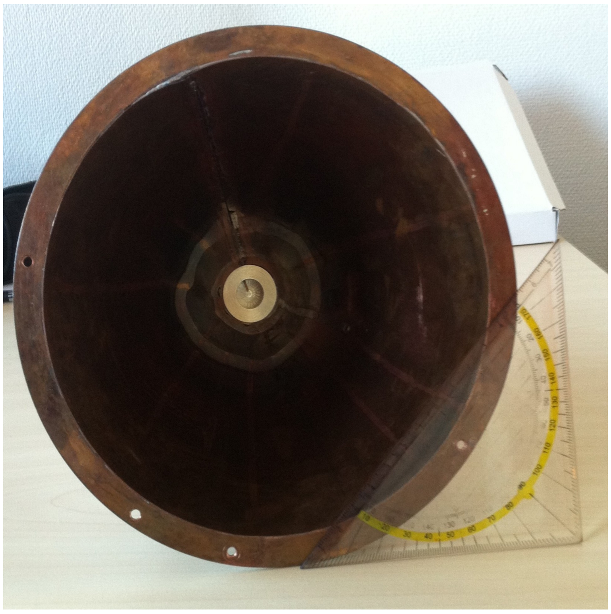

(c) The pointed area.

Figure 38: The measurement setup for measuring the reflection of the probe.

8 Discussion

In this section, the performance of the constructed Pickett-Potter horn is discussed, based on the results shown in section 7. As discussed before, the performance of the constructed Pickett-Potter horn is determined by two parameters; the beam pattern of the Pickett-Potter horn and the reflection of the probe, each of which will be discussed below. The measured results are compared with the simulated results, which are shown in Section 5. This is to verify if the simulation and predictions were a success.

8.1 On the beam pattern of the constructed Pickett-Potter horn

The measured beam pattern for the constructed Pickett-Potter horn is shown in Figure 36a. This figure shows that the beam pattern is not symmetric, as was expected based on the symmetric shape of the aperture. This can be seen in more detail when a cross cut along both axis for the maximum amplitude, i.e. the cross cut where the amplitude reaches 0 db, is taken, as shown in Figure 36b. In this plot the z-axis the beam pattern shows sidelobes at -40 dB, while along the y-axis there are sidelobes at -20 dB. This implies that the beam pattern along the z-axis is as expected, while along the y-axis additional sidelobes appear.

These sidelobes can be explained by imperfections in the horn, which occur at the transition from the flared conical horn section to the circular waveguide or at the gap between the two ends of the conical copper sheet. These imperfections result in geometrically different horn modes. Therefore the behaviour from the horn modes to the circular waveguide modes changes, causing other circular waveguide modes to propagate. However, these imperfections are much smaller than the observed wavelength and are orientated along the probe, hence are not probable to induce such prominent sidelobes.
This asymmetry in sidelobes can also be explained by the coupling of a horn mode to a circular waveguide mode other than TE_{11} circular waveguide mode. This coupling will cause this higher order mode to propagate into the waveguide and to enter the probe. This propagation will change the behaviour of the system, since there is energy, i.e. power, stored in this mode, resulting in the appearance of a sidelobe, causing the beam pattern of the constructed Pickett-Potter horn to be different in shape than was expected from the simulations. In our case this additional sidelobe is expressed in a higher sidelobe level along the y-axis than along the z-axis.
This possibility, that a higher order mode propagates, can also explain the asymmetric shape of the beam pattern, thus why the sidelobes appear along the y-axis and not along the z-axis. Since this probe would only detect the polarization of the higher order mode that is in the direction of the probe, i.e. along the y-axis.

From Figure 36b it can also be concluded that the y-axis cross cut is, in general, quite symmetric, while the z-axis plot isn't, due to the bumps of -40 dB at 30°and 38°. These peaks in the power along the z-axis can be explained by reflections due to the measurement setup. The main reflection, with a power of -20 dB, is shown in Figure 35a at (20 cm,10 cm) till (40 cm,-10 cm). The smaller reflections are next to the main reflection at a level of - 24 dB. These reflection features are also shown in Figure 35c. When comparing the left side of the plot, were the phase is nicely distributed in a circular shape (as expected for a circular shaped aperture), with the right side of the plot, there is a huge difference. At the right side of the plot the phase is not as circularly distributed as at the left, indicating some form of resonance. Since the left side doesn't show this feature, it is not a result of the horn. Therefore it has to be a feature caused by the measurement setup, i.e. reflections. Hence the sidelobe level of -40 dB for the z-axis cross cut described above will be even lower. Namely the z-axis cross cut will have a sidelobe level of -50 dB.

8.2 On the reflection of the probe

The results for the reflection of the probe are shown in Section 7.2.2. When comparing Figure 37 with Figure 29, it can be seen that only the predicted shape of the reflection, in the range from 10 - 11.5 GHz, corresponds with the measured reflection. Both the simulation and the measured data show a lowest point at 11 GHz. This is exactly what is needed for this horn antenna, since the main observing frequency is 11 GHz, thus at this frequency most of the energy must be transferred and not reflected. This being the reason why a low reflection at 11 GHz is preferred. The major differences between Figure 37 and the figures shown in Figure 29 is the measured power levels for the power and the shape of the graph outside the 10-11.5 GHz. There are two reasons that can explain these differences.

The first being the fact the simulation was done with the horn consisting of Perfectly Electrical Conducting (PEC) material, while the horn was made of copper. This would imply that the approximation of copper being a PEC is not entirely correct. Hence despite the fact that copper is, by approximation, a perfectly electrically conducting material, the material differences with PEC may result in difference regarding the reflections. Even though the differences will be small, they are visible, since the S_{11} parameter is shown on a log scale (dB's), showing a more drastic effect than on a linear scale.

The second explanation is, as discussed in Section 8.1, that there are horn modes coupling to a higher order circular

waveguide mode. This propagation will, next to the beam pattern, also influence the behaviour of the system. From the probe optimization this can be seen in a different behaviour of the S_{11} parameter.
An indication for this is given by Figure 37. From this figure it can be seen that there is a cutoff of a higher order mode at 11.55 GHz, shown by the characteristic cutoff feature at 11.55-11.6 GHz. This figure also displays the bandwidth of our system, by the red lines that are drawn in the graph. As a result, it can be seen that the maximum frequency within our bandwidth is very close to this cutoff frequency. Asymmetries in the shape of the horn and/or the circular waveguide, due to imperfections, might cause the cutoff frequency to shift such that it falls in the observed bandwidth. Hence it will be detected by our measurement system, causing the measured probe reflection to deviate from the simulated probe reflection.

8.3 Conclussion performance and horn specifics

Since we will be measuring the atmospheric temperature as function of zenith angle [7][21] to determine the temperature of the CMB, precision in the zenith direction is important. In the current orientation the constructed beam pattern is not suited to observe the CMB, since the sidelobe levels are too high. Therefore we can not make the distinction between power received by the main beam or by a sidelobe.
Despite the fact that the sidelobes along the y-axis are -20 dB, as discussed in Section 8.1, the constructed Pickett-Potter horn is still suited for the measurement of the CMB. Since the entire Pickett-Potter horn can be turned 90°, resulting in a horizontal orientated probe, causing the beam pattern to rotate with 90°. In this way the 'bad' part of the beam pattern (the previous y-axis cross cut) will see the same uniform sky, while the 'good' part of the beam pattern (the previous z-axis cross cut) will give the desired precision. Hence we can be sure that the power we measure is from a uniform sky at a certain zenith angle.

The above rotation of the constructed Pickett-Potter horn can be applied if the beam size of the z-axis cross cut is lower than 15°, otherwise the number of samples that can be measured in one sweep is to low [7][21]. The design parameters of this horn were chosen such that the beam size would be 12.92°(see Table 4). As seen from Figure 36c the beam size for the y-axis cross cut is 10.2°and for the z-axis cross cut 12.78°. Thus the beam size of z-axis cross cut is close to beam size gained from the simulations and smaller than 15°. Hence by placing the constructed Pickett-Potter horn in a horizontal probe orientation the CMB can still be measured.

An observation of the CMB thus seems feasible. However, the remaining question is whether or not the reflection of the probe will cause problems for our measurement. As seen from Figure 37 the measured reflection of the probe has a much lower power level when compared with the simulated reflection of the probe. This means that the reflection of the probe in reality is lower, which is good. Since there is less reflection off the probe then expected, i.e. more energy that falls onto the probe will enter the probe. Hence, the reflection of the probe will not cause problems for our measurement.

With the beam size of the Pickett-Potter horn determined, the other Pickett-Potter horn specifics could be calculated. These specifics are shown in Table 9. For completeness, Table 9 also shows the final result of the design parameters, which where obtained in Section 5.4.

Horn specifics	Value
Observed frequency	11 GHz
Observed wavelength	27 mm
Bandwidth	1 GHz
Observed bandwidth	10.5 - 11.5 GHz
Half Power Beam Width (HPBW)	11.49°or 0.20 radians [14]
Beam Solid angle (Ω_A)	0.032 str. See equation 2.1
Maximum Gain	397.86. See equation 2.2
Effective Area	235.16 cm^2. By rewritting equation 2.2
Aperture Area	249.24 cm^2
Farfield distance	2.33 m. See equation 2.3
Design specifics	**Value**
Slant angle	13.5°
Length horn	289.64 mm
a_w	10 mm
A	19 mm
λ_g	33.3 mm
Length waveguide	19 mm
Wall thickness of the flared Connical horn	2 mm
Position Probe	15.1 mm
Length probe	7.18 mm
Diameter teflon	4.2 mm
Diameter copper probe	1.2 mm

Table 9: Specifics constructed Pickett-Potter Horn.

[14] Calculated by taking the average of the values obtained in Figure 36c

9 Conclusion

The objective of this Bachelor Thesis was to design a horn antenna to measure the Cosmic Microwave Background (CMB) at 11 GHz. With the theory of electromagnetism, shown in Section 2, and the related horn theory and characteristics (Section 3), four selected horn antenna types were investigated. For each of these horn antennas the beam pattern was calculated. Next, the performance of each horn antenna type was judged, based on three selection criteria, i.e. the sidelobe level, HPBW and the construction level. Finally, the Pickett-Potter horn was the selected horn antenna type.
For this horn antenna type, simulations were done to obtain the preferred beam pattern. A maximum sidelobe level of -40 dB and a maximum beam size of 15° were used as design constraints. The final horn design parameters obtained from the optimization was a step-radius (A) of 19 mm and a circular waveguide (a_w) radius of 10 mm. These parameters were used for the Pickett-Potter horn design, which was based on the original design by Pickett himself. Based on this blueprint (see Figure 30 and Figure 32a), the Pickett-Potter horn was constructed.
After which the reflection off the probe and the beam pattern of the horn were measured. The results from these measurements show that, for both the reflection of the probe and for the beam pattern of the Pickett-Potter horn, the measured data deviates from the simulated data, due to the excitation of a higher order mode. Despite the beam pattern being different than expected, the constructed Pickett-Potter horn was still suited for the observation of the CMB, since a horizontal orientation of the probe would provide us with the preferred beam pattern in the zenith direction.

After the design, construction and testing phase the Pickett-Potter horn was integrated into a measurement system, as shown in Figure 39.

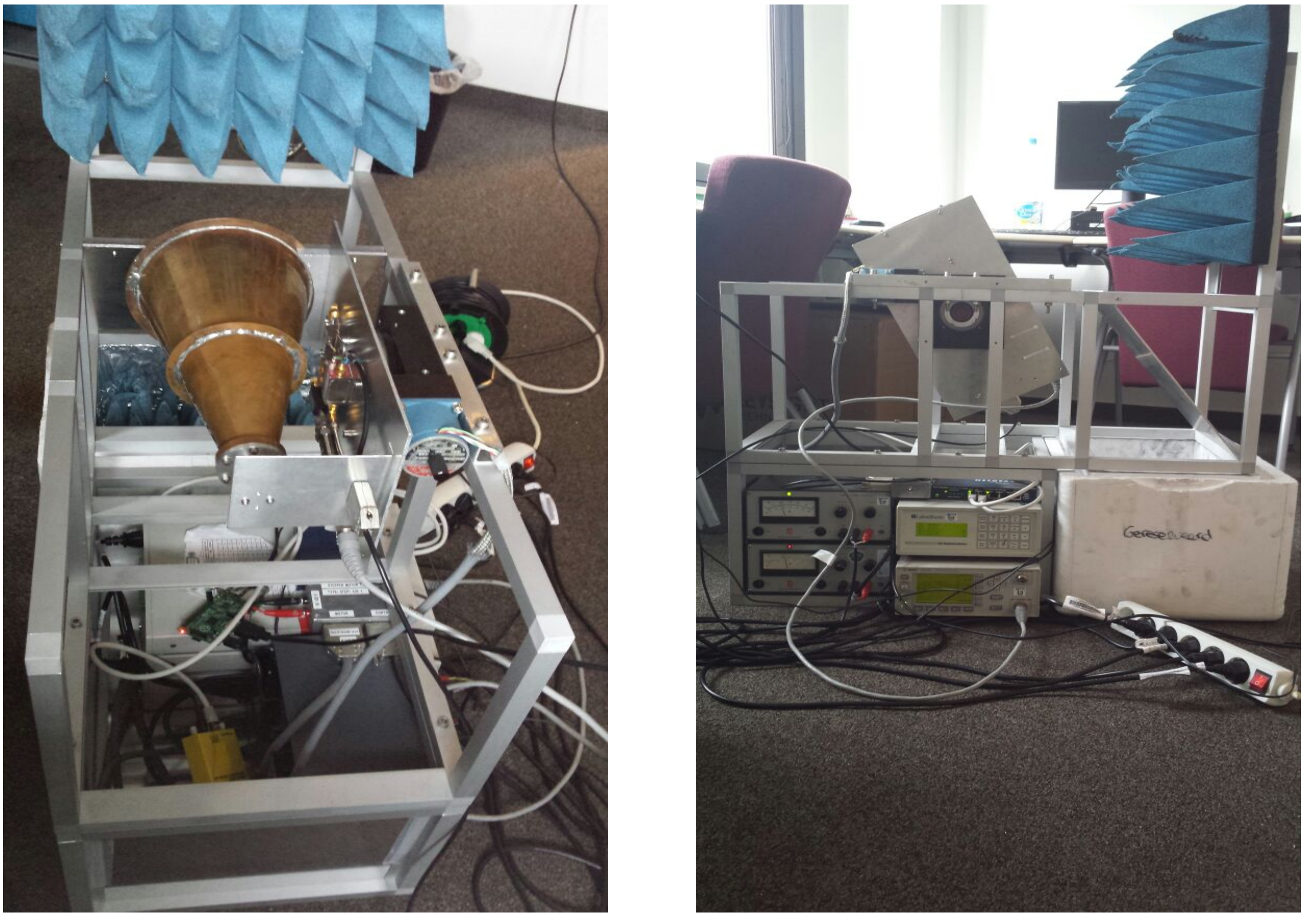

(a) The constructed Pickett-Potter horn mounted on the mount.

(b) The constructed Pickett-Potter horn integrated into the measurement system (side).

Figure 39: The CMB measurement system by: Willeke Mulder, Maik Zandvliet, Frits Sweijnen & Bram Lap.

9.1 Improvements

The objective of this Bachelor thesis is achieved, since a horn antenna type was selected, designed, constructed and finally integrated in a measurement system to measure the CMB temperature. Despite this, further optimization of our horn design is possible. The options for this are discussed below.

Clearly improvements can be made regarding the beam pattern, that is to fully understand from which propa-

gating modes the beam pattern originates. A first check can be done by adding more modes to the simulation in CST MWS. One possibility is to redo the simulation discussed in Section 5.2.1.1, where the number of modes at Port 1 and Port 2 is increased. The number of modes in the circular waveguide need to be increased to determine which mode, other than the TE_{11}, is able to propagate into the circular waveguide.
When the behaviour and the origin of the beam pattern is completely understood, different options for canceling this higher order mode propagation can be investigated. The first step would be to redo the simulation of Section 5.2.2.2 (the beam pattern optimization) with these additional modes. This would investigate how a different step-size and circular waveguide radius affects the propagation of the higher order mode. The most interesting will be how the cutoff frequency of the other mode behaves, since we would like it to be further away from the bandwidth we're observing in, such that is doesn't affect our beam pattern.
If the propagation can not be canceled by changing the step or circular waveguide radii, other possibilities can be investigated, such as tapering the circular aperture or adding an object (such as a pin) to the circular waveguide.
When the propagation of the mode can not be canceled, it needs to be minimized, such that the sidelobe level is as low as possible. The different possibilties, which are discussed above, can be used to achieve this.
With a higher mode propagating, the behaviour of the system changes. Hence a new optimization of the S_{21} parameter is needed to assure the best possible performance in the observed bandwidth. The first step would be to check if an optimization of the current circular waveguide design, shown in Section 5.3, still gives the preferred output, i.e. a S_{21} parameter that on average deviates from the ideal value by -0.15 dB. When such an optimization is not possible more degrees of freedom needed to be added to the optimization of the probe. This can be done by selecting different probe geometries, adding multiple probes to the waveguide or by adding a different object to the circular waveguide. All to obtain the optimal configuration for the transmission of the TE_{11} circular waveguide mode into the probe.
With the above checked, the final optimization needs to be done with a flared Conical horn made out of copper, while the circular waveguide should consist of aluminum. This would make the simulation in CST MWS as realistic as possible.

Another improvement of our measurement system is the observation of other sources. However, as discussed in [7], the received brightness has to be increased. For this the performance of our horn antenna in the observed bandwidth needs to be improved.
A method to increase this is by making the flared conical horn corrugated, where the grooves are approximately one-quarter of the wavelength deep [17]. But, as it is in most design projects, somewhere a trade off has to be made. Here the improved performance would result in a horn that is close to impossible to construct by hand. Therefore improving the bandwidth performance is not realistic.

Besides further optimization of the Pickett-Potter horn, the measurement setup of the near-field scan can also be improved, since the data in Figure 35 still show reflections due to the measurement setup of the beam pattern. These reflections can be removed by changing the attachment of the absorption material to the horn or the source described in Section 7.1.2.

Another improvement that can be made is by using another method to measure the beam pattern of the constructed Pickett-Potter horn. For instance by measuring the far-field pattern of the horn directly. The result obtained from this direct measurement of the far-field pattern, will be used to check the far-field pattern obtained from the near-field, especially to determine if the beam pattern, shown in Figure 36a, is a result of the horn itself, e.g. imperfections in the shape of the horn, or originates from the measurement setup, e.g. due to reflections. To actually do the far-field measurement, one has to travel to ASTRON, since the equipment present at SRON is not ideal for this type of measurement, i.e. the person preforming this measurement has a good excuse to go to ASTRON!

10 Acknowledgements

I want to thank my fellow students, Willeke Mulder, Frits Swijenen and Maik Zandvliet, for cooperation, support and the fun time we had during this project. I would also like to thank my supervisors John McKean and Andrey Baryshev for helping me in completing the project. Ronald Hesper receives special thanks for being the key to assuring the construction of the horn was properly done. Finally, I would like to thank the people from the workshop for giving us a hand where possible.

11 Appendices

11.1 Appendix I: Code for plotting the beam patterns

```
#!/usr/bin/env python
# -*- coding: utf-8 -*-

import numpy as np
import matplotlib.pylab as plt
from scipy import special

nx = 1
ny = nx
wavelength = np.array([0.075,0.0375,0.0273])

D = np.linspace(-1,1,1000)
u = 1

x = np.char.lower(raw_input("Which Beam pattern do you want? A: Rectangular, B: Circular
     or C: Diagonal? "))

if x == 'a':
        theta = np.linspace(-np.pi/2,np.pi/2,1000)
        Lx = np.array([0.2,0.4,0.6])
        Ly = np.linspace(-1,1, 1000)
        fig = plt.figure(1)
        fig.set_size_inches(15, 10)
        P_rectangular1 = (np.sin((np.pi*Lx[0]/wavelength[2])*np.sin(theta))/ ((np.pi*Lx
            [0]/wavelength[2])*np.sin(theta)) )
        P_rectangular2 = (np.sin((np.pi*Lx[1]/wavelength[2])*np.sin(theta))/ ((np.pi*Lx
            [1]/wavelength[2])*np.sin(theta)) )
        P_rectangular3 = (np.sin((np.pi*Lx[2]/wavelength[2])*np.sin(theta))/ ((np.pi*Lx
            [2]/wavelength[2])*np.sin(theta)) )

        ax = plt.subplot(131)
        plt.plot(np.degrees(theta),10*np.log10((P_rectangular1/np.amax(P_rectangular1))
            **2),'b',label='0.2 m')
        plt.xlabel('Angle $\\theta$ ($^\circ$)')
        plt.ylabel('Power (dB)')
        plt.yticks(np.linspace(-40,0,5))
        plt.ylim([-40,0])
        plt.grid(True)
        plt.title('Dx = 0.2 m')

        ax = plt.subplot(132)
        plt.plot(np.degrees(theta),10*np.log10( (P_rectangular2/np.amax(P_rectangular2)
            )**2 ), 'g',label='0.4 m')
        plt.xlabel('Dy $\\theta$ ($^\circ$)')
        plt.ylabel('Power (dB)')
        plt.yticks(np.linspace(-40,0,5))
        plt.ylim([-40,0])
        plt.grid(True)
        plt.title('Dx = 0.4 m')

        ax = plt.subplot(133)
        plt.plot(np.degrees(theta),10*np.log10((P_rectangular3/np.amax(P_rectangular3))
            **2 ),'purple',label='0.6 m')
        plt.xlabel('Dy (m)')
        plt.ylabel('Power $\\theta$ ($^\circ$)')
        plt.yticks(np.linspace(-40,0,5))
        plt.ylim([-40,0])
        plt.grid(True)
        plt.title('Dx = 0.6 m')

        plt.tight_layout()
        plt.savefig('Rectangular_x_Beam_pattern.png')
        plt.show()
```

```
if x == 'b':
        u = 1.841
        r = [0.1,0.3,0.5]
        theta = np.linspace(-np.pi/2,np.pi/2,1000)

        fig = plt.figure(2)
        fig.set_size_inches(15, 10)

        P_circular1 = (wavelength[2]/(np.pi*r[0]*np.sin(theta)) ) * special.jn(1,((2*np.
            pi*r[0]*np.sin(theta))/wavelength[2]))
        P_circular2 = (wavelength[2]/(np.pi*r[1]*np.sin(theta)) ) * special.jn(1,((2*np.
            pi*r[1]*np.sin(theta))/wavelength[2]))
        P_circular3 = (wavelength[2]/(np.pi*r[2]*np.sin(theta)) ) * special.jn(1,((2*np.
            pi*r[2]*np.sin(theta))/wavelength[2]))


        ax = plt.subplot(131)
        plt.plot(np.degrees(np.linspace(-np.pi/2,np.pi/2,1000)),10*np.log10((P_circular1
            /np.amax(P_circular1))**2),'b')
        plt.title('a = '+str(0.1)+' m')
        plt.xlabel('Angle $\\theta$ ($^\circ$)')
        plt.ylabel('Power (dB)')
        plt.grid(True)
        plt.ylim([-60,0])
        plt.legend()

        ax = plt.subplot(132)
        plt.plot(np.degrees(np.linspace(-np.pi/2,np.pi/2,1000)),10*np.log10((P_circular2
            /np.amax(P_circular2))**2), 'g')
        plt.title('a = '+str(0.3)+' m')
        plt.xlabel('Angle $\\theta$ ($^\circ$)')
        plt.ylabel('Power (dB)')
        plt.grid(True)
        plt.ylim([-60,0])
        plt.legend()

        ax = plt.subplot(133)
        plt.plot(np.degrees(np.linspace(-np.pi/2,np.pi/2,1000)),10*np.log10((P_circular3
            /np.amax(P_circular3))**2),'purple')
        plt.title('a = '+ str(0.5) +' m')
        plt.xlabel('Angle $\\theta$ ($^\circ$)')
        plt.ylabel('Power (db)')
        plt.grid(True)
        plt.ylim([-60,0])
        plt.legend()
        #plt.title('Lambda =' + str(wavelength[j]))

        plt.tight_layout()
        plt.savefig('Circular_Beam_pattern.png')
        plt.show()

if x == 'd':
        fig = plt.figure(4)
        fig.set_size_inches(15, 10)
        theta = np.linspace(-np.pi,np.pi,1000)
        k = (2*np.pi)/(wavelength[2])
        r = [0.1,0.095,0.105]
        alpha = 0.653

        K11E1 = 3.832/r[0]
        K11H1 = 1.841/r[0]
        betaH1= np.sqrt(k**2 - K11E1**2)
        betaE1 = np.sqrt(k**2 - K11H1**2)
        P_potter1 = ( ( 1 + (betaH1*np.cos(theta)/k)) - alpha*(((betaE1/k) + np.cos(
            theta))/(1-(K11E1/(k*np.sin(theta)))**2))) * (special.jv( 1, (k*r[0]*np.sin(
            theta)))/np.sin(theta))

        K11E2 = 3.832/r[1]
        K11H2 = 1.841/r[1]
        betaH2= np.sqrt(k**2 - K11E2**2)
```

```
print k**2, K11E2**2
betaE2 = np.sqrt(k**2 - K11H2**2)
P_potter2 = ( ( 1 + (betaH2*np.cos(theta)/k)) - alpha*(((betaE2/k) + np.cos(
    theta))/(1-(K11E2/(k*np.sin(theta)))**2))) * (special.jv( 1, (k*r[0]*np.sin(
    theta)))/np.sin(theta))

K11E3 = 3.832/r[2]
K11H3 = 1.841/r[2]
betaH3= np.sqrt(k**2 - K11E3**2)
print k**2, K11E3**2
betaE3 = np.sqrt(k**2 - K11H3**2)
P_potter3 = ( ( 1 + (betaH3*np.cos(theta)/k)) - alpha*(((betaE3/k) + np.cos(
    theta))/(1-(K11E3/(k*np.sin(theta)))**2))) * (special.jv( 1, (k*r[0]*np.sin(
    theta)))/np.sin(theta))
#P_potter1 = ( 1 -  (alpha/(1 - (3.832**2 / ( (k*r[0]*np.sin(theta))**2) )   )))
      * (special.jv( 1, (k*r[0]*np.sin(theta)) ) / k*r[0]*np.sin(theta))
#P_potter2 = ( 1 -  (alpha/(1 - (3.832**2 / ( (k*r[1]*np.sin(theta))**2) )   )))
      * (special.jv( 1, (k*r[1]*np.sin(theta)) ) / k*r[1]*np.sin(theta))
#P_potter3 = ( 1 -  (alpha/(1 - (3.832**2 / ( (k*r[2]*np.sin(theta))**2) )   )))
      * (special.jv( 1, (k*r[2]*np.sin(theta)) ) / k*r[2]*np.sin(theta))


ax = plt.subplot(131)
plt.plot(np.degrees(theta),10*np.log10((P_potter2/np.amax(P_potter2))**2), 'b')
plt.title('a = '+str(r[1])+' m')
plt.ylim([-60,0])
plt.xlabel('Angle $\\theta$ ($^\circ$)')
plt.ylabel('Power (dB)')
plt.legend()

ax = plt.subplot(132)

plt.plot(np.degrees(theta),10*np.log10((P_potter1/np.amax(P_potter1))**2),'g')
plt.title('a = '+str(r[0])+' m')
plt.xlabel('Angle $\\theta$ ($^\circ$)')
plt.ylabel('Power (dB)')
plt.ylim([-60,0])
plt.legend()

ax = plt.subplot(133)
plt.plot(np.degrees(theta),10*np.log10((P_potter3/np.amax(P_potter3))**2),'
    purple')
plt.title('a = '+ str(r[2]) +' m')
plt.xlabel('Angle $\\theta$ ($^\circ$)')
plt.ylabel('Power (db)')
plt.ylim([-60,0])
plt.legend()
#plt.title('Lambda =' + str(wavelength[j]))

plt.tight_layout()
plt.savefig('Potter_Beam_pattern.png')
plt.show()
```

11.2 Appendix II: Code for analyzing data from the first parameter sweep

```
#!/usr/bin/env python
from matplotlib.pyplot import figure, show
import numpy as np

def intersect(value, x, y):
    ''' Find the x left coordinate corresponding to y = value assuming a symmetric
        function w.r.t. x.
    Intersect fits a straight line through the points just above and just below the
        wanted value and then iterpolates the wanted number.
    '''
    N = len(y)
    # Go halfway
    for i in range(N//2 + 1):
        if y[i] > value:
            y_low = y[i-1]
            y_high = y[i]
            x_low = x[i-1]
            x_high = x[i]
            break
    # Linear interpolation.
    slope = (y_high - y_low) / (x_high - x_low)
    x = (value - y_low) / slope + x_low
    return x

r_step, r_waveguide, theta, directivity = np.loadtxt('beampattern1.txt', usecols=(2, 3,
   6, 7), unpack=True)

fig = figure(); fig2 = figure()
pattern = 0
tikker = 1
fig.set_size_inches(15, 10)
print 'Half Power Beam Width'
print '====================='
print 'Pattern'.ljust(10) + 'R_step'.ljust(10) + 'R_wguide'.ljust(10) + 'HPBW'.ljust(10)
while pattern < 10:
    x = theta[73*pattern:73*(pattern+1)]
    y = directivity[73*pattern:73*(pattern+1)]
    step = r_step[73*pattern]
    waveg = r_waveguide[73*pattern]
    ax = fig.add_subplot(2, 5, pattern+1)
    ax2 = fig2.add_subplot(2, 5, pattern+1)
    ax.plot(x, y - np.max(y), '-', label='Pattern %d' % pattern)
    ax.set_xticks(np.linspace(-180,180,5))
    ax.set_xlabel('Angle ($^\circ$)')
    ax.set_ylabel('Power (dB)')
    ax.set_title('Pattern ' +str(tikker))
    ax2.plot(x, y, '-', label='Pattern %d' % pattern)
    ax2.set_xlim(-20, 20)
    ax2.set_title('Pattern %d' % (pattern+1), fontweight='bold')
    if pattern != 4 and pattern != 9:
        value = np.max(y - 3)
        ang = intersect(value, x, y)
        ax2.axvline(ang, color='r')
        ax2.axvline(np.abs(ang), color='r')
        ax2.axhline(value, color='g')
    print ('%.2d'%(pattern+1)).ljust(10), ('%.2f'%step).ljust(10), ('%.2f'%waveg).ljust
        (10), ('%.2f'%np.abs((ang))).ljust(10)
    pattern += 1
    tikker += 1
fig.tight_layout()
fig2.tight_layout()
show()
fig.savefig('Beam_patterns_parameter_sweep_1(1).png')
fig2.savefig('Beam_patterns_parameter_sweep_1_beamsize(1).png')

fig = figure(); fig2 = figure()
fig.set_size_inches(15, 10)
count = 0
```

```
while pattern < 20:
    x = theta[73*pattern:73*(pattern+1)]
    y = directivity[73*pattern:73*(pattern+1)]
    step = r_step[73*pattern]
    waveg = r_waveguide[73*pattern]
    ax = fig.add_subplot(2, 5, count+1)
    ax2 = fig2.add_subplot(2, 5, count+1)
    ax.plot(x, y - np.max(y), '-', label='Pattern %d' % pattern)
    ax.set_xticks(np.linspace(-180,180,5))
    ax.set_xlabel('Angle ($^\circ$)')
    ax.set_ylabel('Power (dB)')
    ax.set_title('Pattern ' +str(tikker))
    ax2.plot(x, y, '-', label='Pattern %d' % pattern)
    ax2.set_xlim(-20, 20)
    ax2.set_title('Pattern %d' % (pattern+1), fontweight='bold')
    if pattern != 4 and pattern != 9:
        value = np.max(y - 3)
        ang = intersect(value, x, y)
        ax2.axvline(ang, color='r')
        ax2.axvline(np.abs(ang), color='r')
        ax2.axhline(value, color='g')
    print ('%.2d'%(pattern+1)).ljust(10), ('%.2f'%step).ljust(10), ('%.2f'%waveg).ljust
        (10), ('%.2f'%np.abs((ang))).ljust(10)
    pattern += 1
    count += 1
    tikker += 1
fig.tight_layout()
fig2.tight_layout()
show()
fig.savefig('Beam_patterns_parameter_sweep_1(2).png')
fig2.savefig('Beam_patterns_parameter_sweep_1_beamsize(2).png')


fig = figure(); fig2 = figure()
fig.set_size_inches(15, 10)
count = 0
while pattern < 25:
    x = theta[73*pattern:73*(pattern+1)]
    y = directivity[73*pattern:73*(pattern+1)]
    step = r_step[73*pattern]
    waveg = r_waveguide[73*pattern]
    ax = fig.add_subplot(2, 5, count+1)
    ax2 = fig2.add_subplot(2, 5, count+1)
    ax.plot(x, y - np.max(y), '-', label='Pattern %d' % pattern)
    ax.set_xticks(np.linspace(-180,180,5))
    ax.set_xlabel('Angle ($^\circ$)')
    ax.set_ylabel('Power (dB)')
    ax.set_title('Pattern ' +str(tikker))
    ax2.plot(x, y, '-', label='Pattern %d' % pattern)
    ax2.set_xlim(-20, 20)
    ax2.set_title('Pattern %d' % (pattern+1), fontweight='bold')
    if pattern != 4 and pattern != 9:
        value = np.max(y - 3)
        ang = intersect(value, x, y)
        ax2.axvline(ang, color='r')
        ax2.axvline(np.abs(ang), color='r')
        ax2.axhline(value, color='g')
    print ('%.2d'%(pattern+1)).ljust(10), ('%.2f'%step).ljust(10), ('%.2f'%waveg).ljust
        (10), ('%.2f'%np.abs((ang))).ljust(10)
    pattern += 1
    count += 1
    tikker += 1
fig.tight_layout()
fig2.tight_layout()
show()
fig.savefig('Beam_patterns_parameter_sweep_1(3).png')
fig2.savefig('Beam_patterns_parameter_sweep_1_beamsize(3).png')
```

11.3 Appendix III: Code for analyzing data from the second parameter sweep

```
#!/usr/bin/env python
from matplotlib.pyplot import figure, show
import numpy as np

def intersect(value, x, y):
    ''' Find the x left coordinate corresponding to y = value assuming a symmetric
        function w.r.t. x.
    Intersect fits a straight line through the points just above and just below the
        wanted value and then iterpolates the wanted number.
    '''
    N = len(y)
    # Go halfway
    for i in range(N//2 + 1):
        if y[i] > value:
            y_low = y[i-1]
            y_high = y[i]
            x_low = x[i-1]
            x_high = x[i]
            break
    # Linear interpolation.
    slope = (y_high - y_low) / (x_high - x_low)
    x = (value - y_low) / slope + x_low
    return x


# 9 * 7 = 63
r_step, r_waveguide, theta, directivity = np.loadtxt('data_parameter_sweep_2.txt',
    usecols=(2, 3, 6, 7), unpack=True)

fig = figure()
fig.set_size_inches(15, 10)
pattern = 0
tikker = 1
print 'Half Power Beam Width'
print '====================='
print 'Pattern'.ljust(10) + 'R_step'.ljust(10) + 'R_wguide'.ljust(10) + 'HPBW'.ljust(10)
while pattern < 18:
    x = theta[361*pattern:361*(pattern+1)]
    y = directivity[361*pattern:361*(pattern+1)]
    step = r_step[361*pattern]
    waveg = r_waveguide[361*pattern]
    ax = fig.add_subplot(2, 9, pattern+1)
    ax.set_xticks(np.linspace(-180,180,3))
    ax.set_xlabel('Angle ($^\circ$)')
    ax.set_ylabel('Power (dB)')

    #ax2 = fig2.add_subplot(3, 9, pattern+1)
    ax.plot(x, y - np.max(y), '-', label='Pattern %d' % pattern)
    ax.set_title('Pattern '+str(tikker))
    #ax2.plot(x, y, '-', label='Pattern %d' % pattern)
    #ax2.set_xlim(-20, 20)
    #ax2.set_title('Pattern %d' % (pattern+1), fontweight='bold')
    if pattern != 4 and pattern != 9:
        value = np.max(y - 3)
        ang = intersect(value, x, y)
        #ax2.axvline(ang, color='r')
        #ax2.axvline(np.abs(ang), color='r')
        #ax2.axhline(value, color='g')
    print ('%.2d'%(pattern+1)).ljust(10), ('%.2f'%step).ljust(10), ('%.2f'%waveg).ljust
        (10), ('%.2f'%np.abs((ang))).ljust(10)
    pattern += 1
    tikker += 1
fig.tight_layout()
fig.savefig('parametersweep2_fig_1.png')
show()

count = 0
fig = figure()
```

```
fig.set_size_inches(15, 10)
while pattern < 36:
    x = theta[361*pattern:361*(pattern+1)]
    y = directivity[361*pattern:361*(pattern+1)]
    step = r_step[361*pattern]
    waveg = r_waveguide[361*pattern]
    ax = fig.add_subplot(2, 9, count+1)
    ax.set_xticks(np.linspace(-180,180,3))
    ax.set_xlabel('Angle ($^\circ$)')
    ax.set_ylabel('Power (dB)')

    #ax2 = fig2.add_subplot(2, 9, count+1)
    ax.plot(x, y - np.max(y), '-', label='count %d' % pattern)
    ax.set_title('Pattern '+str(tikker))
    #ax2.plot(x, y, '-', label='count %d' % pattern)
    #ax2.set_xlim(-20, 20)
    #ax2.set_title('count %d' % (pattern+1), fontweight='bold')
    if pattern != 4 and pattern != 9:
        value = np.max(y - 3)
        ang = intersect(value, x, y)
        #ax2.axvline(ang, color='r')
        #ax2.axvline(np.abs(ang), color='r')
        #ax2.axhline(value, color='g')
    print ('%.2d'%(pattern+1)).ljust(10), ('%.2f'%step).ljust(10), ('%.2f'%waveg).ljust
       (10), ('%.2f'%np.abs((ang))).ljust(10)
    pattern += 1
    count +=1
    tikker += 1
fig.tight_layout()
fig.savefig('parametersweep2_fig_2.png')
show()

count = 0
fig = figure()
fig.set_size_inches(15, 10)
while pattern < 54:
    x = theta[361*pattern:361*(pattern+1)]
    y = directivity[361*pattern:361*(pattern+1)]
    step = r_step[361*pattern]
    waveg = r_waveguide[361*pattern]
    ax = fig.add_subplot(2, 9, count+1)
    ax.set_xticks(np.linspace(-180,180,3))
    #ax2 = fig2.add_subplot(2, 9, count+1)
    ax.plot(x, y - np.max(y), '-', label='count %d' % pattern)
    ax.set_title('Pattern '+str(tikker))
    ax.set_xlabel('Angle ($^\circ$)')
    ax.set_ylabel('Power (dB)')

    #ax2.plot(x, y, '-', label='count %d' % pattern)
    #ax2.set_xlim(-20, 20)
    #ax2.set_title('count %d' % (pattern+1), fontweight='bold')
    if pattern != 4 and pattern != 9:
        value = np.max(y - 3)
        ang = intersect(value, x, y)
        #ax2.axvline(ang, color='r')
        #ax2.axvline(np.abs(ang), color='r')
        #ax2.axhline(value, color='g')
    print ('%.2d'%(pattern+1)).ljust(10), ('%.2f'%step).ljust(10), ('%.2f'%waveg).ljust
       (10), ('%.2f'%np.abs((ang))).ljust(10)
    pattern += 1
    count +=1
    tikker += 1
fig.tight_layout()
fig.savefig('parametersweep2_fig_3.png')
show()

fig = figure()
fig.set_size_inches(15, 10)
count = 0
while pattern < 63:
```

```
    x = theta[361*pattern:361*(pattern+1)]
    y = directivity[361*pattern:361*(pattern+1)]
    step = r_step[361*pattern]
    waveg = r_waveguide[361*pattern]
    ax = fig.add_subplot(2, 9, count+1)
    ax.set_xticks(np.linspace(-180,180,3))
    ax.set_xlabel('Angle ($^\circ$)')
    ax.set_ylabel('Power (dB)')

    #ax2 = fig2.add_subplot(2, 9, pattern+1)
    ax.plot(x, y - np.max(y), '-', label='Pattern %d' % pattern)
    ax.set_title('Pattern ' +str(tikker))
    #ax2.plot(x, y, '-', label='Pattern %d' % pattern)
    #ax2.set_xlim(-20, 20)
    #ax2.set_title('Pattern %d' % (pattern+1), fontweight='bold')
    if pattern != 4 and pattern != 9:
        value = np.max(y - 3)
        ang = intersect(value, x, y)
        # ax2.axvline(ang, color='r')
        # ax2.axvline(np.abs(ang), color='r')
        # ax2.axhline(value, color='g')
    print ('%.2d'%(pattern+1)).ljust(10), ('%.2f'%step).ljust(10), ('%.2f'%waveg).ljust
        (10), ('%.2f'%np.abs((ang))).ljust(10)
    pattern += 1
    count +=1
    tikker += 1
fig.tight_layout()
fig.savefig('parametersweep2_fig_4.png')
show()
```

11.4 Appendix IV: Code for analyzing the far-field data

```
#!/usr/bin/env python
# -*- coding: utf-8 -*-
import math
import numpy as np
from matplotlib.pylab import *
from mpl_toolkits.mplot3d import Axes3D


''' week 11-15 May '''

x1, y1 , z1 ,real1 ,imaginary1 = np.loadtxt('vnascan_20cm_test11(2).txt', usecols
    =(0,1,2,5,6), unpack=True)
x2, y2 , z2 ,real2 ,imaginary2 = np.loadtxt('vnascan_20cm_test11-lambda.txt', usecols
    =(0,1,2,5,6), unpack=True)

Nz = 81
Ny = 81

def sort_by_freq(re , im, Ny, Nz, freq_element):
        freq =np.linspace(10,12,21)
        #print "Matrix will be calculated for "+ str(freq[freq_element])+ " GHz"
        matrix = np.zeros((Nz,Ny),dtype=complex)
        real_sorted = []
        imaginary_sorted = []

        k = freq_element
        p = freq_element

        while k < len(re):
                real_sorted.append(re[k])
                k += 21

        while p < len(im):
                imaginary_sorted.append(im[p])
                p += 21

        h = 0
        for i in range(Nz):
                for j in range(Ny):
                        matrix[i][j] = real_sorted[h] + imaginary_sorted[h]*1j
                        h += 1
        return matrix

def intersect(value, x, y):
    ''' Find the x left coordinate corresponding to y = value assuming a symmetric
       function w.r.t. x.
    Intersect fits a straight line through the points just above and just below the
       wanted value and then iterpolates the wanted number.
    '''
    N = len(y)
    # Go halfway
    for i in range(N//2 + 1):
        if y[i] > value:
            y_low = y[i-1]
            y_high = y[i]
            x_low = x[i-1]
            x_high = x[i]
            break
    # Linear interpolation.
    slope = (y_high - y_low) / (x_high - x_low)
    x = (value - y_low) / slope + x_low
    return x

def fieldplots(real1, imaginary1, real2, imaginary2, Ny, Nz, selected): #Calculate the
    field plots.
        A1 = np.zeros((Nz,Ny),dtype=complex)
        A2 = np.zeros((Nz,Ny),dtype=complex)
        frequencies = np.arange(10.5,11.6,0.1)
```

```
A1_fft_sum = 0

lowerfreq = np.round(selected[0], decimals=1)
higherfreq = np.round(selected[len(selected)-1], decimals=1)

for t in range(len(selected)):
        A = sort_by_freq(real1,imaginary1,81,81,selected[t])
        B = sort_by_freq(real2,imaginary2,81,81,selected[t])

        A1 += (A + 1j*B)/2

# Nearfield
A1_near_amp = abs(A1)
A1_near_phase = np.arctan2(np.imag(A1),np.real(A1))

theta = np.linspace(-22,22,81)
maximum = 0
for i in range(Nz):
        for j in range(Ny):
                if A1_near_amp[i][j] > maximum:
                        maximum = A1_near_amp[i][j]
                        index_z = i
                        index_y = j
A1_near_amp_T = A1_near_amp.T

# For one frequency
if lowerfreq == higherfreq:
        fig1 = plt.figure()
        fig1.set_size_inches(15, 10)
        ax = fig1.add_subplot(111)
        ax.set_xlabel('y (cm)')
        ax.set_ylabel('z (cm)')
        #ax.set_xticks(np.linspace(-40,40,9))
        #ax.set_yticks(np.linspace(-40,40,9))
        ax.set_title('Amplitude near-field for '+ str(np.round(lowerfreq,
            decimals=0)) +' GHz')
        cax = ax.imshow(10*np.log10((A1_near_amp/np.amax((A1_near_amp)))**2),
            vmin=-40,vmax=0,extent=[-40,40,-40,40])
        cbar = fig1.colorbar(cax)
        cbar.set_label('Power (dB)',size=12)
        a = str(lowerfreq)
        b = ""
        for c in a:
                if c != ".":
                        b += c
                else:
                        b +=","
        savefig('Nearfield_amplitude_'+ b +'_GHz.png')
        show()

        fig1 = plt.figure()
        fig1.set_size_inches(15, 10)
        ax = fig1.add_subplot(111)
        x = np.linspace(-40,40,81)
        plot(x,10*np.log10((A1_near_amp[index_z]/np.amax(A1_near_amp[index_z]))
            **2), label='maximum along z',linewidth=2)
        plot(x,10*np.log10((A1_near_amp_T[index_y]/np.amax(A1_near_amp_T[index_y
            ]))**2),label='maximum along y',linewidth=2)
        title('Maximum amplitude cross cut near-field for '+ str(np.round(
            lowerfreq,decimals=0)) +'  GHz')
        ax.set_xticks(np.linspace(-40,40,9))
        xlabel("distance from center (cm)")
        ylabel("Power (dB)")
        legend(loc='lower center')
        savefig('Nearfield_amplitude_crosscut_'+b+'_GHz.png')
        show()


        fig1 = plt.figure()
        fig1.set_size_inches(15, 10)
```

```
        ax = fig1.add_subplot(111)
        ax.set_xlabel('y (cm)')
        ax.set_ylabel('z (cm)')
        ax.set_title('Phase near-field for '+ str(np.round(lowerfreq,decimals=0)
            )+' GHz')
        cax = ax.imshow(A1_near_phase,extent=[-40,40,-40,40])
        fig1.colorbar(cax)

        savefig('Nearfield_phase_'+b+'_GHz.png')
        show()

# For multiple frequencies
else:
        a = str(lowerfreq)
        b = ""
        for c in a:
                if c != ".":
                        b += c
                else:
                        b +=","

        a = str(higherfreq)
        d = ""
        for e in a:
                if e != ".":
                        d += e
                else:
                        d +=","

        fig1 = plt.figure()
        fig1.set_size_inches(15, 10)
        ax = fig1.add_subplot(111)
        ax.set_xlabel('y (mm)')
        ax.set_ylabel('z (mm)')
        ax.set_title('Amplitude nearfield for '+ str(lowerfreq) + '-' + str(
            higherfreq) +' GHz')
        cax = ax.imshow(10*np.log10((A1_near_amp/np.amax((A1_near_amp)))**2),
            vmin=-40,vmax=0,extent=[-40,40,-40,40])
        fig1.colorbar(cax)
        cax.set_label("Power (dB)")
        savefig('Nearfield_amplitude_'+b+'-'+d+'_GHz.png')
        show()

        fig1 = plt.figure()
        fig1.set_size_inches(15, 10)
        ax = fig1.add_subplot(111)
        x = np.linspace(-40,40,81)
        plot(x,10*np.log10((A1_near_amp[index_z]/np.amax(A1_near_amp[index_z]))
            **2), label='maximum along z',linewidth=2)
        plot(x,10*np.log10((A1_near_amp_T[index_y]/np.amax(A1_near_amp_T[index_y
            ]))**2),label='maximum along y',linewidth=2)
        title('Maximum amplitude cross cut nearfield for '+ str(lowerfreq) + '-'
             + str(higherfreq) +'  GHz')
        xticks(np.linspace(-40,40,9))
        xlabel('distance from center (cm)')
        ylabel('Power (dB)')
        legend(loc='lower center')
        savefig('Nearfield_amplitude_crosscut_'+b+'-'+d+'_GHz.png')
        show()

        fig1 = plt.figure()
        fig1.set_size_inches(15, 10)
        ax = fig1.add_subplot(111)
        ax.set_xlabel('y (cm)')
        ax.set_ylabel('z (cm)')
        ax.set_title('Phase nearfield for '+ str(lowerfreq) + '-' + str(
            higherfreq) +' GHz')
        cax = ax.imshow(A1_near_phase,extent=[-40,40,-40,40])
        fig1.colorbar(cax)
```

```
        savefig('Nearfield_phase'+b+'-'+d+'_GHz.png')
        show()

# Farfield
c = 299792458000 #cm/s
f = 11e9
unit = 400/81
lambda_0 = c/f #mm

element_number1 = np.arange(1,41,1)*(lambda_0/400)                          #Hier
    moet jij van maken: np.arange(1,41,1)*(lambda_0*D/400) waarbij de D de
    afstand tot de spiegel is
element_number2 = -1*np.arange(40,0,-1)*(lambda_0/400)          # Hetzelfde hier
     als in regel 295
zero = np.array(0)
x = np.hstack((element_number2,zero,element_number1))

theta_y = np.degrees(np.arctan(x))
theta_z = np.degrees(np.arctan(x))

A1_far_amp = abs(np.fft.fftshift(np.fft.fft2(A1)))
A1_far_phase = np.arctan2(np.imag(A1),np.real(A1))

theta = np.linspace(-22,22,81)
maximum = 0
for i in range(Nz):
        for j in range(Ny):
                if A1_far_amp[i][j] > maximum:
                        maximum = A1_far_amp[i][j]
                        index_z = i
                        index_y = j
A1_far_amp_T = A1_far_amp.T

y = 10*np.log10((A1_far_amp[index_z]/np.amax(A1_far_amp[index_z]))**2)
z = 10*np.log10((A1_far_amp_T[index_y]/np.amax(A1_far_amp_T[index_y]))**2)

# For one frequency
if lowerfreq == higherfreq:
        a = str(lowerfreq)
        b = ""
        for c in a:
                if c != ".":
                        b += c
                else:
                        b +=","

        fig2 = plt.figure()
        fig2.set_size_inches(15, 10)
        ax = fig2.add_subplot(111)
        ax.set_xlabel('y-angle ($^\circ$)')
        ax.set_ylabel('z-angle ($^\circ$)')
        ax.set_xticks(np.linspace(-70,70,15))
        ax.set_title('Amplitude far-field '+ str(np.round(lowerfreq,decimals=0))
             +' GHz')
        cax = ax.imshow(10*np.log10((A1_far_amp/np.amax((A1_far_amp)))**2),vmin
            =-40,vmax=0,extent=[-70,70,-70,70])
        cbar=fig2.colorbar(cax)

        cbar.set_label('Power (dB)',size=12)
        savefig('Farfield_amplitude_'+ b +'_GHz.png')
        show()

        ax = fig2.add_subplot(122)
        #x = np.linspace(-40,40,81)
        plot(theta_y,z, label='maximum along y',linewidth=2)
        plot(theta_y,y,label='maximum along z',linewidth=2)
        title('Maximum ampltude cross cut far-field '+ str(np.round(lowerfreq,
            decimals=0)) +' GHz')
        legend(loc='lower center')
        xlim([-70,70])
```

```
            #xticks(np.linspace(-40,40,9))
            xlabel('Angle ($^\circ$)')
            ylabel('Power (dB)')
            savefig('Farfield_amplitude_crosscut_'+ b +'_GHz.png')
            show()

    # For more than one frequency
    else:
            a = str(lowerfreq)
            b = ""
            for c in a:
                    if c != ".":
                            b += c
                    else:
                            b +=","

            a = str(higherfreq)
            d = ""
            for e in a:
                    if e != ".":
                            d += e
                    else:
                            d +=","

            fig2 = plt.figure()
            fig2.set_size_inches(15, 10)
            ax = fig2.add_subplot(121)
            ax.set_xlabel('y (mm)')
            ax.set_ylabel('z (mm)')
            ax.set_title('Amplitude farfield '+ str(lowerfreq) + '-' + str(
                higherfreq) +' GHz')
            cax = ax.imshow(10*np.log10((A1_far_amp/np.amax((A1_far_amp)))**2),vmin
                =-40,vmax=0)
            fig2.colorbar(cax)
            cax.set_label("Power (dB)")
            savefig('Farfield_amplitude_'+b+'-'+d+'_GHz.png')
            show()

            ax = fig2.add_subplot(122)
            x = np.linspace(-40,40,81)
            plot(x,z, label='maximum along y',linewidth=2)
            plot(x,y,label='maximum along z',linewidth=2)
            title('Maximum amplitude cross cut nearfield '+ str(lowerfreq) + '-' +
                str(higherfreq) +' GHz')
            legend(loc='lower center')
            xticks(np.linspace(-40,40,9))
            xlabel('distance from center (cm)')
            ylabel('Power (dB)')
            savefig('Farfield_amplitude_crosscut_'+b+'-'+d+'_GHz.png')
            show()


    return z, y, lowerfreq, higherfreq

def beamsize(z,y, Ny, Nz, lowerfreq, higherfreq): # bepalen van de beamsize
    c = 299792458000 #cm/s
    f = 11e9
    unit = 400/81
    lambda_0 = c/f #mm

    element_number1 = np.arange(1,41,1)*(lambda_0/400)                      #Hier
        moet jij van maken: np.arange(1,41,1)*(lambda_0*D/400) waarbij de D de
        afstand tot de spiegel is
    element_number2 = -1*np.arange(40,0,-1)*(lambda_0/400)          # Hetzelfde hier
         als in regel 295
    zero = np.array(0)
    x = np.hstack((element_number2,zero,element_number1))

    theta_y = np.degrees(np.arctan(x))
    theta_z = np.degrees(np.arctan(x))
```

```
# along y-axis
y_min_beamsize = intersect(-3, theta_y, y)
y_min_beamsize_rad = np.radians(y_min_beamsize)
           # Half angle in radians
y_min_beamsize_deg = y_min_beamsize
                   # Half angle in degrees

y_max_beamsize = intersect(-3,-1*theta_y,y)-4
y_max_beamsize_rad = np.radians(y_max_beamsize)
           # Half angle in radians
y_max_beamsize_deg = y_max_beamsize
                   # Half angle in degrees

y_beamsize_avg_deg = (abs(y_min_beamsize_deg)+abs(y_max_beamsize_deg))/2
y_beamsize_avg_rad = (abs(y_min_beamsize_rad)+abs(y_max_beamsize_rad))/2

print 'Beamsize (full angle) along z-axis: ', np.round((2*y_beamsize_avg_deg),
    decimals=2), ' degrees'
print 'Beam solid angle along z-axis: ', (y_beamsize_avg_rad**2)*np.pi, '
    steradian'

# along z-axis
z_min_beamsize = intersect(-3, theta_z, z)+0.1
z_min_beamsize_rad = np.radians(z_min_beamsize)
           # Half angle in radians
z_min_beamsize_deg = z_min_beamsize
                   # Half angle in degrees

z_max_beamsize = intersect(-3,-1*theta_z,z)-2
z_max_beamsize_rad = np.radians(z_max_beamsize)
           # Half angle in radians
z_max_beamsize_deg = z_max_beamsize
                   # Half angle in degrees

z_beamsize_avg_deg = (abs(z_min_beamsize_deg)+abs(z_max_beamsize_deg))/2
z_beamsize_avg_rad = (abs(z_min_beamsize_rad)+abs(z_max_beamsize_rad))/2

print 'Beamsize (full angle) along y-axis: ', np.round((2*z_beamsize_avg_deg),
    decimals=2), ' degrees'
print 'Beam solid angle along y-axis: ', (z_beamsize_avg_rad**2)*np.pi, '
    steradian'
print 'Average beam size ', (y_beamsize_avg_deg+z_beamsize_avg_deg) , ' degrees'


#r_line = np.linspace(-60,0,2)
#theta_line1 = [x_beamsize, x_beamsize]
#theta_line2 = [-x_beamsize+np.pi, -x_beamsize+np.pi]

if lowerfreq == higherfreq:
        a = str(lowerfreq)
        b = ""
        for c in a:
                if c != ".":
                        b += c
                else:
                        b +=","

        y_min = y_min_beamsize_deg
        y_max = y_max_beamsize_deg
        fig3 = plt.figure()
        fig3.set_size_inches(15, 10)
        ax = fig3.add_subplot(121)
        ax.plot(theta_y,y, 'b', label="Measured data",linewidth=2)
        ax.vlines(y_min,-80,0, 'r', label='Beamsize: '+str(np.round((2*
            y_beamsize_avg_deg),decimals=2))+'$^\circ$',linewidth=2)
        ax.vlines(y_max,-80,0, 'r',linewidth=2)
        #ax.vlines(4.4,-60,0, 'k', label='Theoretical: 8.8$^\circ$')
        #ax.vlines(-4.4,-60,0, 'k')
        ax.hlines(-3,-100,100,'g',label="-3 dB line",linewidth=2)
```

```
        ax.set_xticks(np.linspace(-100,100,11))
        ax.xaxis.set_minor_locator(MultipleLocator(5))
        ax.set_xlim([-70,70])
        ax.set_xlabel('Angle y (degrees)')
        ax.set_ylabel('Power (dB)')
        ax.set_title('Beampattern along z-axis max. amp '+ str(np.round(
            lowerfreq,decimals=0))  +' GHz')
        legend()

        z_min = z_min_beamsize_deg
        z_max = z_max_beamsize_deg
        ax = fig3.add_subplot(122)
        ax.plot(theta_z,z,label='Measured data',linewidth=2)
        ax.vlines(z_min,-80,0, 'r', label='Beamsize:'+str(np.round((2*
            z_beamsize_avg_deg),decimals=2))+'$^\circ$',linewidth=2)
        ax.vlines(z_max,-80,0, 'r',linewidth=2)
        #ax.vlines(4.4,-60,0, 'k', label='Theoretical: 8.8$^\circ$')
        #ax.vlines(-4.4,-60,0, 'k')
        #ax.vlines(-38,-60,0, 'y', label='Beam: 74$^\circ$')
        #ax.vlines(36,-60,0, 'y')
        ax.set_xlim([-70,70])
        ax.hlines(-3,-100,100,'g',label="-3 dB line",linewidth=2)
        ax.set_xticks(np.linspace(-100,100,11))
        ax.xaxis.set_minor_locator(MultipleLocator(5))
        xlim([-70,70])
        ax.set_xlabel('Angle z (degrees)')
        ax.set_ylabel('Power (dB)')
        ax.set_title('Beampattern along y-axis max. amp '+ str(np.round(
            lowerfreq,decimals=0))  +' GHz')
        legend()

        tight_layout()

        savefig('Beamsize_'+ b  +'_GHz.png')
        show()

else:
        a = str(lowerfreq)
        b = ""
        for c in a:
                if c != ".":
                        b += c
                else:
                        b +=","

        a = str(higherfreq)
        d = ""
        for e in a:
                if e != ".":
                        d += e
                else:
                        d +=","

        y_min = y_min_beamsize_deg
        y_max = y_max_beamsize_deg
        fig3 = plt.figure()
        fig3.set_size_inches(15, 10)
        ax = fig3.add_subplot(121)
        ax.plot(theta_y,y, 'b', label='beamsize: '+str(np.round((2*
            y_beamsize_avg_deg),decimals=2))+'$^\circ$')
        ax.vlines(y_min,-60,0, 'r', label='Script')
        ax.vlines(y_max,-60,0, 'r')
        ax.vlines(4.4,-60,0, 'k', label='Theoretical: 8.8$^\circ$')
        ax.vlines(-4.4,-60,0, 'k')
        ax.hlines(-3,-160,160,'g')
        ax.set_xticks(np.linspace(-200,200,21))
        ax.xaxis.set_minor_locator(MultipleLocator(5))
        ax.set_ylim([-60,0])
        ax.set_xlabel('Angle y (degrees)')
        ax.set_ylabel('Power (dB)')
```

```
                ax.set_title('Beampattern along z-axis max. amp '+ str(lowerfreq) + '-'
                    + str(higherfreq) +' GHz')
                legend()

                z_min = z_min_beamsize_deg
                z_max = z_max_beamsize_deg
                ax = fig3.add_subplot(122)
                ax.plot(theta_z,z,label='beamsize: '+str(np.round((2*z_beamsize_avg_deg)
                    ,decimals=2))+'$^\circ$')
                ax.vlines(z_min,-60,0, 'r', label='Script')
                ax.vlines(z_max,-60,0, 'r')
                ax.vlines(4.4,-60,0, 'k', label='Theoretical: 8.8$^\circ$')
                ax.vlines(-4.4,-60,0, 'k')
                ax.vlines(-38,-60,0, 'y', label='Beam: 74$^\circ$')
                ax.vlines(36,-60,0, 'y')
                ax.hlines(-3,-160,160,'g')
                ax.set_ylim([-60,0])
                #ax.xaxis.set_major_locator()
                ax.set_xticks(np.linspace(-200,200,21))
                ax.xaxis.set_minor_locator(MultipleLocator(5))
                ax.set_xlabel('Angle z (degrees)')
                ax.set_ylabel('Power (dB)')
                ax.set_title('Beampattern along y-axis max. amp '+ str(lowerfreq) + '-'
                    + str(higherfreq) +' GHz')
                legend()

                tight_layout()

                savefig('Beamsize_'+b + '-' + d+'_GHz.png')
                show()

def resonance(real1, imaginary1, real2, imaginary2, Ny, Nz, selected):
        A1 = np.zeros((Nz,Ny),dtype=complex)
        A2 = np.zeros((Nz,Ny),dtype=complex)
        freq = np.arange(10.5,11.6,0.1)
        A1_fft_sum = 0
        lowerfreq = np.round(selected[0], decimals=1)
        higherfreq = np.round(selected[len(selected)-1], decimals=1)

        for t in range(len(selected)):
                A = sort_by_freq(real1,imaginary1,81,81,selected[t])
                B = sort_by_freq(real2,imaginary2,81,81,selected[t])

                A1 += (A - 1j*B)/2

        # Nearfield
        A1_near_amp = abs(A1)
        A1_near_phase = np.arctan2(np.imag(A1),np.real(A1))

        fig1 = plt.figure()
        fig1.set_size_inches(15, 10)
        ax = fig1.add_subplot(111)
        ax.set_xlabel('y (mm)')
        ax.set_ylabel('z (mm)')
        ax.set_title('Standing wave nearfield for '+ str(lowerfreq) + '-' + str(
            higherfreq) +' GHz')
        cax = ax.imshow(10*np.log10((A1_near_amp/np.amax((A1_near_amp)))**2),vmin=-40,
            vmax=0)
        fig1.colorbar(cax)
        savefig('Standing_wave_horn_'+str(lowerfreq) + '-' + str(higherfreq) +'_GHz.png'
            )
        show()


selected = np.arange(10.5,11.6,.1)
field = fieldplots(real1, imaginary1, real2, imaginary2, Ny, Nz, selected)
z = field[0]
y = field[1]
lowerfreq = field[2]
higherfreq = field[3]
```

```
beamsize(z,y, Ny, Nz, lowerfreq, higherfreq)
#resonance(real1, imaginary1, real2, imaginary2, Ny, Nz, selected)
```

11.5 Appendix V: Code for plotting the probe reflection

```
#!/usr/bin/env python
# -*- coding: utf-8 -*-
import math
import numpy as np
from matplotlib.pylab import *
from mpl_toolkits.mplot3d import Axes3D

freq, y1 , y2 = np.loadtxt('short_probe.txt', usecols=(0,1,2), unpack=True)

fig = plt.figure()
fig.set_size_inches(15, 10)
plot(freq/10e8,10*np.log10(y2**2),'g',linewidth=2)
xticks(np.linspace(8,16,9))
xlabel("Frequency (GHz)")
ylabel("Power (dB)")
axvline(x=10.5, ymin=10, ymax=-30,color='r',linewidth=2)
axvline(x=11.5, ymin=10, ymax=-30,color='r',linewidth=2)
grid(b=True, which='minor',color='k',linestyle='-')
grid(b=True, which='major',color='k',linestyle='-')
minorticks_on()
title("$S_{11}$ for the probe")
savefig("s11_probe.png")
show()
```

12 References

[1] National radio astronomy observatory website.

[2] *Radiall SMA - RIM miniature coaxial connectors.* 1980.

[3] IRE A. P. KING, SENIOR MEMBER. The radiation characteristics conical horn antennas.

[4] Research & Special Development Group University of Massachusetts Christopher J. Mosher, Microwave/RF Antenna Engineer. Mie 605 term project (final report), March, 1998.

[5] Robert E. Collin. *Field Theory of Guided Waves.* 1960.

[6] CST. Cst microwave studio.

[7] F. Sweijen (Frist). Software Design of a Computer Controlled Horn antenna and Measuring the Temperature of the CMB at 11 GHz. jul 2015.

[8] Paul F. Goldsmith. *Quasioptical Systems - Gaussian Beam Quasioptical Propagation and Applications.*

[9] John C. Hardy Herbert M. Pickett and Jam Farhoomand. Characterization of a dual-mode horn for submillimeter wavelengths. *IEEE - Transactions on Microwave Theory and Techniques, vol. MTT-32, No. 8*, August 1984.

[10] Margaret Rouse (image).

[11] Marco Antonio Brasil Terada Leandro de Paula Santos Pereira. New method for optimum design of pyramidal horn antennas. *Journal of Microwaves, Optoelectronics and Electromagnetic Applications, Vol. 10, No. 1*, June 2011.

[12] M. Zandvliet (Maik). Back-end and mechanics of a pickett-potter horn telescope at 11 ghz.

[13] Sophocles J. Orfanidis. *Electromagnetic Waves and Antennas.*

[14] A.A. Penzias and R.W. Wilson. A Measurement of Excess Antenna Temperature at 4080 Mc/s. *apj*, 142:419–421, jul 1965.

[15] A.A. Penzias and R.W. Wilson. Measurement of the Flux Density of CAS a at 4080 Mc/s. *apj*, 142:1149, oct 1965.

[16] P. D. Potter. A new horn antenna with suppressed sidelobes and equal beamwidths. *Technical Report No. 32-354*, February 1963.

[17] P.D. Potter. Efficient antenna systems: A new computer programm for the design and analysis of high-preformance conical feedhorns. *JPL Technical report 32-1526, VOL. XIII.*

[18] Matthew N.O. Sadiku. *Elements of Electromagnetics.* 2nd edition.

[19] John R. Whinnery Simon Ramo and Theodore van Duzer. *Field and Waves in Communication Electronics.* 2nd edition.

[20] Kristen Rohls Thomas L.Wilson and Susanne Hüttemeister. *Tools of Radio Astronomy.*

[21] W. Mulder (Willeke). Calibration.

[22] M.A. Zaman, M. Gaffar, S.M. Choudhury, and M.A. Matin. Optimization and analysis of a ka band pickett potter horn antenna with low cross polarization. In *Electrical and Computer Engineering (ICECE), 2010 International Conference on*, pages 542–545, Dec 2010.